10-4-2010

Study of load transfer efficiency of airfield rigid pavement joints based on stresses and deflections

Ashish Wadkar

STUDY OF LOAD TRANSFER EFFICIENCY OF AIRFIELD RIGID PAVEMENT JOINTS BASED ON STRESSES AND DEFLECTIONS

by
Ashish Wadkar

A Thesis

Submitted in partial fulfillment of the requirements of the
Master of Science in Engineering Degree
of
The Graduate School
at
Rowan University
July 12, 2010

Thesis Chair: Yusuf Mehta, Ph.D., P.E.

Dedicated to:
My professors, my family and my friends

ABSTRACT

Ashish Wadkar
STUDY OF LOAD TRANSFER EFFICIENCY OF AIRFIELD RIGID PAVEMENT JOINTS BASED ON STRESSES AND DEFLECTIONS
2009/10
Yusuf Mehta, Ph.D., P.E.
Master of Science in Civil Engineering

The concept of joint load transfer efficiency is very important and fundamental to Federal Aviation Administration's (FAA) airfield rigid pavement thickness design procedures. The FAA procedure assumes 25% of stress applied to the edge is transferred to the adjoining slab. Moreover, since it is not convenient or practical to measure stress-based load transfer efficiency [LTE (S)], field measurement of load transfer efficiency includes computation of the ratio of unloaded slab deflection to loaded slab deflection. Falling weight deflectometer (FWD) generally serves the purpose of measurement of deflection-based load transfer efficiency [LTE (δ)]. The true load transfer is defined by stress (or strain) ratio [LTE (S)]. The current FAA specification prescribes the evaluation of LTE (S) from deflection based load transfer efficiency [LTE (δ)] which suggests that LTE (S) of 25 % is same as LTE (δ) of 70-90 %. However, the equivalency of LTE (δ) and LTE (S) depends on the effect of single plate loads of FWD versus multiple gear loads of aircraft and short duration impulse loads of FWD verses a comparatively longer duration moving aircraft wheel loading. In addition, unknown differences may exist due to differential slab bending phenomena under different aircraft gear configurations and various gear positions as an aircraft traverses a joint. There is a need to determine the sensitivity of appropriate variables such as pavement structure, static or moving modern aircraft gear loads in different positions along the joint etc. on the LTE (S) of the rigid airfield pavement joints. The FAA currently uses a single slab model for thickness design using FAARFIELD. The design philosophy is now being extended to multi-slabs.

Hence there is also a need to study the above effect considering multi-slabs in finite element modeling. The three objectives of the study were: 1) To determine how 25% stress-based load transfer efficiency compares considering above mentioned variables; 2) To study the effect of various load types such as static versus moving loads, various aircraft gear configurations and position of gears with respect to the joint on the LTE of joint; 3) Justify the commonly used correlation between LTE (S) and LTE (δ) considering the above mentioned effects. The full scale test data collected at National Airport Pavement Test Facility (NAPTF) was used in this study. Available strain gage records obtained during the slow rolling tests were analyzed to obtain LTE (S) under moving aircraft gear loading. Deflection data from FWD was analyzed to obtain LTE (δ) of the test item joints. The pavement stresses and deflections under static aircraft loading were also determined using 2D and 3D-finite element analysis programs. The pavement configuration and the aircraft gear similar to those at NAPTF was simulated in a 2D-finite element program JSLAB and LTE (S) under static load was determined and compared with that obtained under the moving loads. Finally, a 3D-finite element program FEAFAA developed by the FAA, was used to study the effect of different modern day aircrafts with different gear configurations in various positions along the joint on joint load transfer. Thus, the effect of static versus dynamic loading, footprint shapes, gear configurations and gear positions on joint load transfer was studied using the full scale data as well as finite element analysis programs. Overall the results demonstrated that stress based LTE under a moving aircraft gear was significantly higher than that under a static aircraft gear loading. Under static loading, when the main axis of aircraft gear was perpendicular to the joint, LTE (S) under a single wheel was lower by 27% as compared to the same under a 6-wheel, 4-wheel and 2-wheel gear configuration. It was also observed that number of loaded areas along a joint also governed the LTE of joint however; the difference in LTE was statistically insignificant. Overall, the 25% LTE (S) criterion was met in all the cases while it was highly conservative in case of moving aircraft gear loading.

ACKNOWLEDGEMENTS

I would like to express the deepest appreciation to my Thesis Chair, Dr. Yusuf Mehta, who has the attitude and the substance of a genius: he continually and convincingly conveyed excellence in his guidance and teaching which boosted me to explore in-depth learning and added to my excitement in this research. I would also like to convey my deepest gratitude to my Thesis co-Chair, Dr. Douglas Cleary, whose guidance demonstrated the quality attained in the reports and papers published by the virtue of this research. Without the guidance and persistent help of my Thesis Chair and co-Chair this research would not have been possible.

In addition I would like to thank Dr. Edward Guo and Dr. Gordon Hayhoe from the Federal Aviation Administration (FAA) for serving on my thesis committee and the support and appreciation in carrying out this research at Rowan University. Special thanks to Dr. David Brill from FAA for his determined effort in making all the resources in terms of data and software programs available for this research. I would also like to thank Dr. Qiang Wang from SRA International for his efforts in making us fully acquainted with the software programs and relentlessly helping us in case of any queries.

I am also indebted to my colleagues in Civil & Environmental Engineering department at Rowan University who assisted me in this research. I owe my deepest admiration to William Kettleson, Alejandro Zapata, Laura Musumeci, Alan Norton, Christopher Tomlinson, Stephen Schwandt and Patrick Hoffman for their effort and dedicated help in this research. Lastly, I offer my regards and blessings to all of those who supported me in any respect during the completion of the research project.

TABLE OF CONTENTS

LIST OF FIGURES

LIST OF TABLES

CHAPTER 1

Introduction

1.1 Background

Jointed plain concrete pavements are commonly constructed at taxiways, runways and aprons of many airports in the world. The main purpose of the joint is to accommodate the slab movements due to temperature and moisture variations and eliminate cracking during cure. Load transfer mechanisms are used between adjoining slabs because such discontinuities constitute intrinsic planes of weakness. When traffic load is applied near a pavement joint, both the loaded slab and the adjoining unloaded slab undergo a certain amount of deflection depending upon the ability of the joint to transmit part of the applied load to the adjoining slab. As a result, deflection and stress in the loaded slab will be lower than that at the free edge. The term load transfer efficiency (LTE) is commonly used to evaluate degree of load transfer in case of jointed concrete pavements.

When traffic load is applied near a pavement joint, both the loaded slab and the adjoining unloaded slab undergo a certain amount of deflection depending upon the ability of the joint to transmit part of the applied load to the adjoining slab. As a result, deflection and stress in the loaded slab will be lower than that at a free edge. The following definitions are most routinely used in providing quantitative measure of load transfer efficiency (LTE) (Ioannides and Korovesis 1992; Khazanovich and Gotlif 2005; Hammons 1998).

Deflection based load transfer efficiency is defined as,

$$LTE(\delta) = \frac{\delta_{unloaded}}{\delta_{loaded}} \tag{1.1}$$

Where, δ_{unloaded} and δ_{loaded} are the deflections of unloaded and loaded slabs respectively.

Stress based load transfer efficiency as defined by Federal Highway Administration (FHWA) is shown below:

$$LTE(\sigma) = \frac{\sigma_{unloaded}}{\sigma_{loaded}} = \frac{\varepsilon_{unloaded}}{\varepsilon_{loaded}} \quad (1.2)$$

Where, $\sigma_{unloaded}$ and σ_{loaded} are the maximum slab bending stresses while $\varepsilon_{unloaded}$ and ε_{loaded} are corresponding strains on the unloaded and loaded slabs respectively.

The concept of load transfer is very important and fundamental to FAA's rigid pavement thickness design procedures. The FAA procedure (FAA 1995; Kawa et al., 2002; Kawa et al., 2007) assumes 25% of stress applied to the edge is transferred to the adjoining slab. The value of 0.25 or 25% for LTE (S) was based upon the findings of US Army Corps of Engineers from the testing conducted at Lockbourne Army field, Ohio in early 1940's (Hammons et al. 1995; Ahlvin 1991). In the Lockbourne tests (War Department Corps of Engineers 1946), the load transfer efficiency of keyed, dowelled and keyed joints with tie bars was studied using stationary and moving wheel loads of 20000 lbs, 37000 lbs, 60000 lbs. Based on the performance data, it was concluded that 25% load transfer value was conservative (Hammons et al. 1995). Hence, LTE (S) as defined by the FAA, is the portion of edge stress that is carried by the adjacent unloaded slab which can be represented as below (Hammons 1998).

$$LTE(S) = \frac{\sigma_{unloaded}}{\sigma_{free\ edge}} = \frac{\sigma_{unloaded}}{(\sigma_{loaded}+\sigma_{unloaded})} = \frac{\varepsilon_{unloaded}}{(\varepsilon_{loaded}+\varepsilon_{unloaded})} \quad (1.3)$$

Where, $\sigma_{free\ edge}$ is the maximum bending stress at free edge of a loaded slab. Guo (2003) proved that the assumption that the sum of stresses on two sides of a joint is equal to the free edge stress is true only for flat slabs. This assumption is also true for deflections. Therefore, the sum of deflections on loaded and unloaded sides can be thus directly obtained from the free edge deflection. Moreover, since it is not convenient or practical to measure LTE (S), field measurement of load transfer efficiency includes computation of ratio of unloaded slab deflection to loaded slab deflection. Falling weight deflectometer (FWD) generally serves the purpose of measurement of deflection based load transfer efficiency [LTE (δ)]. However, the true load transfer is defined by stress (or

strain) ratio [LTE (S)]. The current FAA specification prescribes the conversion to LTE (S) from deflection based load transfer efficiency [LTE (δ)] which suggests that LTE (S) of 25 % is same as LTE (δ) of 70-90 %. Figure 1 shows the correlation between LTE (S) and LTE (δ). The correlation is based upon results obtained by a 12 inch diameter loading plate. Furthermore, as per FAA definition, the range of LTE (S) is from 0 (when, $\sigma_{unloaded} = 0$) and 50% (when, $\sigma_{unloaded} = \sigma_{loaded}$). Theoretically and logically, $\sigma_{unloaded} \leq \sigma_{loaded}$ must be satisfied. However, the horizontal axis showing LTE (S) in figure 1 exceeds beyond 50% and continues up to 100% which is not practical as per FAA's definition for LTE (S).

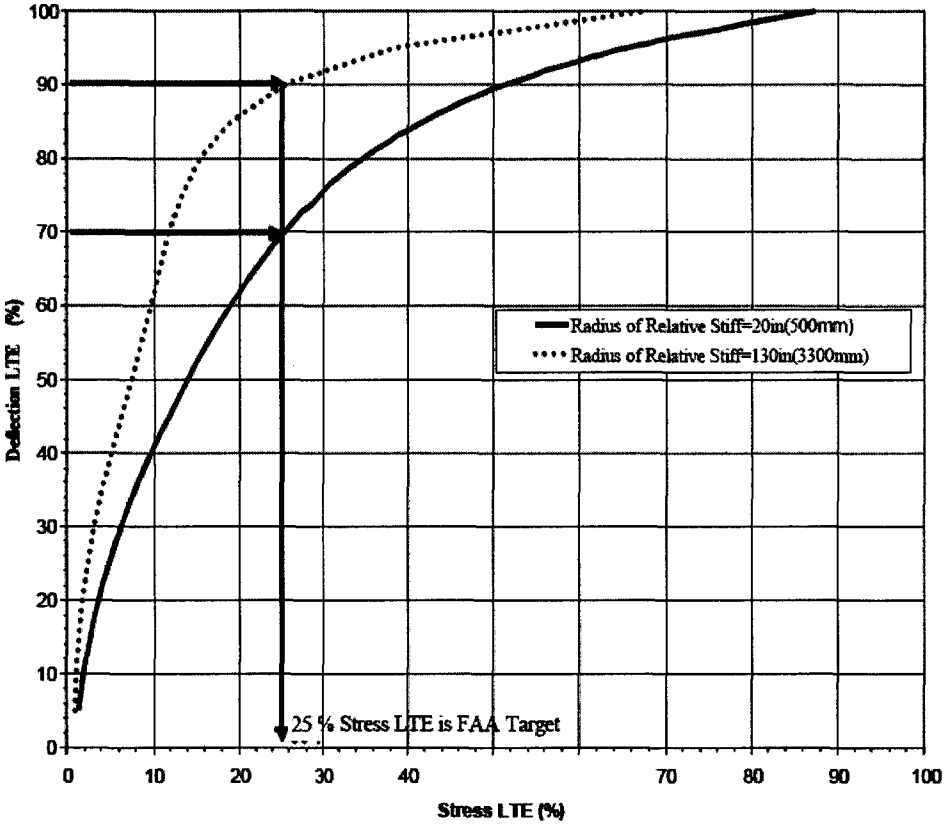

FIGURE 1: LTE (δ) versus LTE(S) for 12 inch diameter load plate. (FAA 2004)

The accuracy of relationship between LTE (S) and LTE (δ) depends on how good the match is between predicted and true load transfer in the field (Guo 2009). Some unknown differences may arise due to differences in techniques used to measure LTE (δ) and LTE (S) in the field. As mentioned earlier field measurement of LTE (δ) is based upon the deflections caused due to short duration impulse load using a 12 inch load plate.

The mechanical responses such as stresses and deflections in an airfield pavement are induced by multiple wheels of an aircraft gear which might be static or moving. Thus, the equivalency of LTE (δ) and LTE(S) depends on the effect of single plate loads of FWD versus multiple gear loads of aircraft and short duration impulse loads of FWD verses a comparatively longer duration dynamic aircraft wheel loading. In addition, unknown differences may exist due to different aircraft gear configurations and various gear positions as an aircraft traverses a joint. Therefore, there is a need to determine the sensitivity of appropriate variables such as pavement structure, static or moving modern aircraft gear loads in different positions along the joint etc. on the LTE (S) of the rigid airfield pavement joints. The FAA currently uses a single slab model for thickness design using FAARFIELD. The design philosophy is now being extended to multi-slabs. Hence there is also a need to study the above effect considering multi-slabs in finite element modeling.

1.2 Problem Statement

The following questions arise due to single plate loads of FWD versus multiple gear loads of aircraft and static loads of FWD verses dynamic aircraft wheel load considerations on the correlation between LTE (S) and LTE (δ).

1) A FWD, static or moving wheel provide different types of load distribution, in both time and space, and the responses under the three types of load have unknown differences even if their magnitudes and load center locations are the same. FWD produces impact load of very short duration and the tensile stresses are produced for that short duration. The load transfer during FWD is calculated in terms of LTE (δ). The mechanism of load transfer such as transmission of dowel forces from loaded side to unloaded side and closure of void between dowel and concrete for transmission of forces from dowel to concrete slab takes place within this short duration. However, in the case of static loading, the slab is gradually stressed to cause peak tensile stresses at the bottom of slab and remains in a state of stresses for the entire duration of loading. In the case of moving wheels, totally different mechanical responses such as tensile stresses are produced which vary with speed and position of wheels. Thus, the effect of this

difference in load types on joint load transfer needs to be studied by comparing results of FWD with slow rolling test data available from full scale testing conducted by the FAA.

2) The quality of a joint is traditionally determined using a single wheel (FWD load). This is appropriate because it provides a standard way for making the measurement. However, the stress distribution along the joint would be different in the case of single wheel or FWD load and multiple wheel of an aircraft gear. The tire pressures would also be different for a constant gross weight under a single wheel and multiple wheels. Thus, it is still of interest to find out how a joint behaves when the front and the rear axle of a wheel crosses the joint. The characteristics of LTE under a multiple-wheel gear can be understood by analyzing full-scale test data.

3) An aircraft might traverse a joint with the main axis of landing gear oriented perpendicular, parallel or at an angle with respect to the joint. The slab bending phenomena and the stress distribution across the joint tends to vary under different aircraft gear positions with respect to the joint. Thus, it is also essential to understand the impact of various gear positions on the ability of join to transmit loads from loaded slabs to unloaded slabs.

1.3 Hypothesis

The effect of different load types, aircraft gear position and gear configurations on load transfer efficiency of joints can be studied to determine whether the commonly used correlation between LTE (S) and LTE (δ) holds true. The degree of load transfer was studied using full scale test data collected by the FAA and finite element programs considering the variables in current airfields due to modern day aircraft in various positions and different pavement structures. The full scale test data collected during Construction Cycle 2 (CC2) at the FAA's National Airport Pavement Test Facility is a good source for the research for load transfer mechanism (dowels).

1.4 National Airport Pavement Test Facility

The Federal Aviation Administration (FAA) operates a state-of-the-art, full-scale pavement test facility dedicated solely to airport pavement research. Located at the

William J. Hughes Technical Center near Atlantic City, New Jersey, the National Airport Pavement Test Facility (NAPTF) provides high quality, accelerated test data from rigid and flexible pavements subjected to simulated aircraft traffic. The original test pavement of construction cycle 1 (CC1) consisted of 3 rigid pavement test items and 4 flexible pavement test items constructed over varying strengths of subgrades namely LRS, MRS and HRS. The test items were loaded with two different gear loads on nine different tracks simulating the movement of B747 and B777 airplane. Distresses were observed unexpectedly early as during the first wander itself. Because of unsatisfactory results from CC1, new construction cycle CC2 was initiated. CC2 consisted of a test strip on LRS with different slab sizes and a free standing instrumented slab with high fly ash content. Finally, based on the results of preceding tests, three test items were constructed on medium strength subgrade: econocrete subbase (MRS), aggregate subbase (MRC), and slab-on-subgrade (MRG) (Hayhoe 2004).

1.5 Overview of CC1 and CC2 at NAPTF

The construction cycle 1 (CC1) consisted of 3 rigid pavement test items and 4 flexible pavement test items constructed over varying strengths of subgrades: Low Strength Subgrade (LRS), Medium Strength Subgrade (MRS) and High Strength Subgrade (HRS) (www.airtech.tc.faa.gov/NAPTF/). However, the scope of this research is limited to rigid pavement test sections. The concrete slab size was 20 ft by 20 ft and the slab thickness was 11 inches over LRS, 9.75 inches over MRS and, 9 inches over HRS. A large amount of curling in these slabs was observed and its causes were related to excessive drying shrinkage and large vertical moisture gradient in the slab in combination with thicknesses and mix prone to moisture shrinkage (Hayhoe 2004). Trafficking on CC1 started in February 2000 with all of test items loaded at 45000 lbs per wheel. Distresses were observed unexpectedly early as during the first wander. The test was stopped and the distresses were analyzed to discover some major findings. All the slabs of HRS and MRS showed major cracking while only the central slabs of LRS cracked during the first 28 passes. Because of unsatisfactory results from CC1, new construction cycle CC2 was initiated.

The data from construction cycle 2 (CC2) at NAPTF was used in this study for evaluation of LTE (S) and LTE (δ) based on full scale tests. The test items of CC2 consisted of three rigid pavements constructed on conventional base (MRC), on grade (MRG) and on stabilized econocrete base (MRS). A medium strength subgrade of CBR value 7 was adopted. Each test item was 75 feet long and 60 feet wide, comprised of 20 slabs of size 15 feet x 15 feet. Thickness of slabs was 12 inches. Figure 2 represents the plan and sectional view of the test items. The slabs were designed such that, in the inner lanes, they would be connected with steel dowels on all four sides. The slabs in the outer lanes were doweled on three sides, leaving only the free outer edges non-doweled (NAPTF).

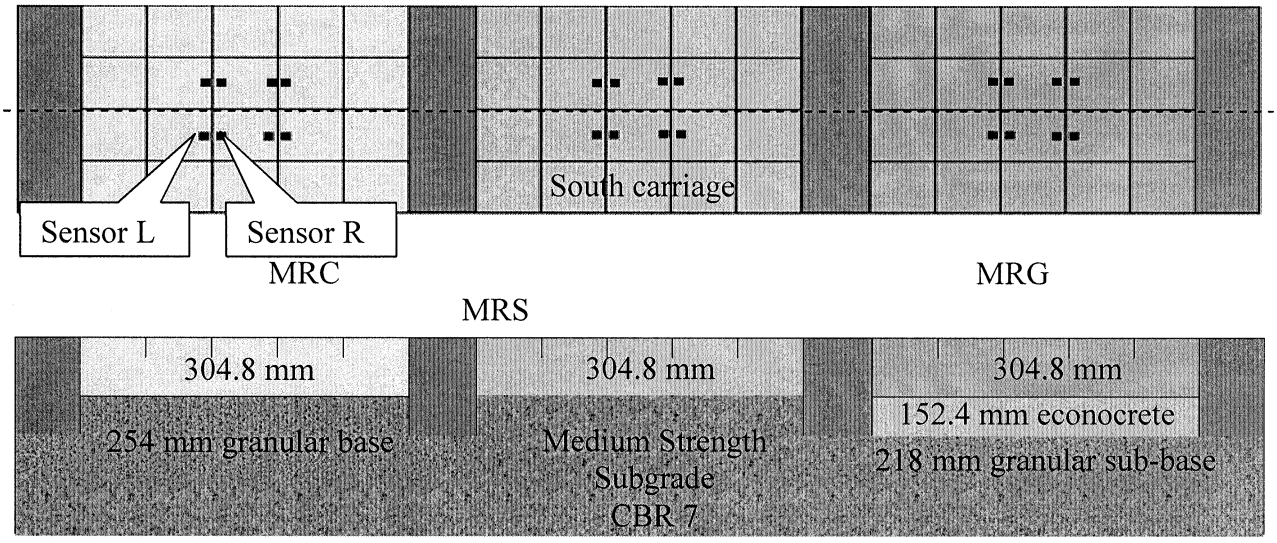

FIGURE 2: Plan and sectional view of CC2 test items along with position of concrete strain gages used in this study.

Curling of test item slabs was limited to around 20 mils or less (Hayhoe 2004). Concrete strain gages were installed at various locations to measure the strains. Traffic loading was applied by National Airport Pavement Test Vehicle (NAPTV) which is programmed for controlled aircraft wander simulation. The basic wander pattern consisted of 66 discrete positions centered on the outside edge of the inside slab, approximating a normal traffic distribution. While the original plan called for all three test items to be trafficked by 6-wheel gears on the north side and 4-wheel gears on the south side, this was actually done only for test items MRG and MRS. For test item MRC, both lanes were trafficked

by 4-wheel gears; the difference being that the south side was trafficked by a full wander pattern (i.e., traffic on both the inside and outside slabs), while on the north side, a truncated wander pattern was used (traffic applied to the inside lanes only). The gear dimensions used for trafficking the test items are shown in Figure 3.

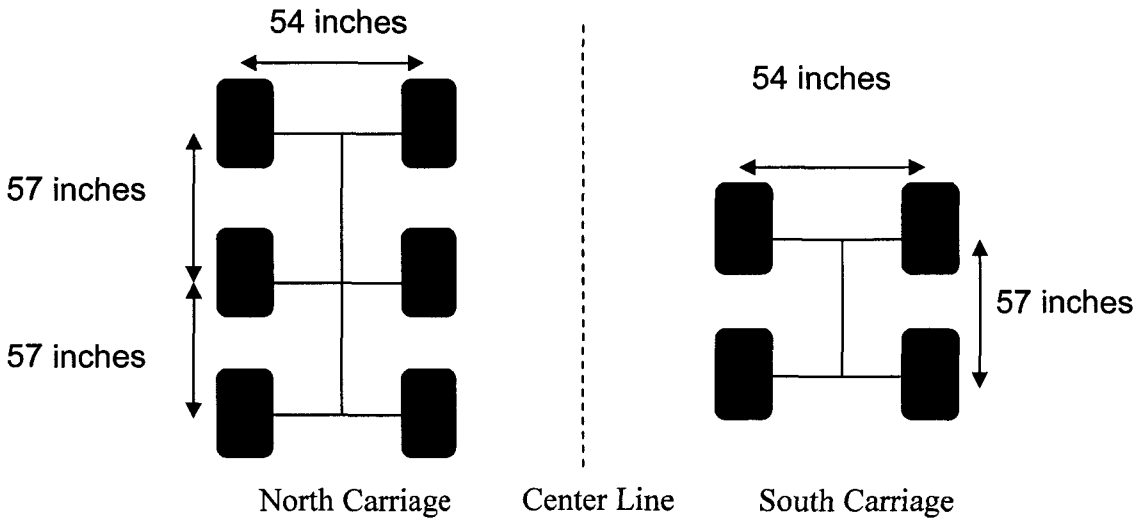

FIGURE 3: Loading gear configuration used for trafficking CC2 test items

1.6 Goal

The goal of the research is:

1) To obtain and compare LTE (S) and LTE (δ) measured during the full scale testing of airfield pavements.
2) To calculate LTE (S) under 4-wheel/ 6-wheel static loading using finite element (FE) analysis program and compare it with LTE (S) under moving loads with similar axle configuration measured from full scale test data.
3) To determine any differences in LTE due to differential slab bending or stress distribution along the joint face under different modern day aircraft gears in various positions with respect to the joint.

1.7 Research Approach

The approach adopted to achieve the above goal is as follows:

Task I: *Determining LTE (S) from slow rolling wheel responses*

Concrete strain gage records were obtained for slow rolling tests conducted at FAA's National Airport Pavement Test Facility (NAPTF). The tests were conducted using a 4-wheel and 6-wheel gear loading configurations. A protocol was formulated (described in Chapter 3) depending on forward speed of the loading vehicle and the sensor location to synchronize the raw strain record and making it reliable for analysis. Ultimately, the LTE (S) was computed under moving wheel loads from the synchronized strain records for the test item joints at NAPTF.

Task II: *Determining LTE (δ) from Heavy Weight Deflectometer (HWD) testing*

Deflection data from heavy weight deflectometer (HWD) tests conducted at NAPTF was analyzed to compute the ratio of deflections and to determine LTE (δ) of transverse joints of test items at NAPTF. In addition to transverse joints, data obtained from testing done at the slab centers was also analyzed. Deflection data at slab centers was used to estimate the modulus of subgrade reaction and modulus of elasticity of concrete by conventional method (Hall and Mohseni 1991). Data from testing at transverse and longitudinal joints was analyzed to study the importance of sum of deflection parameter to estimate curling and ability of dowelled joint in uniform load transfer.

Task III*: Determining and validating the inputs for 2D-finite element (FE) program*

The modulus of subgrade reaction (k-value) and elastic modulus of concrete slab (E_{PCC}) were required to be used as an input parameter in the 2D-FE program. These input parameters were determined using conventional back-calculation techniques (Hall and Mohseni 1991) and FAA Advisory circulars (FAA 1995). The joint stiffness parameter was then determined by simulating HWD in a 2D-FE program and using trial and error method. An equivalent joint stiffness value can be defined in the FE-program for dowelled joint assuming the joint to be fully interlocked (Ioannides and Korovesis 1992; Guo & Brill 2001). The equivalent joint stiffness value was selected when the calculated

values of LTE (δ) from FE program matched with the average LTE (δ) of field transverse joints.

Task IV: *Determining LTE (S) and LTE (δ) from static 4-wheel and 6-wheel loading using 2D- FE program*

After the joint stiffness parameter was calculated, the LTE (S) under static 4-wheel/ 6-wheel loading was determined from the stresses calculated by the 2D-FE program. In order to determine the difference in joint behavior under static and dynamic loading, the value of LTE (S) under moving wheel load computed from Task I was compared with LTE (S) under static load predicted by 2D-FE program. The LTE (δ) was also determined from this task which was compared to the values obtained from task II. In addition, the influence of different gear configurations on joint stiffness was determined in this task by comparing LTE under single wheel, 4-wheel and 6-wheel loading. The differences in LTE were also examined under parallel and perpendicular gear positions with respect to the joint. This was critical because unknown differences may arise due to differential slab bending phenomena under different gear configuration in parallel and perpendicular position.

Task V: *Determining the effect of different modern day aircraft gears in various position along a joint using 3D-Finite Element Analysis program FEAFAA*

The objective of this task was to understand the impact of various modern day aircraft gear configuration in different positions with respect to the joint on load transfer efficiency using a 3D- FE analysis program FEAFAA, developed by the FAA. FEAFAA makes use of the same 3D-FE model as used by FAA's new thickness design program FAARFIELD. In addition, the LTE (S) under different modern day aircraft gears with different gross weights was also determined to see if 25% LTE (S) assumption was valid for a typical pavement layer configuration.

1.8 Summary

This chapter presented a brief introduction of the joint load transfer efficiency concept and the importance of this study to understand the various parameters such as load types, aircraft gears, pavement structure which might influence the load transfer efficiency of a joint in airfield pavements. The goal of this study was also presented in this chapter. Finally the research approach adopted for this study was presented. The approach adopted was based on the specific objectives outlined. The next chapter presents an in depth literature review that was conducted for better understanding of joint modeling concept for finite element studies and other aspects of airfield pavement design.

CHAPTER 2

Literature Review

2.1 Jointed Plain Concrete Pavements

Concrete, like all materials, expand and contract with variation in temperature. In addition, concrete shrinks as it cures. Concrete slabs curl and warp due to excessive drying shrinkage and moisture gradients from top to bottom of slabs. These natural responses cause concrete to crack at fairly regular intervals. Jointed plain concrete pavements are commonly constructed to account for slab movements due to temperature and moisture variations. Because of joints, an intrinsic plane of weakness exists, and hence some means of transferring load from loaded slab to adjacent unloaded slab is essential. This is accounted by providing load transfer systems which are capable of transferring load by bending and shear in case of doweled joints and purely by shear in case of dummy or aggregate interlock joints. Design factors for doweled joints include the diameter, the length of embedment, the spacing of dowels required to limit and control the magnitude of stresses developing in each bar and surrounding concrete matrix. Design of aggregate interlock joints is primarily governed by width of joint and depth of saw-cut (Ioannides & Korovesis 1992). Various joint models are developed and embedded in finite element programs in recent past for design and analysis of rigid pavements.

2.2 Finite Element analysis and joint models

The finite element analysis (FEA) methods offer a solid basis for understanding rigid pavement behavior. Recent FEA methods have been proven to be reliable tools for prediction of pavement responses such as stresses, strains, deflections under traffic and

environmental loading. These finite element programs make use of various foundation models as well as joint models and the predicted data such as stresses due to edge and interior loading, strain distribution, deflections has been proven to be valid by experimentally measured data.

The efficiency of a joint in transferring the applied wheel load depends on a number of dowel-joint parameters including modulus of dowel support, dowel diameter, embedded length of dowel, dowel spacing, dowel looseness, joint opening, properties of both steel and concrete and also to a lesser extent on sub-grade strength (Maitra et al. 2009). Joints modeling was studied in the past using a number of approaches and finite element method of analysis. In an early attempt to model dowel joints, a linear elastic spring element was placed connecting the adjacent slab directly where the stiffness of spring represented the stiffness of the joint (Huang and Wang 1973). In another study, the dowel bar was modeled as an elastic beam element across the joint and relative deformation of dowel bar and the surrounding concrete was represented by the stiffness of a vertical spring connecting the two (Tabatabaie and Barenberg 1978). Nishizawa et al. (1989) developed a refined model for dowelled joints with narrow and wide joint openings. This model considers appropriate interaction between dowel and surrounding concrete. The mechanism of load transfer at the joint was characterized by aggregate interlock for dummy joints with narrow openings and dowel-concrete interaction for dowelled joints. The dowel section between the two vertical surfaces of the joint was modeled by a bending beam. The study also highlighted that stress based load transfer efficiency is much lower than deflection based load transfer efficiency where the load transfer efficiency was calculated in terms of ratio of unloaded values to the loaded values. Guo et.al. (1995) replaced the bending beam portion of the dowel by a shear beam with considerations of dowel bar geometry and physical properties of the dowel. The effect of dowel embedment length was also studied and it was stated that higher the embedment length of dowel, higher is the load-transfer capability of dowel bar system which leads to an increase of maximum displacement and stresses in the unloaded slab and a decrease of maximum displacements in the loaded slab. Table 1 summarizes some of the studies carried out to understand the rigid pavement behavior using finite element

techniques. The studies include development of various finite element programs, foundation models, joint models and their verification concordant to past full scale test data.

One of the major successes in joint modeling history is the equivalency model. There exists an equivalency in model for dowelled joint and aggregate interlock joint in which distributed shear stiffness replaces the shear stiffness contributed by individual dowelled bar (Ioannides and Korovesis 1992). The next section details equivalency between aggregate interlock and dowelled joints.

2.3 Equivalency in aggregate interlock and dowelled joint

Ioannides and Korovesis (1990) showed that for a joint equipped with pure-shear load-transfer device, the governing variable is the joint stiffness per unit length of the joint. The major load transfer mechanism in dowelled joint is also shear since bending of bars over very small span afforded by the joint opening has relative small effect. In finite element analysis, a doweled joint may be modeled as an array of shear-bending beams embedded in the slabs or as an equivalent interlock joint in which distributed shear stiffness replaces the shear stiffness contributions afforded by individual dowel bars. In past efforts have been made to develop a formula to convert dowel bar properties into an effective uniformly distributed shear stiffness (Huang & Chou 1978; Ioannides & Korovesis 1992). Guo and Brill (2001) presented a correction in dowel-concrete interaction stiffness to account for bearing of dowel on both loaded as well as unloaded slab. Guo used 2D-FE program JSLAB to compute the load transfer efficiencies and compared it with dimensionless parameter comprising of ratio of equivalent joint stiffness and product of radius of relative stiffness and subgrade modulus. The results of this analysis also demonstrated that load transfer efficiency based on deflection is insensitive to slab size. Also doweled joints transfer load more uniformly than interlock joints but they do not necessarily increase the load transfer efficiency (Guo and Brill, 2001).

The equivalence model was used in the finite element program JSLAB (2D-FEA) and FEAFAA (3D- FEA) used in this research.

The equivalent joint stiffness (k_q) was defined by the following expression:

$$k_q = \frac{1}{s\left(\frac{\omega}{0.9\,G_d\,A_d} + \frac{\omega^3}{12\,E_d I_d} + \frac{2+\beta\omega}{2\,\beta^3 E_d I_d}\right)} \quad (2.1)$$

Where, $\beta = \sqrt[4]{\frac{K\,d}{4\,E_d I_d}}$

ω is the joint opening in inches

G_d is the dowel bar shear modulus in psi

A_d is the cross sectional area of dowel bar in inch^2

E_d is the Young's modulus in psi

I_d is the moment of inertia in inch^4

K is the modulus of dowel bar support for the concrete matrix in pci

d is the diameter of dowel in inches

Thus, the efficiency of a joint in transferring the applied wheel load depends on a number of dowel-joint parameters like modulus of dowel support, dowel diameter, embedded length of dowel, dowel spacing, dowel looseness, joint opening, properties of both steel and concrete and also to a lesser extent on sub-grade strength.

The success and pending problems of the past joint models were analyzed by Guo (2009) based on a 4-point model evaluation criteria. The models were evaluated based on logical, theoretical, experimental and practical feasibility criterion. Logically, the loaded slab stresses should be more critical than the unloaded slab stresses. Tabatabie and Nishizawa model failed to pass the logical criteria. The Huang model failed the practical criteria as it required the deflection ratios as an input parameter to be defined in the model which is difficult to predict before analysis (Guo 2009). Mechanistic evaluation of pavement behavior based on full scale testing (experimental) proves to be the most appropriate way to calibrate the existing pavement engineering concepts. The next section highlights some of the studies involving field evaluation of load transfer efficiency concepts.

TABLE 1: Past studied based on development of finite element models for rigid pavement structure and joints.

Author and Year	Topic of discussion	FE Modeling Techniques adopted	Summary of Findings
Huang & Wang, 1973	Use of FE technique to determine stress distribution in concrete slabs	• Rectangular element with 4 nodes and 12 DOF for concrete slab. • Rectangular elements on either sides of joints with 12 nodes and 36 DOF to model joint forces.	• Load transfer efficiency has relatively small effect on interior stress but large effect on stress at joint. • If no load transfer is provided, the most critical stresses occur when load is nearest to transverse joint.
Tabatabaie & Barenberg., 1978	Use of FE program ILLI-SLAB (verified using Westergaard's equations, Pickett's and Ray's influence charts, AASHO road tests and testing conducted by Teller and Sutherland (1935)	• Rectangular plate elements for concrete slab and pavement layers • Joint modeled using a bar element for dowelled joint with a vertical displacement and rotational component. For an aggregate interlock or keyway, a spring element with vertical displacement component was used	• Dowelled and key joints have largest reduction in maximum edge stress and deflections under an edge load. • Maximum stress reduction in loaded slab due to presence load transfer system was found to be approximately 50%. • Depending on the modulus of dowel support, the edge stresses in dowelled joint can vary considerably.
Huand & Chou, 1978	Discrepancy of above ILLI-SLAB FE model	• Used dowel concrete interaction parameter in joint modeling	• Because of larger effect of dowel concrete interaction, the stress reduction in loaded slab due to presence of joint is about 22%.
T. Nishizawa et.al., 1989	Refined model for dowelled joints (verified by laboratory experiments and full scale experiments conducted by Ministry of Construction)	• Use of rectangular element for joint with 4 nodes and 12 DOF's. • Joints stiffness distinguished by aggregate interlock and dowel action	• Strains computed by finite element method using refined model matched well with full scale data for loaded slabs. • Joint opening has little impact on LTE of dowelled joints. Stress based LTE is much smaller than deflection based LTE.

Author and Year	Topic of discussion	FE Modeling Techniques adopted	Summary of Findings
Ioannides & korovesis, 1992	Use of dimensionless variables and ILLI-SLAB FE code to study load transfer mechanism	• Shear stiffness of dowel distinguished by dowel bar stiffness and stiffness of spring acting as dowel-concrete interaction.	• Increase in k-value or slab stiffness will result in lower LTE. • While LTE (δ) was insensitive to the ratio of loaded area to radius of relative stiffness, LTE (S) decreased with increase in the same ratio.
H. Guo et.al., 1995	Component dowel bar model to simulate dowelled joint (verified using U.S. Naval Civil Engineering airfield tests)	• Dowel bar modeled with two bending segments embedded in concrete and one shear segment in joint. • Eliminated the non equilibrium force system existing in two spring system model for dowel bars	• Bending stress due to non equilibrium stiffness matrix model for dowelled joint overestimates the longitudinal stress in unloaded slab by 18.7% and longitudinal edge stresses near joint in loaded slab by 81%.
D. Brill, 1998	Study the effect of base layer and load geometry on load transfer efficiency using a new 3D- Finite Element analysis program	• Four-node shell elements used for the PCC slab and eight-node solid elements for other pavement components, including the subgrade. • Three-dimensional solid elements for joints with linear elastic, orthotropic material properties.	• Critical pavement stresses and LTE are less sensitive to joint stiffness value when stabilized base is used • Joint efficiency in the field is a function of the loading gear characteristics as well as the joint properties.
Khazanovich & Gotlif, 2005	Justification of Tabatabaie-Barenberg (TB) joint model by LTPP FWD data	• Use of spring element for aggregate interlock • Use of beam element resting over spring for dowelled joints	• LTE is not load level dependent in majority of cases seen from LTPP dataset which also justified T-B model • Typical back-calculated stiffness of dowelled joints was recommended to be 58000 psi to 145000 psi
Yu et al., 2010	A dynamic analysis approach to study LTE under single moving load	• Pavement layers modeled as homogeneous linear elastic characterized by damping coefficients • Aggregate interlock or dowel bar embedment is reflected by a set of joint shearing springs	• LTE (S) increases with increase in vehicle speed or higher pavement damping coefficient • Ratio of dynamic to static LTE (S) changes from 1 to 2 depending on speed of vehicle

2.4 *Field measurement of Load Transfer Efficiency*

Load transfer efficiency is typically measured by means of non-destructive testing devices such as a Falling Weight Deflectometer (FWD). The FWD testing includes dropping of load on one side of joint and measurements of deflection on either side of joint. Deflection based load transfer efficiency is computed by taking the ratio of unloaded slab deflection to the loaded slab deflection. The deflection ratio has been extensively used by most pavement engineers to evaluate the joint load transfer capability due to ease of FWD testing. Some of the studies related to field evaluation of load transfer efficiency using FWD data are listed in the table below.

TABLE 2: Past studied based on field measurement of LTE

Author and Year	Topic of discussion	Summary of Findings
Guo and Brill (2001)	• Evaluation of performance of hinged (tied) joints and dowelled joints at Denver International Airport using FWD • Evaluation of subgrade strength effect on degree of load transfer during construction cycle 1 at NAPTF using FWD	• Hinged joint exhibited better performance than dowelled joints in terms of degree of load transfer as well as better joint performance even after 1 year of service. A larger decrease in LTE of dummy joints was observed in the same period. • Direction of load transfer has a significant effect on LTE. However, this effect is less significant in dowelled joints. • Subgrade CBR had less influence on LTE.
Guo & Marsey (2001)	• Analysis of FWD data from NAPTF's construction cycle 1 to study the joint load transfer. • Investigation of sum of deflection parameter as a curling indicator	• LTE of dummy joints was higher than dowelled joints in summer, however LTE dropped in fall and the drop was more for dummy joints. Dowelled joints showed uniform load transfer. • Sum of deflection on two-sides of a dummy joint increases proportionally to the slab curling.

Khazanovich & Gotlif (2003)	• Study of LTE of joints and crack from LTPP deflection data	• Testing time and season were found to have profound effects on LTE. • LTEs from leave and approach side deflection testing data were found to be statistically different the difference being more prominent in joints with low LTE • LTE of doweled joints was found to have lower variability, load level dependency, and load position dependency than LTE of non-doweled joints
Shoukry et. al. (2005)	• Examined the effect of load position, joint opening, slab temperatures and temperature differential on LTE of joints. • Examining the accuracy of measuring load transfer efficiency of transverse joints using FWD data and study its correlation of actual shear forces transferred across the joint	• LTE along wheel-path was found to be higher than LTE along pavement edge. Loading position had significant effect on LTE of joints with smaller dowel diameter. • Testing time and season had significant effect on joint LTE • Poor correlation was found between deflection based LTE and actual percentage shear forces transmitted across joints.
Ricalde & McQueen (2003)	• Study the joint formation of rigid pavement test strip initiated during CC2 at NAPTF	• Cracks were first initiated as loading was applied at free edges or joint with low LTE • Concrete strain gauge readings proved valuable for detecting the exact time of the joint formation in which was also verified by FWD testsing

2.5 Summary

This chapter covered the technical summary of past studies on jointed concrete pavements pertaining to finite element modeling of rigid pavement structure and joints in addition to analysis of field evaluation of load transfer efficiency concept. A brief summary of factors affecting LTE and other important parameter related to LTE was also emphasized in this chapter. The next two chapters presents the analysis of full scale test data collected during construction cycle 2 initiated at FAA's NAPTF.

CHAPTER 3

Concrete Stain Gage Data Analysis

3.1 Introduction

Concrete strain gage records were obtained for slow rolling tests conducted at NAPTF. The purpose of using the CC2 strain gage data was to compute the LTE (S) based on moving wheels and study the effect of dynamic loading on load transfer across the joint. Analyses of concrete strain gages located across the transverse joint of the of the CC2 test items is included in the study.

3.2 Concrete strain gage data available in the NAPTF database

The raw data available in the database needed processing in order to make the strain record reliable for LTE(S) computations. A reliability criterion was formulated depending on speed of test vehicle and sensor location to synchronize the raw strain records and making it reliable for analysis. LTE (S) was computed from the synchronized strain records for all three test items. The basic knowledge of axle configuration and speed of test vehicle was used to deduce a reliability criterion. Based on sensor location along the wheel path, the order of strain gage excitation can be easily estimated. Under a dual axle configuration, the strain gage must emit two distinct peak values. The time lag between two peaks must be equal to the time required for the vehicle to travel a distance equal to the axle spacing. In addition to the timings of peaks, the sequence of occurrence of peaks of two different strain records must also comply with the sensor location. Thus, the raw strain records were closely scrutinized to determine the peaks and were synchronized as explained with an example below.

Synchronization of strain record for MRC south wheel track gages CSG-6 and CSG-8 during Event 5 and Event 6 is considered as an example. CSG-6 which is located on the left side of the transverse joint should show the first peak followed by a peak of CSG-8 located on right side of the joint when the first axle traverses the joint from west to east. The time lag between the first peaks of the sensors as the first axle crosses or the second peaks as rear axle crosses the joint must be equal to the time require for the vehicle to travel a distance equal to the sensor spacing. The gages were located at a distance of 3 inches from the joint. The speed of test vehicle was set to be 2.5 mph during the slow rolling tests and the loading module of test vehicle was positioned such that the distance between the front and rear axle was 57 inches. Based on the sensor position, test vehicle configuration and speed it can be stated that the lag between the peaks of CSG-6 and CSG-8 which are 6 inches apart is expected to be 0.136 seconds or approximately 3 time units defining the strain history. Similarly, the time period between the two peaks of the same gage is expected to be 1.29 seconds or approximately 26 time units based on the wheel spacing. Also CSG-6 is expected to be excited before CSG-8 during "Go" event 5 and vice-versa during "Return" event 6.

Not all strain records followed the estimated sequence as described. The probable reason can be attributed to non-excitation of the gage at the exact time of wheel passage over them. Figure 4 and 5 shows the raw strain gage records for CSG-6 and CSG-8 during Event 5 and Event 6 respectively on the first day of loading MRC i.e. April 27th, 2004. It is important to note that only those events with the wheel path directly over the strain gage have been considered in this analysis. As per CC2 wander pattern, these events are typically known as Track 0 events.

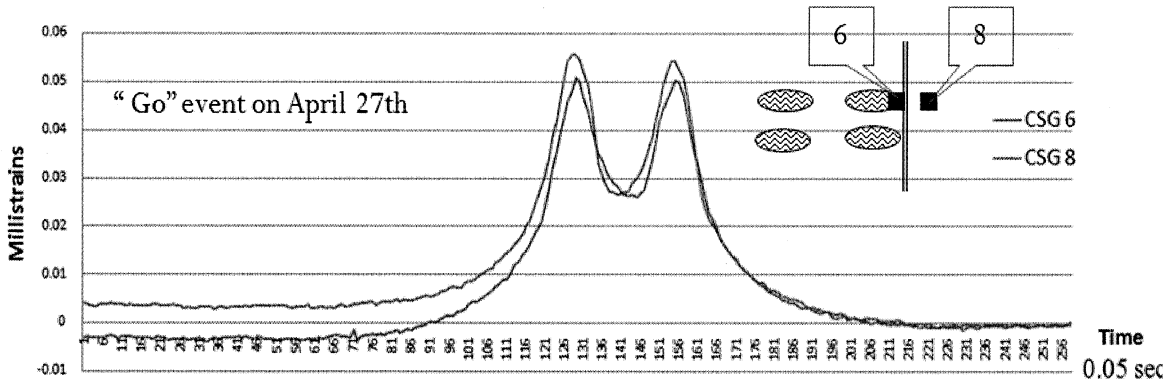

FIGURE 4: Raw strain history of CSG-6 and CSG-8 during go event number 5

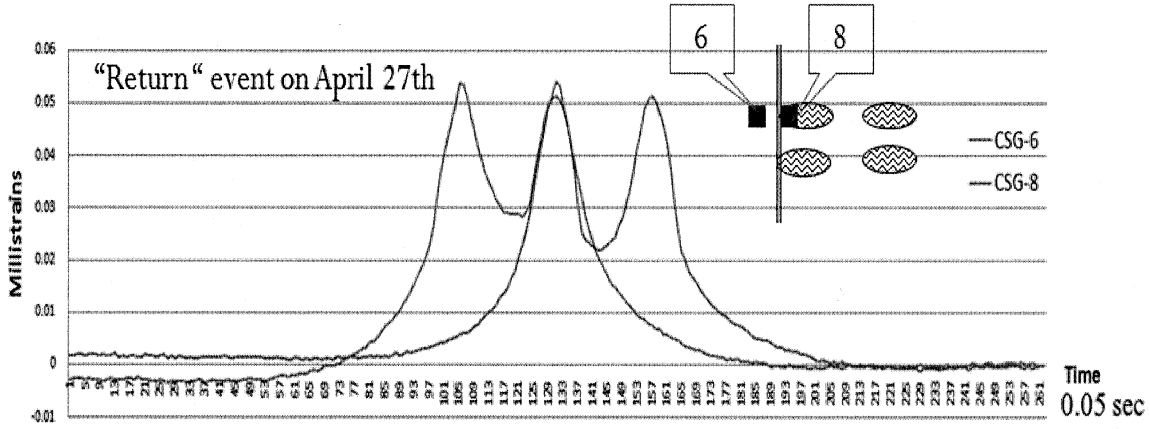

FIGURE 5: Raw strain history of CSG-6 and CSG-8 during return event number 6

Synchronized strain gage record for same gages during same loading event as per the criteria explained above is shown in figure 6 and 7. The typical computation of LTE (S) based on synchronized strain history is also shown in figure 6 and 7. Loaded slab strain is recorded at the instant when the first axle is directly over the gage. The unloaded slab strain is recorded at the same instant and ratio of unloaded strain to sum of loaded and unloaded strains is taken to determine LTE (S).

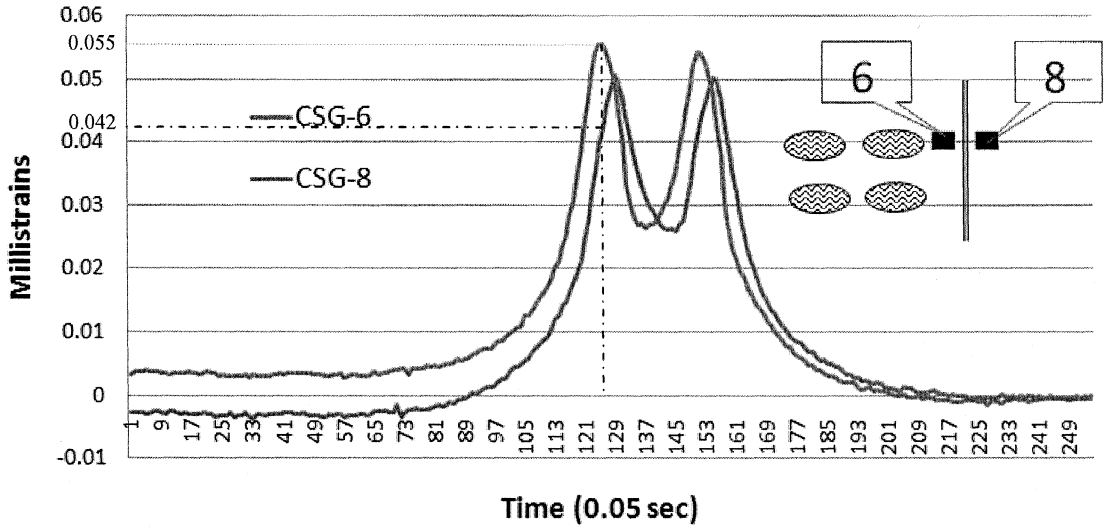

$$\text{LTE(S)} = \frac{0.042}{0.042 + 0.055} = 0.43$$

FIGURE 6: Synchronized strain history of CSG-6 and CSG-8 during go event 5

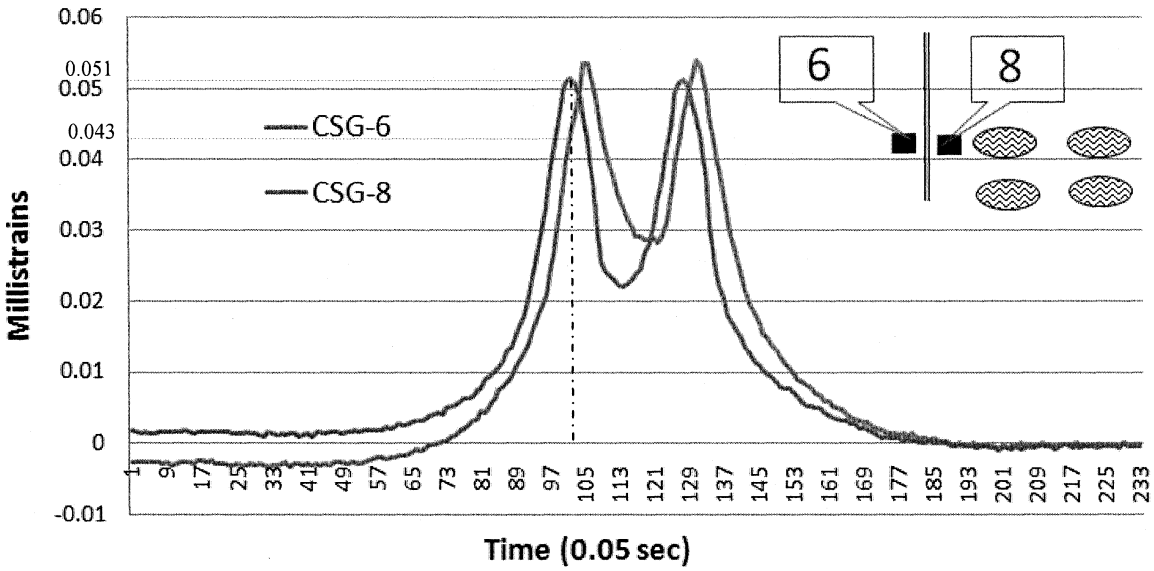

$$\text{LTE(S)} = \frac{0.043}{0.043 + 0.051} = 0.46$$

FIGURE 7: Synchronized strain history of CSG-6 and CSG-8 during return event 6

Similarly, the LTE (S) was calculated for "Go" and Return "Events" for four different wheel positions shown in figure 8 as the test vehicle traverses the joint. The initial phase of trafficking consisting of first 40 Track 0 events was analyzed in this study. The exact

event numbers and day of loading considered can be found in subsequent tables. In some cases, the value of LTE (S) is found to be higher than 50%. The probable reason for this can be attributed to the damping effects due to dynamic wheel loading. Also during synchronization process, as the first peaks were adjusted to be separated by 0.136 seconds or approximately 3 time units defining the strain history the second peaks were not lagged exactly by the same amount. Ideally, as mentioned above, the time lag between the first peaks of the sensors as the first axle crosses or the second peaks as rear axle crosses the joint must be equal. However, in rare cases it happens that these time lags are equal. This is the limitation of synchronization process which can be attributed to rounding off error and a joint opening of 0.25 inches.

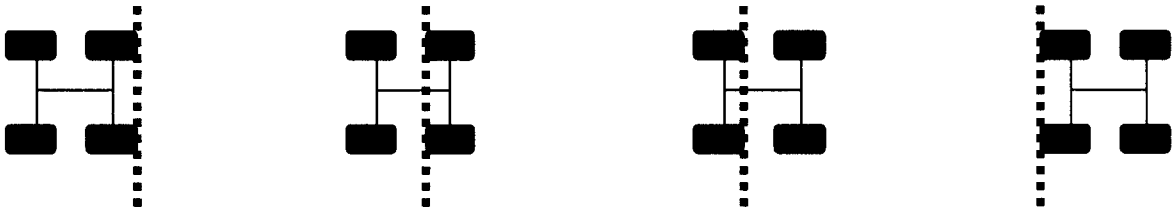

FIGURE 8: Position of wheels across the joint

The average LTE (S) values for the two south transverse joints TJ1 and TJ2 as shown in figure1 of all three test item for early phase of trafficking are tabulated in table 3a through 5. TJ1 is the first joint and TJ2 is the second joint (equipped with concrete strain gages) intercepted as the vehicle moves from west to east over the south carriage. Again, only those passes (Track 0 events) with wheels traversing directly over the gages were considered in the analysis. The strain responses only in wheel position 1 and position 4 were considered in this analysis. Vehicle passes from west to east (W to E) as well as east to west (E to W) were considered. The average LTE (S) of south transverse joints under moving wheels was found to be 0.45, 0.47 and 0.47 for MRC, MRG and MRS respectively.

TABLE 3a: Strains in mils and stress based LTE of MRC south transverse joint TJ1

Event #	Position 1					Position 4				
	ε_{loaded}	$\varepsilon_{unloaded}$	LTE(σ)	LTE(S)	Sum	ε_{loaded}	$\varepsilon_{unloaded}$	LTE(σ)	LTE(S)	Sum
5	0.056	0.042	0.762	0.430	0.098	0.050	0.048	0.945	0.490	0.098
6	0.054	0.046	0.849	0.460	0.100	0.052	0.044	0.848	0.460	0.095
23	0.055	0.046	0.837	0.460	0.101	0.052	0.051	0.982	0.500	0.103
24	0.055	0.046	0.849	0.460	0.101	0.051	0.044	0.870	0.470	0.095
47	0.053	0.045	0.848	0.460	0.098	0.052	0.051	0.966	0.490	0.103
48	0.055	0.045	0.813	0.450	0.100	0.050	0.045	0.912	0.480	0.095
53	0.054	0.046	0.866	0.460	0.100	0.052	0.049	0.938	0.480	0.101
54	0.056	0.045	0.809	0.450	0.100	0.050	0.046	0.903	0.470	0.096
65	0.054	0.044	0.822	0.450	0.098	0.053	0.046	0.862	0.460	0.098
66	0.055	0.045	0.824	0.450	0.100	0.051	0.046	0.900	0.470	0.097
71	0.054	0.045	0.820	0.451	0.099	0.052	0.049	0.948	0.487	0.102
72	0.058	0.046	0.791	0.442	0.104	0.051	0.044	0.861	0.463	0.094
89	0.054	0.045	0.842	0.457	0.099	0.054	0.051	0.940	0.485	0.104
90	0.055	0.047	0.851	0.460	0.102	0.051	0.046	0.916	0.478	0.097
113	0.054	0.046	0.847	0.459	0.100	0.054	0.045	0.830	0.453	0.099
114	0.057	0.047	0.820	0.450	0.104	0.050	0.044	0.870	0.465	0.094
119	0.053	0.045	0.853	0.460	0.099	0.053	0.049	0.928	0.481	0.102
120	0.055	0.047	0.847	0.459	0.102	0.050	0.046	0.919	0.479	0.096
131	0.054	0.046	0.860	0.462	0.100	0.054	0.051	0.943	0.485	0.106
132	0.056	0.044	0.789	0.441	0.101	0.051	0.045	0.884	0.469	0.097
137	0.055	0.045	0.818	0.450	0.100	0.054	0.048	0.885	0.470	0.102
138	0.056	0.046	0.823	0.451	0.102	0.050	0.042	0.840	0.457	0.093
155	0.055	0.044	0.798	0.444	0.099	0.054	0.048	0.889	0.471	0.101
156	0.057	0.047	0.826	0.452	0.104	0.050	0.045	0.892	0.471	0.095
179	0.054	0.045	0.834	0.455	0.098	0.053	0.049	0.929	0.481	0.102
180	0.057	0.048	0.843	0.457	0.105	0.051	0.047	0.917	0.478	0.097
185	0.054	0.045	0.826	0.452	0.099	0.053	0.048	0.911	0.477	0.101
186	0.058	0.046	0.794	0.443	0.104	0.050	0.044	0.867	0.464	0.094
197	0.053	0.043	0.819	0.450	0.096	0.053	0.044	0.833	0.454	0.097
198	0.057	0.046	0.805	0.446	0.103	0.050	0.045	0.898	0.473	0.094
203	0.054	0.045	0.840	0.457	0.099	0.052	0.050	0.954	0.488	0.102
204	0.057	0.043	0.745	0.427	0.100	0.050	0.043	0.863	0.463	0.093

Event #	Position 1					Position 4				
	ε_{loaded}	$\varepsilon_{unloaded}$	LTE(σ)	LTE(S)	Sum	ε_{loaded}	$\varepsilon_{unloaded}$	LTE(σ)	LTE(S)	Sum
221	0.054	0.044	0.806	0.446	0.098	0.053	0.047	0.876	0.467	0.100
222	0.058	0.043	0.737	0.424	0.101	0.050	0.044	0.880	0.468	0.094
247	0.054	0.044	0.819	0.450	0.098	0.053	0.045	0.850	0.460	0.098
248	0.056	0.043	0.773	0.436	0.099	0.050	0.042	0.842	0.457	0.092
253	0.053	0.043	0.822	0.451	0.096	0.052	0.043	0.822	0.451	0.095
254	0.056	0.043	0.776	0.437	0.099	0.050	0.043	0.868	0.465	0.093
265	0.052	0.042	0.815	0.449	0.095	0.052	0.043	0.829	0.453	0.094
266	0.054	0.043	0.792	0.442	0.098	0.048	0.042	0.874	0.467	0.089

TABLE 3b: Strains in mils and stress based LTE of MRC south transverse joint TJ2

Event #	Position 1					Position 4				
	ε_{loaded}	$\varepsilon_{unloaded}$	LTE(σ)	LTE(S)	Sum	ε_{loaded}	$\varepsilon_{unloaded}$	LTE(σ)	LTE(S)	Sum
5	0.061	0.043	0.709	0.415	0.104	0.056	0.057	1.006	0.501	0.113
6	0.054	0.054	1.003	0.501	0.107	0.064	0.042	0.660	0.398	0.106
23	0.059	0.048	0.808	0.447	0.108	0.058	0.058	1.000	0.500	0.115
24	0.054	0.048	0.885	0.470	0.101	0.061	0.043	0.701	0.412	0.104
47	0.058	0.047	0.804	0.446	0.105	0.058	0.057	0.987	0.497	0.115
48	0.053	0.058	1.083	0.520	0.111	0.060	0.039	0.655	0.396	0.099
53	0.058	0.046	0.792	0.442	0.104	0.058	0.053	0.901	0.474	0.111
54	0.054	0.044	0.819	0.450	0.098	0.061	0.037	0.617	0.382	0.098
65	0.058	0.043	0.747	0.428	0.101	0.058	0.053	0.912	0.477	0.111
66	0.053	0.054	1.025	0.506	0.107	0.061	0.037	0.606	0.377	0.098
71	0.059	0.043	0.737	0.424	0.102	0.058	0.037	0.632	0.387	0.095
72	0.058	0.044	0.768	0.434	0.102	0.061	0.036	0.580	0.367	0.097
113	0.058	0.042	0.725	0.420	0.100	0.056	0.040	0.708	0.415	0.096
114	0.057	0.045	0.791	0.442	0.101	0.060	0.038	0.630	0.386	0.098
119	0.058	0.043	0.741	0.426	0.100	0.056	0.037	0.667	0.400	0.094
120	0.056	0.046	0.813	0.448	0.102	0.059	0.036	0.606	0.377	0.095
131	0.056	0.039	0.688	0.408	0.095	0.056	0.041	0.723	0.420	0.097
132	0.055	0.037	0.663	0.399	0.092	0.061	0.034	0.551	0.355	0.095
137	0.056	0.040	0.711	0.415	0.096	0.058	0.049	0.854	0.461	0.107
138	0.051	0.052	1.010	0.502	0.103	0.059	0.035	0.598	0.374	0.094
155	0.057	0.042	0.728	0.421	0.099	0.057	0.051	0.902	0.474	0.108

Event #	Position 1					Position 4				
	ε_{loaded}	$\varepsilon_{unloaded}$	LTE(σ)	LTE(S)	Sum	ε_{loaded}	$\varepsilon_{unloaded}$	LTE(σ)	LTE(S)	Sum
156	0.050	0.048	0.950	0.487	0.098	0.059	0.038	0.642	0.391	0.096
179	0.057	0.036	0.639	0.390	0.093	0.055	0.044	0.799	0.444	0.099
180	0.050	0.048	0.949	0.487	0.098	0.059	0.035	0.599	0.375	0.094
185	0.056	0.040	0.712	0.416	0.096	0.054	0.050	0.920	0.479	0.104
186	0.049	0.048	0.967	0.491	0.097	0.057	0.036	0.625	0.385	0.093
197	0.055	0.037	0.668	0.400	0.092	0.053	0.041	0.778	0.438	0.095
198	0.050	0.042	0.850	0.459	0.092	0.057	0.034	0.591	0.371	0.091
203	0.055	0.036	0.648	0.393	0.091	0.054	0.042	0.781	0.438	0.096
204	0.049	0.047	0.951	0.487	0.096	0.057	0.034	0.607	0.378	0.091
221	0.055	0.038	0.680	0.405	0.093	0.054	0.048	0.888	0.470	0.102
222	0.050	0.046	0.924	0.480	0.095	0.057	0.033	0.575	0.365	0.089
247	0.055	0.038	0.681	0.405	0.093	0.053	0.048	0.898	0.473	0.101
248	0.049	0.050	1.021	0.505	0.099	0.056	0.035	0.630	0.386	0.091
253	0.054	0.037	0.677	0.404	0.090	0.053	0.041	0.779	0.438	0.094
254	0.048	0.049	1.019	0.505	0.097	0.056	0.036	0.638	0.389	0.092
265	0.054	0.036	0.664	0.399	0.089	0.051	0.045	0.881	0.468	0.096
266	0.048	0.045	0.944	0.486	0.093	0.055	0.035	0.640	0.390	0.090

TABLE 4a: Strains in mils and stress based LTE of MRG south transverse joint TJ1

Event #	Position 1					Position 4				
	ε_{loaded}	$\varepsilon_{unloaded}$	LTE(σ)	LTE(S)	Sum	ε_{loaded}	$\varepsilon_{unloaded}$	LTE(σ)	LTE(S)	Sum
14091	0.052	0.040	0.771	0.440	0.093	0.043	0.051	1.192	0.540	0.094
14092	0.047	0.040	0.855	0.460	0.087	0.047	0.044	0.940	0.480	0.091
14109	0.052	0.039	0.753	0.430	0.091	0.042	0.052	1.229	0.550	0.094
14110	0.047	0.043	0.914	0.480	0.090	0.046	0.046	0.985	0.500	0.092
14133	0.052	0.037	0.716	0.420	0.089	0.042	0.046	1.089	0.520	0.087
14134	0.047	0.038	0.794	0.440	0.085	0.047	0.042	0.905	0.480	0.089
14139	0.051	0.037	0.727	0.420	0.089	0.041	0.044	1.068	0.520	0.085
14140	0.047	0.039	0.835	0.460	0.086	0.047	0.044	0.941	0.480	0.090
14151	0.051	0.038	0.740	0.430	0.089	0.042	0.047	1.122	0.530	0.089
14152	0.046	0.040	0.862	0.460	0.086	0.046	0.042	0.912	0.480	0.088
14157	0.052	0.040	0.780	0.438	0.092	0.042	0.051	1.219	0.549	0.093
14158	0.046	0.039	0.861	0.463	0.085	0.046	0.040	0.870	0.465	0.087

Event #	Position 1					Position 4				
	ε_{loaded}	$\varepsilon_{unloaded}$	LTE(σ)	LTE(S)	Sum	ε_{loaded}	$\varepsilon_{unloaded}$	LTE(σ)	LTE(S)	Sum
14175	0.050	0.038	0.756	0.430	0.088	0.041	0.045	1.105	0.525	0.086
14176	0.044	0.038	0.858	0.462	0.082	0.046	0.042	0.900	0.474	0.088
14199	0.049	0.035	0.715	0.417	0.084	0.041	0.039	0.949	0.487	0.079
14200	0.044	0.038	0.852	0.460	0.082	0.046	0.042	0.909	0.476	0.087
14205	0.050	0.038	0.756	0.430	0.088	0.040	0.044	1.087	0.521	0.084
14206	0.045	0.039	0.879	0.468	0.084	0.046	0.040	0.862	0.463	0.085
14217	0.050	0.037	0.733	0.423	0.086	0.040	0.041	1.038	0.509	0.081
14218	0.045	0.039	0.881	0.468	0.084	0.046	0.040	0.867	0.464	0.086
14223	0.049	0.034	0.697	0.411	0.084	0.040	0.039	0.987	0.497	0.079
14224	0.045	0.038	0.859	0.462	0.083	0.046	0.040	0.876	0.467	0.086
14241	0.049	0.035	0.704	0.413	0.084	0.040	0.039	0.973	0.493	0.078
14242	0.045	0.040	0.895	0.472	0.085	0.046	0.042	0.909	0.476	0.087
14265	0.049	0.035	0.718	0.418	0.085	0.040	0.045	1.145	0.534	0.085
14266	0.045	0.037	0.822	0.451	0.083	0.045	0.040	0.900	0.474	0.085
14271	0.050	0.033	0.667	0.400	0.083	0.040	0.041	1.022	0.505	0.080
14272	0.045	0.039	0.849	0.459	0.084	0.045	0.040	0.884	0.469	0.085
14283	0.051	0.036	0.711	0.416	0.087	0.039	0.044	1.133	0.531	0.084
14284	0.045	0.039	0.858	0.462	0.084	0.045	0.042	0.928	0.481	0.087
14289	0.050	0.035	0.690	0.408	0.085	0.039	0.043	1.096	0.523	0.083
14290	0.045	0.042	0.926	0.481	0.087	0.045	0.042	0.922	0.480	0.087
14307	0.051	0.036	0.705	0.414	0.087	0.040	0.046	1.139	0.532	0.086
14308	0.045	0.036	0.787	0.440	0.081	0.045	0.041	0.916	0.478	0.087
14331	0.051	0.035	0.691	0.409	0.086	0.039	0.046	1.167	0.538	0.085
14332	0.046	0.038	0.831	0.454	0.085	0.045	0.043	0.961	0.490	0.088
14337	0.051	0.036	0.702	0.413	0.087	0.040	0.045	1.136	0.532	0.084
14338	0.046	0.042	0.897	0.473	0.088	0.045	0.042	0.944	0.486	0.087
14349	0.051	0.038	0.738	0.425	0.089	0.039	0.051	1.330	0.571	0.090
14350	0.046	0.034	0.744	0.426	0.080	0.045	0.039	0.868	0.465	0.084

TABLE 4b: Strains in mils and stress based LTE of MRG south transverse joint TJ2

Event #	Position 1					Position 4				
	ε_{loaded}	$\varepsilon_{unloaded}$	LTE(σ)	LTE(S)	Sum	ε_{loaded}	$\varepsilon_{unloaded}$	LTE(σ)	LTE(S)	Sum
14091	0.052	0.038	0.717	0.417	0.090	0.040	0.048	1.185	0.542	0.088
14092	0.044	0.045	1.006	0.501	0.089	0.048	0.042	0.881	0.468	0.090
14109	0.053	0.039	0.750	0.428	0.092	0.040	0.054	1.345	0.574	0.094
14110	0.045	0.043	0.964	0.491	0.088	0.046	0.041	0.907	0.475	0.087
14133	0.053	0.032	0.600	0.375	0.085	0.034	0.048	1.395	0.583	0.082
14134	0.045	0.039	0.861	0.463	0.084	0.046	0.041	0.882	0.469	0.087
14139	0.054	0.038	0.708	0.414	0.092	0.041	0.047	1.127	0.530	0.088
14140	0.045	0.042	0.941	0.485	0.087	0.048	0.044	0.912	0.477	0.091
14151	0.054	0.036	0.672	0.402	0.090	0.040	0.046	1.154	0.536	0.086
14152	0.045	0.045	0.992	0.498	0.090	0.047	0.042	0.897	0.473	0.089
14157	0.054	0.036	0.660	0.397	0.090	0.045	0.040	0.892	0.471	0.085
14158	0.055	0.037	0.678	0.404	0.092	0.046	0.042	0.908	0.476	0.088
14175	0.054	0.037	0.690	0.408	0.090	0.044	0.042	0.940	0.485	0.086
14176	0.055	0.036	0.660	0.397	0.091	0.046	0.039	0.866	0.464	0.085
14199	0.053	0.035	0.652	0.395	0.088	0.046	0.041	0.896	0.473	0.086
14200	0.055	0.034	0.618	0.382	0.088	0.045	0.042	0.930	0.482	0.087
14205	0.054	0.034	0.636	0.389	0.088	0.060	0.050	0.830	0.454	0.109
14206	0.062	0.037	0.596	0.373	0.099	0.045	0.041	0.895	0.472	0.086
14217	0.053	0.037	0.697	0.411	0.090	0.058	0.048	0.829	0.453	0.106
14218	0.061	0.041	0.668	0.401	0.102	0.045	0.040	0.898	0.473	0.085
14223	0.053	0.033	0.629	0.386	0.087	0.037	0.048	1.279	0.561	0.085
14224	0.045	0.037	0.842	0.457	0.082	0.045	0.041	0.901	0.474	0.086
14241	0.053	0.035	0.654	0.395	0.088	0.038	0.048	1.257	0.557	0.086
14242	0.044	0.040	0.913	0.477	0.085	0.046	0.039	0.855	0.461	0.085
14265	0.053	0.032	0.601	0.375	0.085	0.038	0.042	1.107	0.525	0.079
14266	0.044	0.036	0.814	0.449	0.080	0.044	0.042	0.954	0.488	0.085
14271	0.053	0.030	0.571	0.364	0.084	0.037	0.048	1.292	0.564	0.086
14272	0.045	0.041	0.913	0.477	0.085	0.044	0.040	0.912	0.477	0.084
14283	0.053	0.035	0.659	0.397	0.088	0.038	0.048	1.258	0.557	0.087
14284	0.044	0.038	0.872	0.466	0.082	0.044	0.039	0.888	0.470	0.083
14289	0.053	0.033	0.630	0.387	0.087	0.037	0.047	1.254	0.556	0.084
14290	0.044	0.042	0.961	0.490	0.086	0.044	0.041	0.936	0.484	0.085
14307	0.053	0.033	0.617	0.381	0.086	0.038	0.046	1.198	0.545	0.084
14308	0.044	0.035	0.789	0.441	0.079	0.043	0.038	0.891	0.471	0.081
14331	0.052	0.032	0.609	0.378	0.084	0.037	0.041	1.119	0.528	0.078

Event #	Position 1					Position 4				
	ε_{loaded}	$\varepsilon_{unloaded}$	LTE(σ)	LTE(S)	Sum	ε_{loaded}	$\varepsilon_{unloaded}$	LTE(σ)	LTE(S)	Sum
14332	0.044	0.035	0.796	0.443	0.079	0.043	0.039	0.925	0.480	0.082
14337	0.053	0.035	0.660	0.397	0.087	0.036	0.048	1.332	0.571	0.084
14338	0.044	0.035	0.796	0.443	0.079	0.044	0.039	0.881	0.468	0.083
14349	0.053	0.036	0.676	0.403	0.089	0.039	0.049	1.256	0.557	0.087
14350	0.044	0.042	0.956	0.489	0.086	0.046	0.039	0.860	0.462	0.085

TABLE 5: Strains in mils and stress based LTE of MRS south transverse joints TJ1

Event #	Position 1					Position 4				
	ε_{loaded}	$\varepsilon_{unloaded}$	LTE(σ)	LTE(S)	Sum	ε_{loaded}	$\varepsilon_{unloaded}$	LTE(σ)	LTE(S)	Sum
14091	0.050	0.047	0.948	0.487	0.097	0.055	0.046	0.827	0.453	0.101
14092	0.056	0.045	0.800	0.444	0.100	0.048	0.047	0.979	0.495	0.095
14109	0.051	0.048	0.944	0.486	0.099	0.055	0.052	0.938	0.484	0.107
14110	0.055	0.044	0.794	0.443	0.100	0.046	0.046	0.994	0.498	0.093
14133	0.052	0.043	0.824	0.452	0.094	0.053	0.050	0.948	0.487	0.104
14134	0.055	0.048	0.872	0.466	0.104	0.047	0.049	1.046	0.511	0.096
14139	0.052	0.051	0.975	0.494	0.103	0.054	0.049	0.902	0.474	0.103
14140	0.056	0.047	0.846	0.458	0.103	0.046	0.050	1.081	0.520	0.096
14151	0.052	0.043	0.825	0.452	0.095	0.053	0.038	0.722	0.419	0.091
14152	0.056	0.047	0.831	0.454	0.103	0.046	0.046	1.003	0.501	0.093
14223	0.053	0.045	0.855	0.461	0.098	0.053	0.046	0.859	0.462	0.099
14224	0.056	0.045	0.799	0.444	0.101	0.044	0.047	1.078	0.519	0.091
14241	0.053	0.043	0.812	0.448	0.096	0.053	0.050	0.954	0.488	0.103
14242	0.057	0.042	0.740	0.425	0.098	0.046	0.047	1.016	0.504	0.094
14265	0.053	0.048	0.912	0.477	0.101	0.053	0.046	0.860	0.462	0.099
14266	0.056	0.047	0.833	0.454	0.103	0.043	0.050	1.171	0.539	0.093
14271	0.053	0.040	0.753	0.430	0.092	0.052	0.043	0.826	0.452	0.094
14272	0.057	0.040	0.713	0.416	0.097	0.045	0.050	1.094	0.522	0.095
14283	0.052	0.044	0.852	0.460	0.096	0.053	0.045	0.860	0.462	0.098
14284	0.057	0.039	0.686	0.407	0.096	0.042	0.051	1.206	0.547	0.093

Strain gages located along the north carriage joints were also analyzed for MRC and MRS. Table 6a and 6b contains the average LTE (S) values for the two north transverse joints TJ3 and TJ4 as shown in figure 11 for first 20 events (Track 0) of trafficking MRC. TJ3 is the first joint and TJ4 is the second joint (equipped with concrete strain gages)

intercepted as the vehicle moves from west to east over the south carriage. It is important to note that MRC north carriage was loaded with a modified wander pattern and using a 4-wheel configuration. The average LTE (S) for MRC north carriage was found to be 0.47.

MRS North carriage was loaded with a 6 wheel configuration as shown in figure 9. The LTE (S) values under 6-wheel loading for MRS are tabulated in table 7. Only strain responses in wheel position 1 and position 2 (figure 2) were considered in this analysis. Vehicle passes from west to east (W to E) as well as east to west (E to W) were considered. The average LTE (S) under moving 6-wheel load was found to be 0.46 for MRS which is almost same as that obtained under moving 4-wheel load for MRS.

Position1 Position 2

FIGURE 9: Position of wheels across the joint as test vehicle traverses the joint

TABLE 6a: Strains in mils and stress based LTE of MRC North transverse joint TJ3

Event #	Position 1					Position 2				
	ε_{loaded}	$\varepsilon_{unloaded}$	LTE(σ)	LTE(S)	Sum	ε_{loaded}	$\varepsilon_{unloaded}$	LTE(σ)	LTE(S)	Sum
1394	0.055	0.044	0.802	0.445	0.098	0.055	0.044	0.802	0.445	0.098
1395	0.057	0.045	0.787	0.440	0.103	0.048	0.048	1.019	0.505	0.096
1404	0.055	0.046	0.842	0.457	0.101	0.055	0.046	0.832	0.454	0.100
1405	0.058	0.048	0.832	0.454	0.107	0.049	0.049	0.999	0.500	0.097
1412	0.056	0.049	0.875	0.467	0.105	0.057	0.055	0.964	0.491	0.112
1413	0.060	0.048	0.801	0.445	0.107	0.050	0.052	1.045	0.511	0.102
1420	0.057	0.047	0.827	0.453	0.104	0.057	0.049	0.856	0.461	0.106
1421	0.060	0.049	0.808	0.447	0.109	0.049	0.052	1.052	0.513	0.101
1426	0.057	0.049	0.856	0.461	0.106	0.058	0.056	0.978	0.495	0.114

Event #	Position 1					Position 2				
	ε_{loaded}	$\varepsilon_{unloaded}$	LTE(σ)	LTE(S)	Sum	ε_{loaded}	$\varepsilon_{unloaded}$	LTE(σ)	LTE(S)	Sum
1427	0.062	0.053	0.854	0.461	0.114	0.052	0.054	1.043	0.510	0.105
1442	0.060	0.052	0.872	0.466	0.112	0.060	0.058	0.965	0.491	0.118
1443	0.062	0.052	0.839	0.456	0.113	0.053	0.052	0.982	0.496	0.105
1450	0.060	0.053	0.887	0.470	0.113	0.060	0.057	0.954	0.488	0.117
1451	0.062	0.047	0.755	0.430	0.109	0.053	0.052	0.988	0.497	0.105
1458	0.061	0.047	0.775	0.437	0.108	0.060	0.051	0.841	0.457	0.111
1459	0.062	0.050	0.794	0.442	0.112	0.053	0.051	0.947	0.486	0.104
1464	0.057	0.044	0.774	0.436	0.101	0.058	0.049	0.838	0.456	0.107
1465	0.061	0.053	0.880	0.468	0.114	0.052	0.048	0.937	0.484	0.100

TABLE 6b: Strains in mils and stress based LTE of MRC North transverse joint TJ4

Event #	Position 1					Position 2				
	ε_{loaded}	$\varepsilon_{unloaded}$	LTE(σ)	LTE(S)	Sum	ε_{loaded}	$\varepsilon_{unloaded}$	LTE(σ)	LTE(S)	Sum
1394	0.053	0.042	0.792	0.442	0.095	0.056	0.057	1.006	0.501	0.113
1395	0.054	0.054	1.003	0.501	0.107	0.050	0.047	0.935	0.483	0.096
1404	0.053	0.045	0.854	0.461	0.098	0.052	0.055	1.064	0.516	0.107
1405	0.059	0.048	0.818	0.450	0.107	0.051	0.051	1.007	0.502	0.102
1412	0.054	0.046	0.855	0.461	0.100	0.058	0.057	0.988	0.497	0.115
1413	0.053	0.058	1.083	0.520	0.111	0.051	0.050	0.979	0.495	0.102
1420	0.054	0.044	0.816	0.449	0.098	0.053	0.058	1.083	0.520	0.111
1421	0.060	0.047	0.785	0.440	0.107	0.051	0.049	0.947	0.487	0.100
1426	0.055	0.046	0.838	0.456	0.101	0.053	0.057	1.071	0.517	0.110
1427	0.060	0.052	0.866	0.464	0.113	0.053	0.051	0.955	0.489	0.103
1432	0.053	0.042	0.782	0.439	0.095	0.052	0.053	1.025	0.506	0.105
1433	0.060	0.051	0.850	0.459	0.111	0.052	0.050	0.978	0.494	0.102
1442	0.056	0.047	0.845	0.458	0.104	0.054	0.053	0.970	0.492	0.107
1443	0.061	0.050	0.821	0.451	0.111	0.053	0.048	0.897	0.473	0.101
1450	0.056	0.043	0.765	0.433	0.098	0.057	0.051	0.896	0.473	0.107
1451	0.051	0.049	0.946	0.486	0.100	0.054	0.053	0.971	0.493	0.107
1458	0.056	0.043	0.769	0.435	0.100	0.055	0.057	1.048	0.512	0.112
1459	0.061	0.053	0.868	0.465	0.114	0.055	0.052	0.945	0.486	0.106
1464	0.054	0.041	0.758	0.431	0.094	0.052	0.055	1.060	0.514	0.107
1465	0.060	0.056	0.933	0.483	0.116	0.052	0.050	0.956	0.489	0.102

TABLE 7: Strains in mils and stress based LTE of MRS North transverse joints under 6-wheel loading

TJ3 Event #	Position 1					Position 2				
	ε_{loaded}	$\varepsilon_{unloaded}$	LTE(σ)	LTE(S)	Sum	ε_{loaded}	$\varepsilon_{unloaded}$	LTE(σ)	LTE(S)	Sum
14091	0.063	0.043	0.694	0.410	0.106	0.056	0.049	0.868	0.465	0.105
14092	0.065	0.048	0.739	0.425	0.113	0.055	0.046	0.837	0.456	0.101
14109	0.064	0.045	0.699	0.412	0.108	0.057	0.047	0.829	0.453	0.105
14110	0.066	0.049	0.742	0.426	0.116	0.057	0.045	0.787	0.441	0.102
14133	0.064	0.044	0.689	0.408	0.109	0.058	0.057	0.993	0.498	0.115
14134	0.066	0.045	0.679	0.405	0.111	0.057	0.042	0.732	0.423	0.099
14139	0.064	0.042	0.652	0.395	0.106	0.057	0.054	0.935	0.484	0.111
14140	0.066	0.048	0.735	0.423	0.114	0.058	0.043	0.750	0.428	0.101
14151	0.064	0.044	0.692	0.409	0.108	0.057	0.056	0.977	0.494	0.114
14152	0.066	0.047	0.712	0.416	0.113	0.058	0.043	0.750	0.428	0.101
TJ4 Event #	Position 1					Position 2				
	ε_{loaded}	$\varepsilon_{unloaded}$	LTE(σ)	LTE(S)	Sum	ε_{loaded}	$\varepsilon_{unloaded}$	LTE(σ)	LTE(S)	Sum
14091	0.059	0.055	0.939	0.484	0.114	0.065	0.058	0.897	0.473	0.123
14092	0.061	0.059	0.982	0.496	0.120	0.065	0.048	0.745	0.427	0.113
14109	0.057	0.052	0.909	0.476	0.109	0.067	0.057	0.850	0.459	0.124
14110	0.062	0.059	0.955	0.488	0.121	0.064	0.049	0.773	0.436	0.113
14133	0.054	0.056	1.029	0.507	0.110	0.069	0.049	0.712	0.416	0.117
14134	0.059	0.063	1.068	0.516	0.122	0.064	0.048	0.750	0.428	0.112
14139	0.055	0.061	1.106	0.525	0.116	0.069	0.051	0.742	0.426	0.121
14140	0.059	0.058	0.990	0.497	0.117	0.065	0.049	0.750	0.429	0.113
14151	0.055	0.058	1.047	0.511	0.113	0.071	0.053	0.741	0.425	0.124
14152	0.059	0.061	1.029	0.507	0.119	0.068	0.050	0.732	0.423	0.117

From the above tables, it becomes clear that the sum of loaded and unloaded stresses is almost the same irrespective of the pavement layer configuration. No significant variation in the strain values on the loaded and unloaded slabs were observed. The above finding demonstrates that the stresses in PCC slab are less governed by the pavement layers or presence of base (stabilized/ un-stabilized) as long as the thickness of PCC slab

and loading parameters remain the same. Moreover, the sum of strains on either sides of the joint was similar for MRC and MRS. Average sum of strains in the slabs on two sides of a joint (for south transverse joints) was 0.099 for MRC, 0.086 for MRG and 0.098 for MRS which was similar as anticipated for a flat slab condition.

3.3 Summary

The analysis of concrete strain gage data was described in this chapter. Thus an average value of LTE (S) under a moving wheel load (about 47%) was obtained from full scale testing during CC2 at NAPTF. The next chapter presents the analysis of FWD data collected during CC2.

CHAPTER 4

Falling Weight Deflectometer Data Analysis

4.1 Introduction

Periodic heavy weight deflectometer (HWD) testing, using a KUAB model 240, was carried out on CC2 test items with an objective of investigation material properties and track the pavement deterioration concurrent to trafficking (Ricalde 2007). The first among the series was primarily aimed at determining back-calculation of layer properties which was conducted before loading the pavement. Deflection data from HWD tests conducted at NAPTF was analyzed to compute the ratio of deflections and determine LTE (δ) of transverse joints. This chapter gives the details of nature of raw HWD data and computation of LTE (δ).

4.2 Background of FWD data analysis from CC1

From a past study (Guo and Marsey 2001) on CC1 at NAPTF, it has been found from the FWD data that the calculated [LTE (δ)] could be very different when the FWD loading is applied on both sides of the joints, indicating that LTE (δ) may be sensitive to the traffic direction. However, the sum of above two deflections (SDs) still remains almost the same for both traffic directions. It was also found that the SDs varied significantly from summer to winter, or it is sensitive to the curling state of the slab.

As mentioned earlier, the longitudinal joints at CC1 were dowelled while the transverse joints were saw-cut. Figure 10 shows details of a dowelled and saw cut joint. The FWD testing was conducted at both longitudinal as well as transverse joints in June 1999 and

October 1999 during CC1 for LRS, MRS and HRS. Comparison of loaded side deflections (deflection under FWD load) indicated that the mean loaded deflections at transverse and longitudinal joints were similar. This was attributed to the fact that joint had not been completely cracked at that time. However, all loaded deflection values measured in October and later were much larger than the values observed in June. The difference between the loaded deflection values in June and October was greater for transverse joints than for longitudinal joints. This finding supported the fact that dowelled joints provide relatively better load transfer especially in winter after the joints are cracked.

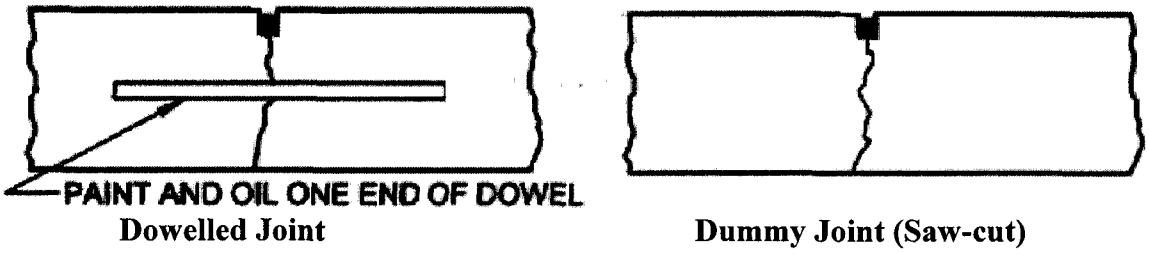

FIGURE 10: Typical details of a dowelled and saw-cut contraction joint

The corners of the CC1 pavement were also tested and the deflection values under the FWD load-plate were found to be higher than those at the joints. In winter, this difference became more significant indicating the different degree of slab curling. In addition, highest curling was observed for HRS (strongest subgrade). Comparison of LTE (δ) indicated that load transfer across transverse joints (saw-cut) was higher or equal to those of the longitudinal joints (dowelled) for testing done in June. However, for testing done in October, the LTE (δ) was much lower as compared to that in June and the difference was more significant for the saw-cut joints. It was believed that the lower temperature from October caused all joints to be cracked which significantly reduced the load transfer capability for the transverse joints (saw-cut) while the load transfer capability of the longitudinal joints were still relatively high through the dowels.

Hammons et al. (1995) suggests the use of following formula for a two-slab system from the theory of statics.

$$\delta_{loaded} + \delta_{unloaded} = \delta_e \qquad (4.1)$$

Where δe is the load induced deflection at a joint edge when the joint load transfer capability is zero. It is often called the free edge deflection. The above equation can also be extended to bending stresses on the loaded and unloaded side of a joint which is shown below.

$$\sigma_{loaded} + \sigma_{unloaded} = \sigma_e \quad (4.2)$$

Where σ_{loaded}, $\sigma u_{nloaded}$, σ_e are the maximum bending stresses in the loaded slab, unloaded slab and at the free edge respectively. The above relationships have been theoretically proved in Guo (2003) and it is further mentioned that the relation is true only for flat slab condition. The analysis of FWD data from CC1 at NAPTF indicated that the measured sum of two deflections (SD) on two sides of dummy joints increase proportionally to the slab curling but were insensitive to the joint LTE (δ) (Guo, 2001). In addition, although the values of LTE (δ) were found to be significantly different in two directions across the joints, the values of SD varied much less. The SD was found to be sensitive only to curling of slabs. Higher SDs was observed for slabs with higher curling which was for HRS in case of CC1.

A 2D-Finite Element (FE) computer program JSLAB 92 (Tayabji, 1986; Guo, 1995) with the capability of considering temperature effects and non-linear elastic behavior was used to analyze the parameter SD. For no curling case (temperature gradient = 0), SD was found to be independent of joint stiffness and always equals the free edge deflection. Both SD and loaded side deflection increased as the temperature gradient increased and the SD were always greater than the free edge deflection.

In this study, data from CC2 is analyzed to understand the importance of parameter SD in addition to computation of LTE (δ) of joints. The next section covers the details of FWD data analysis from CC2.

4.3 FWD data analysis from CC2

The preliminary approach was to import the raw data into a spreadsheet and filter the data for the highest load drop and locations. In addition, slab centre locations were also

recorded for back calculation of subgrade modulus. The slabs were numbered sequentially from west to east starting from north-west corner of MRC and ending with south-east corner of MRS. Thus the slabs were tagged with number 1 to 20 for MRC, 21 to 40 for MRG and 41 to 60 for MRS. Figure 11 shows the numbering of slabs for all three test items in MRC/MRG/MRS format. The first test among the series of HWD tests was primarily directed for back-calculation of layer properties which was conducted before loading the pavement. In this paper, only the first HWD test program is analyzed. Testing was carried out at longitudinal joints, transverse joints and slab center locations. Proper curing and quality control of the CC2 test items was conducted and curling was almost negligible (Hayhoe, 2004). Table 8 summarizes the loaded and unloaded deflections with LTE (δ) and SD computation for MRC. The drop locations are denoted by a specific code comprising of Joint (longitudinal or transverse)/ Slab number. For example, L/4 indicates that the load is dropped at the center of longitudinal joint on the slab number 4. Similarly, T/28 would indicate that the load is dropped at the center of transverse joint with slab number 28. The remark column indicates the direction of load transfer: East to West (E to W) or West to East (W to E) for transverse joint and North to South (N to S) or South to North (S to N) for longitudinal joints.

	1/21/41	2/22/42	3/23/43	4/24/44	5/25/45
North Carriage	6/26/46	7/27/47 **TJ3**	8/28/48	9/29/49 **TJ4**	10/30/50
	11/31/51	12/32/52 **TJ1**	13/33/53	14/34/54 **TJ2**	15/35/55
South Carriage	16/36/56	17/37/57	18/38/58	19/39/59	20/40/60

FIGURE 11: Typical plan view of CC2 test items with slab numbers

TABLE 8: Results of HWD data analysis for test item MRC

Drop Location	Drop weight (lbs)	Loaded Deflection (mils)	Unloaded Deflection (mils)	LTE (δ)	Remark	SD (mils)	Ratio of high to low values	
TRANSVERSE JOINTS							LTE	SD
T/10	36821	14.54	12.04	0.83	E to W	26.58	1.04	1.02
T/9	37066	14.48	12.56	0.86	W to E	27.04		
T/9	36859	15.30	12.57	0.82	E to W	27.87	1.00	1.03
T/8	36732	15.85	12.99	0.82	W to E	28.84		
T/8	36770	15.19	11.74	0.77	E to W	26.93	1.03	1.02
T/7	36872	15.25	12.10	0.79	W to E	27.35		
T/7	36795	15.30	12.18	0.79	E to W	27.48	1.08	1.01
T/6	36884	14.70	12.56	0.85	W to E	27.26		
T/15	37164	15.36	12.15	0.79	E to W	27.51	1.10	1.00
T/14	37075	14.70	12.83	0.87	W to E	27.53		
T/14	37037	15.47	11.99	0.76	E to W	27.46	1.09	1.00
T/13	37126	15.08	12.45	0.83	W to E	27.53		
T/13	37241	15.36	12.57	0.82	E to W	27.93	1.07	1.01
T/12	37164	14.92	13.15	0.88	W to E	28.07		
T/12	36859	16.89	13.04	0.77	E to W	29.93	1.01	1.02
T/11	36795	17.22	13.15	0.76	W to E	30.37		
LONGITUDINAL JOINTS								
L/4	36897	16.84	15.41	0.92	N to S	32.25	1.02	1.02
L/9	36681	16.95	16.01	0.94	S to N	32.96		
L/3	36858	16.35	15.36	0.94	N to S	31.71	1.01	1.03
L/8	36883	16.78	15.91	0.95	S to N	32.69		
L/2	36947	15.58	14.61	0.94	N to S	30.19	1.00	1.13
L/7	36566	17.50	16.47	0.94	S to N	33.97		
L/14	36693	16.84	15.96	0.95	N to S	32.80	1.03	1.05
L/19	36846	16.29	14.97	0.92	S to N	31.26		
L/13	36732	16.51	15.45	0.94	N to S	31.96	1.02	1.04
L/18	36668	17.39	15.96	0.92	S to N	33.35		
L/12	36770	18.10	16.74	0.92	N to S	34.84	1.01	1.10
L/17	36846	16.51	15.30	0.93	S to N	31.81		

From the above table the average LTE (δ) for transverse joints and longitudinal joints was computed to be 0.81 and 0.93 respectively. The average SD was 27.86 mils for transverse joints and 32.48 mils for longitudinal joints. The standard deviation of SD for transverse and longitudinal joints was 1.03 and 1.24 respectively. The coefficient of variation in SD was 3.69% and 3.82% for transverse and longitudinal joints respectively.

Table 9 summarizes the loaded and unloaded deflections with LTE (δ) and SD computation for MRG.

TABLE 9: Results of HWD data analysis for test item MRG

Drop Location	**Drop weight (lbs)**	**Loaded Deflection (mils)**	**Unloaded Deflection (mils)**	**LTE (δ)**	**Remark**	**SD (mils)**	**Ratio of high to low values**	
TRANSVERSE JOINTS							LTE	SD
T/30	36974	11.3	9.31	0.82	E to W	20.61	1.07	1.04
T/29	36910	11.41	9.99	0.88	W to E	21.40		
T/29	36897	11.41	9.61	0.84	E to W	21.02	1.03	1.01
T/28	36884	11.3	9.94	0.88	W to E	21.24		
T/28	36961	11.3	9.53	0.84	E to W	20.83	1.07	1.04
T/27	37025	11.13	9.99	0.90	W to E	21.12		
T/27	37063	11.19	9.67	0.86	E to W	20.86	1.03	1.03
T/26	37025	11.35	10.13	0.89	W to E	21.48		
T/35	37509	12.45	10.69	0.86	E to W	23.14	1.01	1.01
T/34	37305	12.62	10.78	0.85	W to E	23.40		
T/34	37292	12.12	9.56	0.79	E to W	21.68	1.11	1.04
T/33	37253	12.01	10.53	0.88	W to E	22.54		
T/33	37356	11.24	9.86	0.88	E to W	21.10	1.03	1.03
T/32	37202	11.74	9.97	0.85	W to E	21.71		
T/32	37228	11.9	10.14	0.85	E to W	22.04	1.05	1.03
T/31	37190	11.96	10.61	0.89	W to E	22.57		
LONGITUDINAL JOINTS								
L/24	36706	13.16	12.07	0.92	N to S	25.23	1.01	1.07
L/29	36719	12.23	11.42	0.93	S to N	23.65		
L/23	36896	12.29	11.16	0.91	N to S	23.45	1.03	1.08
L/28	36884	13.00	12.21	0.94	S to N	25.21		
L/22	36808	13.27	12.18	0.92	N to S	25.45	1.01	1.03
L/27	36921	12.78	11.88	0.93	S to N	24.66		
L/34	36884	14.32	13.12	0.92	N to S	27.44	1.02	1.10
L/39	36973	13.16	11.88	0.90	S to N	25.04		
L/33	37075	12.95	12.15	0.94	N to S	25.10	1.04	1.05
L/38	37024	13.77	12.46	0.90	S to N	26.23		
L/32	36795	14.04	12.83	0.91	N to S	26.87	1.01	1.08
L/37	36973	13.00	11.96	0.92	S to N	24.96		

From the above table the average LTE (δ) for transverse joints and longitudinal joints was computed to be 0.86 and 0.92 respectively. The average SD was 21.67 mils for transverse joints and 25.27 mils for longitudinal joints. The standard deviation of SD for transverse and longitudinal joints was 0.84 and 1.16 respectively. The coefficient of variation in SD was 3.88% and 4.59% for transverse and longitudinal joints respectively.

Table 10 summarizes the loaded and unloaded deflections with LTE (δ) and SD computation for MRS.

TABLE 10: Results of HWD data analysis for test item MRS

Drop Location	**Drop weight (lbs)**	**Loaded Deflection (mils)**	**Unloaded Deflection (mils)**	**LTE (δ)**	**Remark**	**SD (mils)**	**Ratio of high to low values**	
TRANSVERSE JOINTS							LTE	SD
T/50	36425	12.29	8.34	0.68	E to W	20.63	1.00	1.06
T/49	36361	13.00	8.78	0.68	W to E	21.78		
T/49	36208	12.45	9.06	0.73	E to W	21.51	1.16	1.02
T/48	36527	12.95	8.16	0.63	W to E	21.11		
T/48	36451	11.63	8.92	0.77	E to W	20.55	1.07	1.03
T/47	36489	12.34	8.83	0.72	W to E	21.17		
T/47	36540	13.49	8.09	0.60	E to W	21.58	1.15	1.04
T/46	36387	13.33	9.16	0.69	W to E	22.49		
T/55	36451	11.74	7.98	0.68	E to W	19.72	1.06	1.01
T/54	36515	11.57	8.34	0.72	W to E	19.91		
T/54	36541	11.85	8.76	0.74	E to W	20.61	1.04	1.03
T/53	36451	12.4	8.83	0.71	W to E	21.23		
T/53	36413	11.85	8.59	0.72	E to W	20.44	1.14	1.03
T/52	36451	11.63	9.48	0.82	W to E	21.11		
T/52	36337	13.22	8.53	0.65	E to W	21.75	1.02	1.05
T/51	36464	13.71	9.10	0.66	W to E	22.81		
LONGITUDINAL JOINTS								
L/44	36463	11.63	10.72	0.92	N to S	22.35	1.01	1.06
L/49	36630	12.23	11.37	0.93	S to N	23.60		
L/43	36591	12.23	11.27	0.92	N to S	23.50	1.00	1.04
L/48	36374	12.73	11.77	0.92	S to N	24.50		
L/42	36489	11.68	10.63	0.91	N to S	22.31	1.01	1.09
L/47	36335	12.67	11.61	0.92	S to N	24.28		
L/54	36553	11.35	10.59	0.93	N to S	21.94	1.03	1.06
L/59	36642	10.86	9.78	0.90	S to N	20.64		
L/53	36349	12.62	11.59	0.92	N to S	24.21	1.00	1.03
L/58	36426	12.29	11.27	0.92	S to N	23.56		
L/52	36553	12.12	11.45	0.94	N to S	23.57	1.02	1.08
L/57	36426	11.35	10.39	0.92	S to N	21.74		

From the above table the average LTE (δ) for transverse joints and longitudinal joints was computed to be 0.71 and 0.92 respectively. The average SD was 21.15 mils for transverse joints and 23.02 mils for longitudinal joints. The standard deviation of SD for transverse and longitudinal joints was 0.84 and 1.19 respectively. The coefficient of

variation in SD was 3.97 % and 5.17 % for transverse and longitudinal joints respectively.

The table also shows the ratio of high and low values of LTE (δ) and SD in two directions across a joint. An average value for the ratio of high to low values of LTE (δ) was 1.04, 1.04, 1.05 for MRC, MRG and MRS respectively indicating uniform load transfer in the two directions. However, the average ratios between high and low value of LTE (δ) for three test sections of construction cycle 1 (CC1) on low-strength subgrade, medium-strength subgrade and high-strength subgrade at NAPTF was 1.37, 1.67 and 1.47 respectively (Guo, 2001). The different behavior of CC2 and CC1 joints was due to different joint configurations. As mentioned before, transverse joints at CC2 were dowelled while CC1 joints were saw-cut. Thus the load transfer efficiency is sensitive to traffic direction for saw-cut joints but relatively insensitive for dowelled joints. Similarly, the value of high to low values of SD in two directions across the CC2 joints was determined to be 1.03, 1.05 and 1.05 for MRC, MRG and MRS respectively. Also, the variance in the values of parameter SD was very insignificant which can be anticipated for flat slabs as was the case for the CC2 test items. It is important to note that LTE (δ) and SD values for longitudinal joints were higher than those for transverse joints although the joint configuration was the same. Only, the average LTE (δ) of the transverse joints was considered in further analysis.

The average deflection based LTE for transverse joints of MRS was found to be the least and of the order 0.71 while that for MRG was found to be of highest value 0.86. The LTE (δ) for MRC was 0.81. This trend suggests that non stabilized base tends to increase load transfer as compared to identical joints on stabilized base. In general, non-stabilized bases allow greater deflections as compared to stabilized bases as thus the effect of aggregate interlock or dowels is likely to be greater on non-stabilized bases as compared to stabilized bases. This phenomena was also observed by (Hammons, 1995) in a study conducted at four different US airports.

Deflection data from center drop locations was also considered in the backcalculation of pavement parameters such as modulus of subgrade reaction (k) and elastic modulus of PCC layer using conventional methods (E_{PCC}). The backcalculated parameters were required as inputs for 2D finite element program JSLAB. Table 11 below summarizes the deflection data used for backcalculation pavement parameters. The deflection value directly under the loaded plate is denoted by d_0 and d_{12}, d_{24}, d_{36} are deflection values measured at a distance of 12 inches, 24 inches and 36 inches from the load center respectively. The backcalculation method used is explained in the subsequent chapter.

TABLE 11: HWD test data for slab center load drop locations

	MRS South	**MRS North**	**MRG South**	**MRG North**	**MRC South**	**MRC North**
Load P(lbs)	36566	36642	37133	37063	36896	36948
Slab Number	54	48	32	28	14	8
d_0 (mils)	8.34	8.39	9.65	9.27	10.7	10.31
d_{12} (mils)	7.83	7.78	8.91	8.64	9.97	9.59
d_{24} (mils)	6.87	6.98	7.84	7.51	8.81	8.51
d_{36} (mils)	6.08	6.17	6.74	6.55	7.71	7.46

4.4 Summary

The analysis of HWD data available in NAPTF database for the CC2 test items was described in this chapter. Values of deflection based load transfer efficiency were found to be similar when measured under a HWD or 4-wheel/ 6-wheel gear configuration and is lower for stabilized base as compared to similar configuration of joints over non-stabilized base. The value of LTE (δ) before trafficking started was 0.71 for MRS (stabilized base), 0.81 for MRC (conventional base), 0.86 for MRG (over subgrade). Moreover, it was observed that the LTE (δ) of longitudinal joints was much higher than that of the transverse joint in spite of the joint configuration being the same in both cases. Although, some amount of variation in joint load transfer efficiency was observed, the sum of deflection parameter almost remained a constant which was clear from significantly low coefficient of variation and as anticipated for a flat slab case. The strain

gages records indicated that the sum of strains on either sides of the joint also remained constant for the initial phases of trafficking analyzed in this research. Thus the importance of sum of deflections/ strains to estimate curling was also highlighted in this study.

CHAPTER 5

Input Parameters for 2D-FE Analysis Program

5.1 Introduction

This chapter describes the backcalculation procedure followed to estimate parameters of test items constructed during CC2 at NAPTF. The backcalculated parameters were required as inputs for 2D-Finite Element program JSLAB 2004. The primary input parameters include modulus of subgrade reaction (k) and modulus of elasticity of PCC layer (E_{PCC}). Three methods are described in this chapter for determination of the above mentioned input parameters.

5.2 Procedure described by K. Hall (1991)

K. Hall has described a simple and straightforward method to backcalculate the PCC layer modulii and liquid foundation modulus (k-value) using deflection data (Hall 1991). The k-value was determined for both, north as well as south slab using HWD data at slab center locations. This method assumes the PCC slab as an elastic plate that exhibits pure bending without shear deformation and the foundation as a bed of springs. The area of deflection basin from the maximum deflection is used to backcalulate the k-value as well as the PCC elastic modulus (E_{PCC}). Following equation is used to determine area of deflection basin.

$$A = 6 * \left[1 + 2\frac{d_{12}}{d_0} + 2\frac{d_{24}}{d_0} + \frac{d_{36}}{d_0}\right] \quad (5.1)$$

Where,

A= Area of deflection basin

D_n= Deflection in mils recorded at distance "n" inches from the center of the loading plate (n= 0, 12, 24 & 36)

The radius of relative stiffness (l_k) in inches for a dense liquid foundation is given by the following equation.

$$l_k = \left[\frac{\ln\left(\frac{36-A}{1812.279}\right)}{-2.559}\right]^{\frac{1}{0.228}} \quad (5.2)$$

With the area of deflection basin computed from equation 1 and radius of relative stiffness computed from equation 2, the k- value can be obtained from the following equation.

$$k = \left(\frac{P}{8\, d_o {l_k}^2}\right) \times \left\{1 + \left(\frac{1}{2\pi}\right)\left[\ln\left(\frac{a}{2l_k}\right) + \gamma - 1.25\right]\left(\frac{a}{l_k}\right)^2\right\} \quad (5.3)$$

Where,

P is applied load in lbs

a is the load radius in inches

π is Euler's constant whose value is 0.57721566490

Based on the above mentioned equations and using HWD deflection data for testing at slab centers tabulated in previous chapter, the computation of E_{PCC} k-value for various test items is shown in table 12.

TABLE 12: Results of back-calculation analysis by K.Hall (1991) method

	MRS South	**MRS North**	**MRG South**	**MRG North**	**MRC South**	**MRC North**
Load P(lbs)	36566	36642	37133	37063	36896	36948
d_0 (mils)	8.34	8.39	9.65	9.27	10.7	10.31
d_{12} (mils)	7.83	7.78	8.91	8.64	9.97	9.59
d_{24} (mils)	6.87	6.98	7.84	7.51	8.81	8.51
d_{36} (mils)	6.08	6.17	6.74	6.55	7.71	7.46
A	31.53	31.52	31.02	31.15	31.39	31.41
l_k (inches)	42.11	42.10	38.92	39.66	41.17	41.32
$E_{PCC}(10^6$ psi)	6.5	6.5	5.3	4.8	5.1	4.7
k (pci)	305.83	304.83	313.81	314.01	251.54	259.50

5.3 FAA Advisory Circular method

FAA Advisory Circular (1995) provides guideline curves to determine k-value based on layer thicknesses. The k-value for subgrade is first established based on subgrade CBR and then corrected for effects of base and subbase depending upon their thicknesses. The following equations were used to estimate the elastic modulus Esg in psi and further the modulus of subgrade reaction k in pci.

$$E_{sg} = 1500 \times CBR \tag{5.4}$$

$$\log_{10}E_{sg} = 1.415 + 1.284\log_{10}k_{sg} \tag{5.5}$$

From FAA's NAPTF database, the CBR value of medium strength subgrade was found to be 7. From the above equations, the value of E_{sg} was 10500 psi and k-value for MRG (slab directly over grade) was computed to be 107 pci. The k-value of MRC was determined by using figure 12 below which is published in AC 150 5320-6D (FAA 1995). The k-value of subgrade was first established as above and was corrected for the effect of base. The k-value for MRC with 10 inch thick granular subbase was found to be 300 pci.

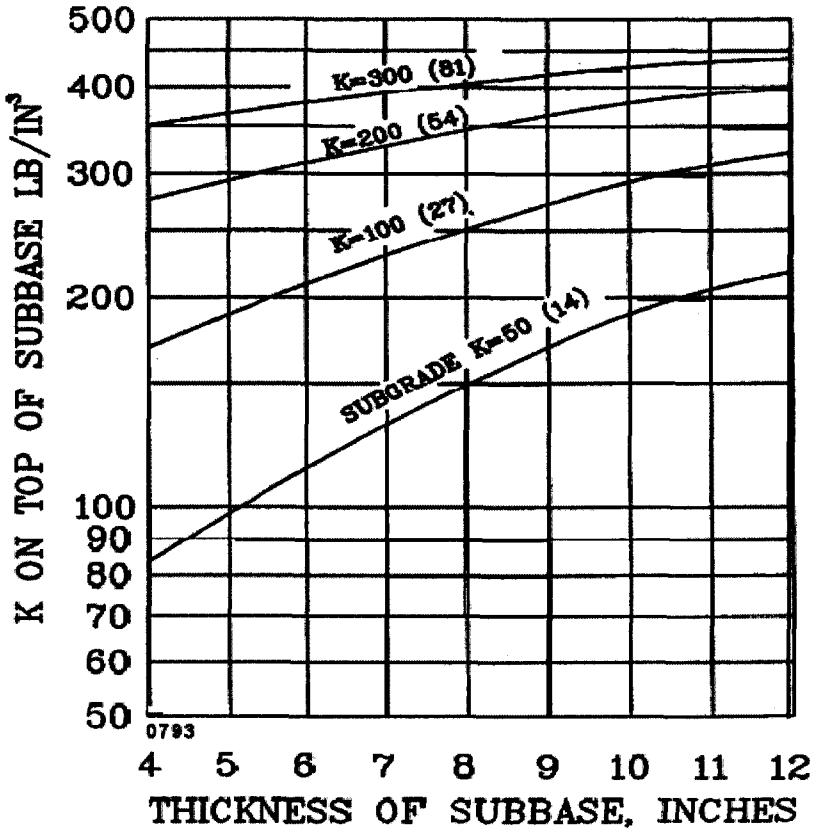

FIGURE 12: Effect of subbase on modulus of subgrade reaction (FAA 1995)

The k- value for MRS with a granular subbase and stabilized base was also determined in a similar manner. The effect of granular subbase was first established and corrected for the presence of 6 inch thick stabilized Econocrete base. Thus k-value for MRS was found to be 380 pci.

While the two methods should produce nearly equal values, it was observed that the difference between k-values was 75 pci and 45 pci for MRS and MRC respectively. However for MRG, the difference in values obtained by the two methods was significantly large. From the table 12, it is clear that the deflection values in case of MRG were lower than those recorded in case of MRC. This contradicts the fact that weaker pavement layer configuration should yield higher deflections as compared to a relatively stronger pavement layers. Since the subgrade soil is not linearly elastic and remains much stiffer under small stress or deflections, it can be stated that lower k-value should be obtained for pavement without a base and subbase. Also, the k-values obtained

were significantly different from the other back-calculation method described below. Furthermore, it was also verified from the FAA testing personnel that the discrepancy in MRG HWD data for slab centers was due to varied moisture content in subgrade during the time of testing. Hence, the k-value obtained from K. Hall's method was eliminated for further analysis. A k-value of 107 pci was assumed for MRG based on FAA Advisory Circular method. An average k-value for MRC (278 pci) and MRS (343 pci) obtained from above methods was selected for the JSLAB analysis. The averaging carried out in order to determine the final k-values with respect to its impact on degree of load transfer was justified by the fact that within the range considered, k-value does not have significant effect on computed stresses and LTE, provided the equivalent joint stiffness remains the same. The elastic modulus of PCC is typically 4 million psi, however, based upon K. Hall's method the value of 5.1 million psi, 5.3 million psi and 6.5 million psi was chosen for MRC, MRG and MRS respectively. In addition, the impact of E_{PCC} on degree of load transfer was also considered and the values chosen were justified for further analysis.

The next section entails the details of computation of equivalent joint stiffness value for MRC, MRG and MRS for further analysis using 2D-FE analysis program JSLAB.

5.4 Joint modeling in 2D-FE analysis program JSLAB

To determine the LTE (S) and LTE (δ) under static loading, a 2-D finite element (FE) program JSLAB 2004 was used. Modulus of elasticity of concrete (E_{PCC}), foundation modulus (k), slab thickness, Poissons ratio are some of the input parameters required by the program. In addition, joint modeling includes defining a joint stiffness parameter. Since the joints at NAPTF CC2 were dowelled with a surface saw-cut, the stiffness of joint can be assumed to be contributed by dowel plus aggregate interlock. However, it has been theoretically proved that a dowelled joint can be transformed into a total aggregate interlock joint (Ioannides & Korovesis 1992). An interlock stiffness parameter which resembles the joint stiffness can be defined in JSLAB for modeling an aggregate interlock joint equivalent to a dowelled joint.

Although the equivalent interlock stiffness can be computed from dowel parameters such as dowel diameter and spacing it becomes essential to capture the true joint stiffness exhibited in the field. Since it is difficult to determine the value of modulus of dowel bar support which is also a parameter required for computing equivalent stiffness, it is a good practice to capture the actual joint stiffness directly from field data. HWD data was again used to determine the joint stiffness. A 9-slab structure was modeled in JSLAB. The parameters used in this analysis for all three test items are shown in table 9. HWD test was simulated in JSLAB by applying a single wheel load of square footprint at the transverse joint. The area of square footprint was same as that of a circular footprint of HWD load plate. Loading pressure was computed for the highest load drop. Multiple trials were simulated until the ratio of deflection computed by the program matched the average LTE (δ) of the transverse joint measured during field HWD testing. The value of joint stiffness obtained through this analysis is shown in table 13 below in addition to other input parameters for JSLAB.

TABLE 13: Input parameters for finite element program JSLAB

	MRC	**MRG**	**MRS**
E_{PCC} (10^6 psi)	5.1	5.3	6.5
k (pci)	278	107	343
Slab width (feet)	15	15	15
Slab length (feet)	15	15	15
Number of elements in slab division	30	30	30
Poisson Ratio	0.15	0.15	0.15
LTE (δ) to be matched	0.81	0.86	0.71
Joint Stiffness (ksi)	75	55	43

5.5 Justification of final input parameters

In order, to determine the sensitivity of E_{PCC} on load transfer efficiency of joints, multiple finite element runs were performed on JSLAB using four different values of E_{PCC} keeping all other variables constant. The joint stiffness value as derived from previous section for

each type of test item was adopted. A 9-slab model was used and HWD test was simulated during each run. The load pressure and plate size used were same as used in determining the joint stiffness for each type of test item. An E_{PCC} value of 4 million psi, 5 million psi, 6 million psi and 7 million psi was used since the actual values finalized were within a range of 5 million to 6.5 million. As shown in figure 13 below variations in E_{PCC} had no effect on load transfer efficiency of joint, as long as the equivalent joint stiffness defined was kept as a constant. Thus the values of E_{PCC} chosen within the above range can be justified for further analysis.

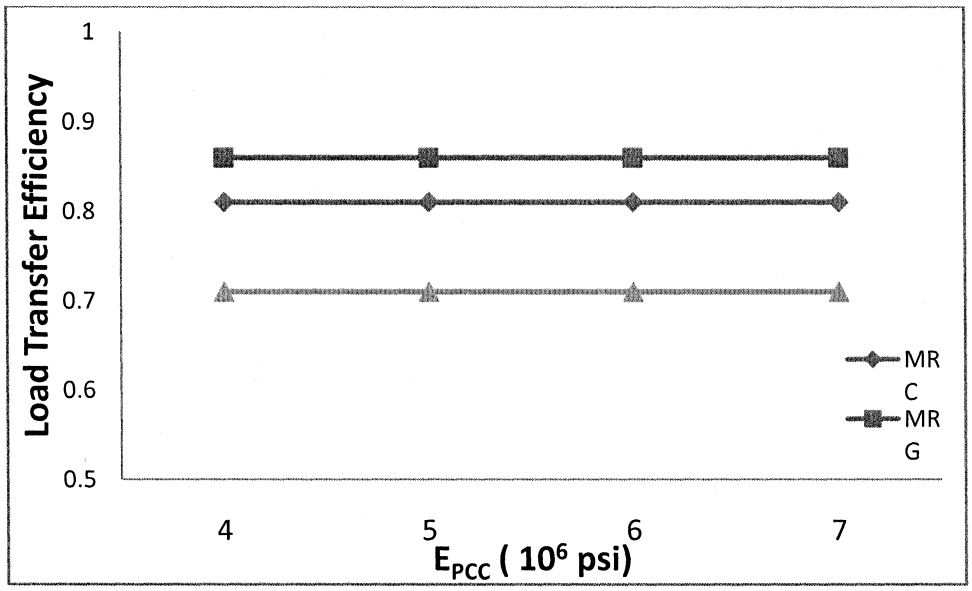

FIGURE 13: Effect of Modulus of Elasticity of Concrete on Load Transfer Efficiency

As stated earlier, the final k-value was taken as an average of values (for MRC and MRS) yielded by K. Hall's back-calculation technique and FAA advisory circular method. However, if the k-value has a very significant effect on degree of load transfer of joint, then the averaging may result in unreliable findings derived from finite element runs. Thus, it is important to determine the effect of k-value on load transfer efficiency. Multiple finite element runs simulating HWD were again performed using the input variables deduced from previous chapter as tabulated in table. Only the k-value was changed while keeping all other variables constant. The analysis was performed with k-values of 250 pci and 300 pci since as an intermediate average value of 278 pci was chosen for MRC. The objective was to determine if a significant variation in load

transfer efficiency of joint existed within the range of k-values selected for a particular value of joint stiffness. As observed in the figure 14 below, no significant variation in load transfer efficiency resulted from variations in k-values. Thus the average k- value chosen for analysis was justified. Similar check was performed for MRS and again it was observed that the load transfer efficiency was approximately similar in the range of k-value used for averaging. No check was performed for MRG since the k-value chosen was based on FAA Advisory Circular method only.

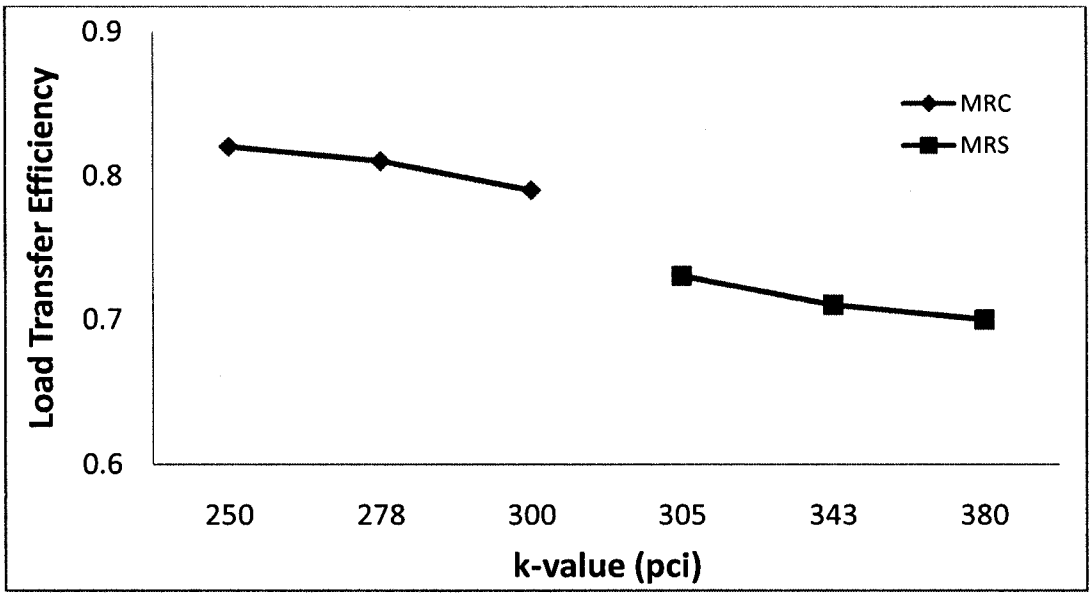

FIGURE 14: Variation in load transfer efficiency over range of k-value considered

5.6 Summary

The values of input variables for 2D-FE program, JSLAB were determined and justified in this chapter on the basis on its effect on joint load transfer efficiency. Insignificant changes in degree of load transfer efficiency of joint due to variation in values of modulus of elasticity of PCC layer and modulus of subgrade layer were considered as a basis of validation. The next chapter presents the results of 2D- FE analysis program runs in order to determine the load transfer efficiencies based on stresses and deflections due to static aircraft gear loadings.

CHAPTER 6

2D-FE Analysis using JSLAB

6.1 Introduction

To determine LTE (S) and LTE (δ) under static aircraft gear loading, a 2-D finite element (FE) program JSLAB 2004 was used. The input parameters for JSLAB were as derived in the previous sections. The LTE values under static loading with various aircraft gear configurations in different position was obtained and the effect of load types (static versus moving), aircraft gear configuration and positions on joint load transfer efficiency was studied.

6.2 Background of 2D- FE program JSLAB

JSLAB is a 2D-FE program which can be used for analysis of jointed concrete pavements. The mechanical responses such as stresses and deflection along any section in the pavements slab can be obtained under particular type of loading for a pavement structure which is defined by E_{PCC}, k-value, slab size, joint parameters, mesh division. The program is equipped with different foundation models such as spring, dense liquid, elastic solid foundation (Boussinesq's theory) etc (FHWA 2004). The program is also validated by comparing the results with other FE analysis program ILLISLAB, H51 (Kreger 1967) as well as full scale test data obtained by Ohio University. The strain measurements during full scale tests conducted at Ohio University were also used for verification of a 3D- FE analysis program (Sargand 1998). Therefore, the results of 2D-FE analysis using JSLAB can be said to be comparable to 3D- FE analysis.

A dense liquid model under a thin plate 2-D model for slabs was used for simulating the foundation in JSLAB. A thin plate 2-D model is justified for use in computation for load transfer efficiencies since the results of 2D and 3D program were found to be similar (Guo 2009). When the load transfer capability was zero, it was found that deformations on unloaded side were zero, as logically anticipated and as found in the 3D finite element program EverFe. In addition, the loaded side deflections in JSLAB were found to be similar as those predicted by EverFe. In another study (Brill and Guo 2001) conducted with the use of JSLAB, comparing the predicted load transfer efficiency values with measured ones, an average standard deviation of 0.05 was found between the measured and predicted values for different strength of subgrades. However, this deviation was attributed to curled slabs in the field which did not yield a proper result for deflection testing. Thus the use of 2D-FE program JSLAB for predicting LTE is justified in this study.

6.3 Effect of load types (moving versus static) on joint LTE

In order to study the differences in load transfer efficiencies during moving and static loading, a 9-slab structure connected by a joint was modeled in JSLAB. The input parameters for JSLAB were as tabulated in table 13 of previous chapter. Figure 15 below shows the location for 4-wheel and 6-wheel loading along with the finite element slab mesh. When the longer axis of either the 4-wheel or 6-wheel aircraft gear is perpendicular to the joint, the gear position is referred as perpendicular gear position. The aircraft gears were modeled in such a way that the center slab becomes loaded with the entire gear with wheels tangential to the joint across which the LTE is computed. The LTE was measured by computing stresses and deflections at a distance of 6 inches away from the joint. This is consistent with the fact that, under a 12 inch HWD loading plate, the center of plate is at 6 inches away from the joint. The output stress and deflection profiles on loaded as well as unloaded sides for 4-wheel and 6 -wheel perpendicular position can be found in Appendix B. Table 14a and 14b summarize the values of LTE (S) and LTE (δ) under static 4-wheel and 6-wheel loading respectively while the gears are in perpendicular position. The stress-based LTE was calculated based on FAA [LTE (S)] as well as FHWA [LTE (σ)] definition.

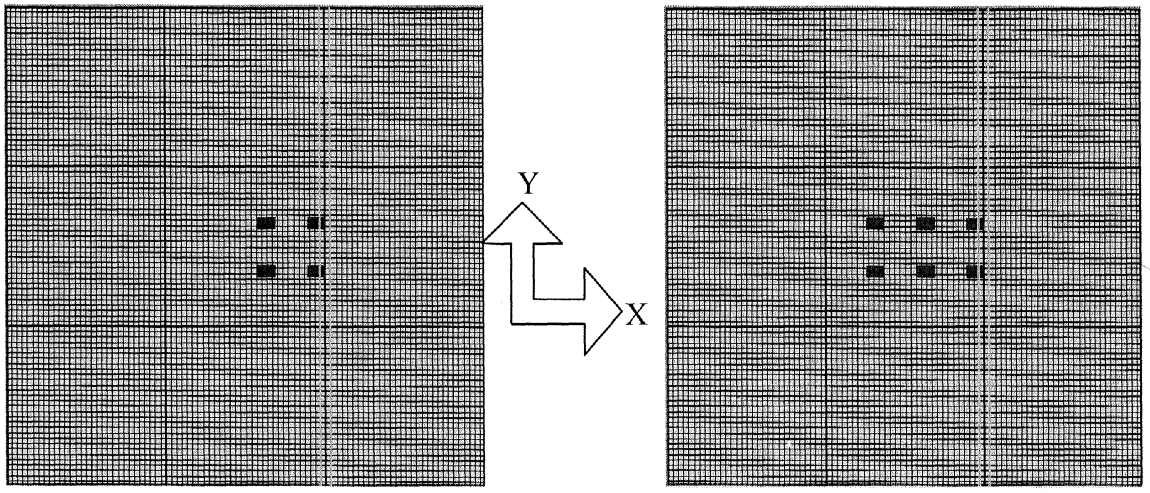

FIGURE 15: Perpendicular gear position for 4-wheel and 6-wheel aircraft gear

TABLE 14a: Deflection and stress based LTE obtained under static loading 4-wheel loading in perpendicular position

	Deflection (inches)		**LTE(δ)**	**Bending stress in Y- direction (psi)**		**LTE(S)**	**LTE(σ)**
	Unloaded	**Loaded**		**Unloaded**	**Loaded**		
MRC	0.041	0.052	0.80	255.75	630.33	0.29	0.41
MRG	0.086	0.102	0.85	401.09	809.67	0.33	0.50
MRS	0.031	0.044	0.70	223.82	668.20	0.25	0.33

TABLE 14b: Deflection and stress based LTE obtained under static loading 6-wheel loading in perpendicular position

	Deflection (inches)		**LTE(δ)**	**Bending stress in Y- direction (psi)**		**LTE(S)**	**LTE(σ)**
	Unloaded	**Loaded**		**Unloaded**	**Loaded**		
MRC	0.041	0.052	0.78	268.42	650.04	0.29	0.41
MRG	0.088	0.107	0.83	433.25	858.67	0.34	0.50
MRS	0.030	0.044	0.68	235.69	692.58	0.25	0.34

No significant difference in the LTE (δ) and LTE (S) or LTE (σ) of joints was observed under 4-wheel or 6-wheel loading case comparing individual test items although the deflection at center of slabs and bending stresses changed by a small value. The value of LTE (δ) obtained from static 4-wheel and 6-wheel loading were compared with the values for single wheel loading (HWD) when the joint stiffness remained the same in both cases. The graph in figure 16 shows that no significant difference in LTE (δ) under 4-wheel/6-wheel loading or single wheel loading (HWD) although the slab bending phenomena tends to be different in the two cases.

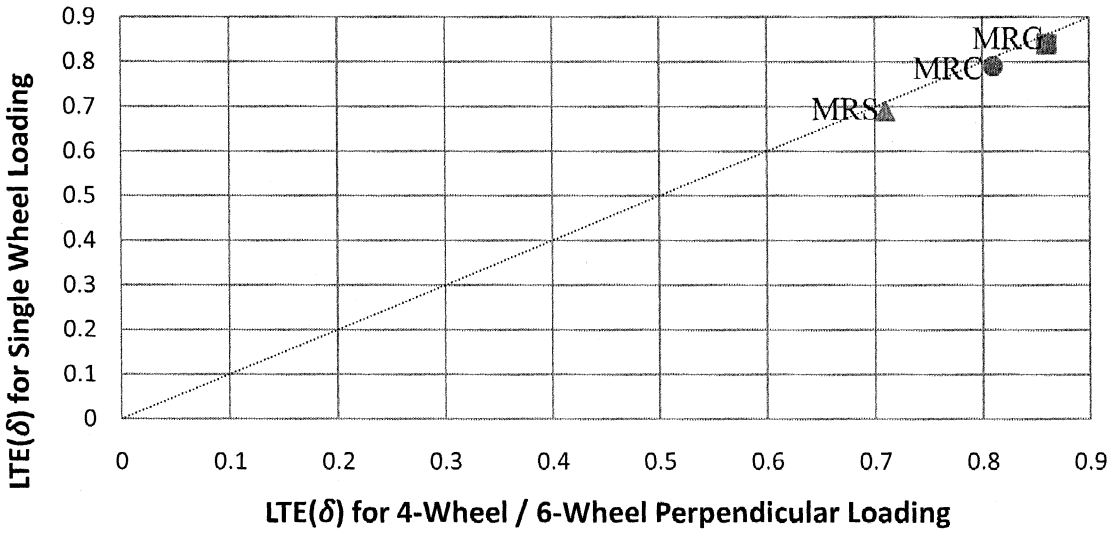

FIGURE 16: Comparison between LTE (δ) due to 4-wheel loading and single wheel loading for MRC, MRG and MRS.

The stress based LTE from static 4-wheel loading was compared with that under moving loads already obtained from the strain record analysis previously. The LTE (S) due to static load was calculated based on the maximum values of tensile stresses along the direction of joint. On an average, the LTE (S) values from static loading were lower by 38% as compared to moving loads. The graph in figure 17 shows the difference in values due to static and moving loading. The above finding raises a question whether a static LTE or dynamic LTE be considered in the design. Majority of studies on load transfer efficiency assume that the load is transferred across a joint under a static load. However,

the true load transfer in the field is based on moving wheels. The LTE in the field is influenced by factors such as speed of the aircraft, pavement and foundation damping coefficients (Yu et al. 2010), and time of year (Brill and Guo, 2001) etc. It also becomes imperative to analyze if low LTE measured by FWD leads to early cracking. More than 15 years data available from Denver airport indicated low LTE but did not lead to early cracking. The full scale tests data available from testing of CC2 test strip at FAA's NAPTF indicated that cracking would occur if LTE was low (Ricalde 2003, Guo et al. 2009). Corner cracks were first observed at slabs with a free edge (no load transfer) since the tensile stresses were higher as compared to the slabs with load transferring devices.

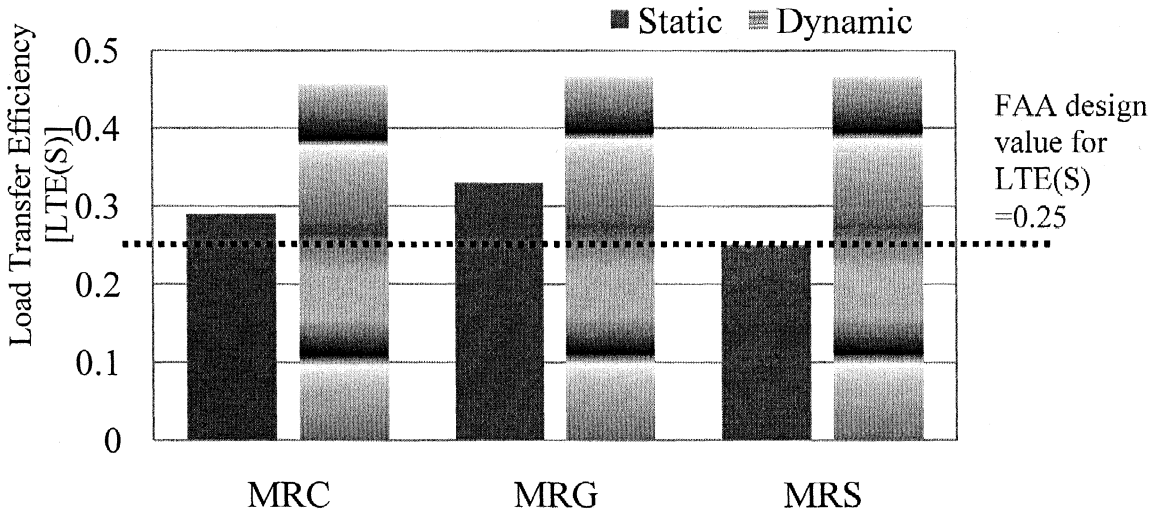

FIGURE 17: Comparison between LTE (S) due to static and dynamic 4-wheel loading for MRC, MRG and MRS

The next section present the results of analysis conducted to determine the effect of gear position on LTE of joints.

6.4 Effect of aircraft gear position with respect to the joint on LTE

In previous section, the value of LTE (S) and LTE (δ) was determined from JSLAB when the aircraft gears were in perpendicular position with respect to the joint. In this section LTE (S) and LTE (δ) is determined under parallel gear position. In order to study the differences in load transfer efficiencies when the aircraft landing gear's longer axis is

perpendicular or parallel to the joint, the LTE values under the two gear positions were compared. Figure 18 below shows the location for 4-wheel and 6-wheel loading along with the finite element slab mesh. Since the main axis of aircraft gear is parallel to the joint, the positions shown in Figure 18 are referred as parallel gear positions. The output was determined along a line at 6 inches from the joint on both loaded as well as unloaded sides. Table 15a and Table 15b summarize the values of LTE (S) and LTE (δ) under static loading 4-wheel and 6-wheel loading respectively while the gears are in parallel position. The output stress and deflection profiles on loaded as well as unloaded sides for 4-wheel and 6 -wheel parallel position can be found in Appendix A.

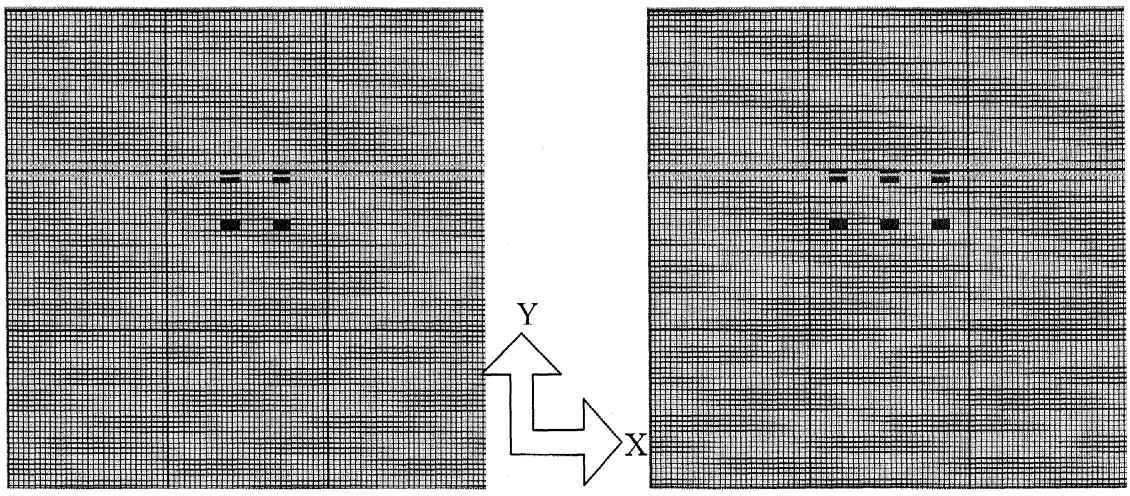

FIGURE 18: Parallel gear position for 4-wheel and 6-wheel aircraft gear

TABLE 15a: Deflection and stress based LTE obtained under static 4-wheel loading in parallel position

4-wheel parallel	Deflection (inches)		LTE(δ)	Bending stress in X- direction (psi)		LTE(S)	LTE(σ)
	Unloaded	Loaded		Unloaded	Loaded		
MRC	0.045	0.055	0.82	256.68	631.84	0.29	0.41
MRG	0.120	0.103	0.86	501.13	1018.9	0.33	0.49
MRS	0.034	0.047	0.71	225.81	668.80	0.25	0.34

TABLE 15b: Deflection and stress based LTE obtained under static 6-wheel loading in parallel position

6-wheel parallel	Deflection (inches)		LTE(δ)	Bending stress in X- direction (psi)		LTE(S)	LTE(σ)
	Unloaded	Loaded		Unloaded	Loaded		
MRC	0.054	0.066	0.82	189.66	549.05	0.26	0.35
MRG	0.117	0.135	0.87	341.07	686.84	0.33	0.50
MRS	0.042	0.056	0.73	165.81	562.07	0.23	0.29

Unlike the perpendicular gear position case, some amount of differences in the LTE values were observed under a 4-wheel and 6-wheel gear load in parallel position. Under 6 wheel loading, the LTE (S) dropped by 6% on an average and LTE (σ) dropped by 9 % on an average for the three test items. The differences in LTE values under different gear configuration can be attributed to the different number of loading areas along the joint under a 4-wheel and a 6-wheel gear. Under a 4-wheel gear in parallel position, the stresses at the joint are governed by two loaded areas. On the other hand, under a 6-wheel loading gear, the stresses at the joint are governed by three loaded areas.

The effect of number of loaded areas along the joint was also evident from comparison of LTE of the same gear in different positions with respect to the joint. In the case of 4 wheel loading, no significant difference was found in LTE (S) when the gears were in parallel or perpendicular position. LTE (δ) was also found to be the same in the case of 4-wheel parallel and perpendicular gear position. The probable reason for similarity of load transfer behavior in 4-wheel parallel and perpendicular position can be attributed to the fact that center of loads was approximately at same location relative to the joint in either of these two gear position. In addition, the number of loaded areas along the joint always remains two in parallel as well as perpendicular position under a 4-wheel loading. Figure 19 shows the comparison of load transfer efficiencies for 4-wheel static loading while the gears are in parallel and perpendicular position. It was observed that, while MRG exhibited the highest degree of load transfer, load transfer efficiency was lowest for

a stabilized base i.e. MRS. This trend applies for both gears in perpendicular as well as parallel position. It is also important to note that the 25% LTE (S) assumption as followed by the FAA thickness design (Kawa et al., 2002; Kawa et al., 2007; FAA 1995) procedure was just met in the case of MRS.

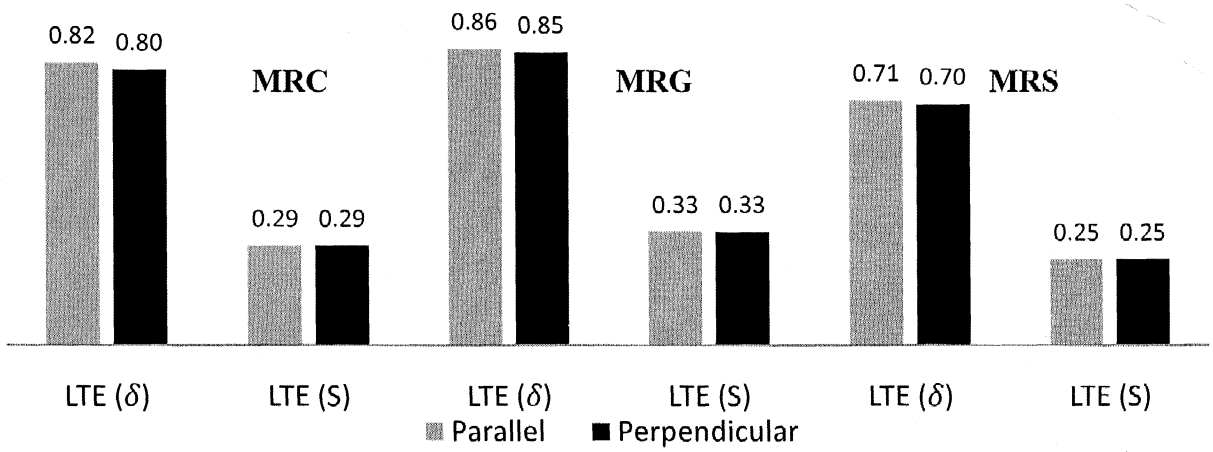

FIGURE 19: Comparison of LTE (S) and LTE (δ) under 4-wheel loading for parallel and perpendicular gear position.

The load transfer efficiencies were also compared for static 6-wheel loading in parallel and perpendicular gear position. Figure 20 shows the comparison of load transfer efficiencies for 6-wheel static loading while the gears are in parallel and perpendicular position.

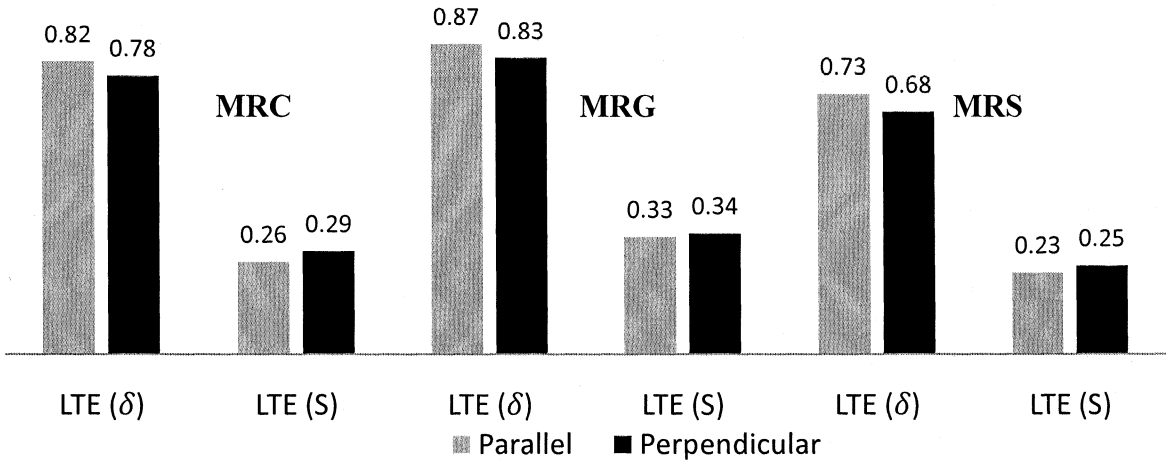

FIGURE 20: Comparison of LTE (S) and LTE (δ) under 6-wheel loading for parallel and perpendicular gear position.

A small difference was observed between the LTE values in the two gear positions. While LTE (δ) in perpendicular position dropped by 5.7% on an average for the three test items, an increase of 7.7% on an average was observed for LTE (S) in perpendicular as compared to parallel gear position. Again, the difference in LTE values can be attributed to difference in number of loaded areas along the joint under a 6-wheel gear in perpendicular or parallel position. Under a 6-wheel gear in parallel position, the stresses at the joint are governed by three loaded areas. On the other hand, in perpendicular position, the stresses at the joint are governed by two loaded areas. It was also observed that the stress based load transfer efficiency was lower than the 25% value while gears were in parallel position in case of MRS.

Another viewpoint of looking at the effect of different gear positions is the position of load center with respect to the joint. It is worthwhile to note that LTE (δ) increased as the load center moved closer to the joint as in the case of parallel gear position. During construction of a dowelled joint, one end of the dowel is bonded in concrete and the other end is painted and greased before pulling the forms for concreting. Thus a void is created by buildup of paint under the unbounded dowel. When load is applied to the slab containing the bonded end of dowel, the unbonded end does not make contact with the concrete and contribute to the load transfer until some amount of deflection occurs at the end. As the load center moves closer to the joint, deflections at slab edges increase causing a full contact of dowel with concrete and resulting in higher degree of load transfer. Thus, an increase in LTE (δ) is observed as the loads move closer to the joint. This phenomenon was first observed by Hammons from the data collected at Lockbourne and Sharonville test track (1995). However, a reverse trend was observed in LTE (S) which is evident from slightly higher values in the case of perpendicular gear position.

6.5 Correlation between LTE (S) and LTE (δ)

The effect of aircraft gear position on the relation between LTE (S) and LTE (δ) was studied by conducting a series of finite element program runs using JSLAB. A plot of LTE (S) versus LTE (δ) was created and compared to a similar plot published in FAA

Advisory Circular AC 150/5370 11-A (FAA 2004). However, the correlation in FAA, 2004 is based on FHWA definition of stress-based load transfer efficiency.

The stress and deflection data used to compute the load transfer efficiencies was generated in JSLAB under 4-wheel and 6-wheel loading. Only the joint stiffness value which is an input parameter that defines the equivalent dowelled joint stiffness was proportionately increased from a relative low value of the order 500 psi until higher values of the order 200000 psi as no significant change in LTE value was observed for higher joint stiffness values. This analysis was performed for gears in perpendicular and parallel position with respect to the joint. The relationship between LTE(S) and LTE (δ) for different gear configurations in static perpendicular position for each type of CC2 test item is displayed in Figure 21(a), 21(b) and 21(c) for MRC, MRG and MRS respectively.

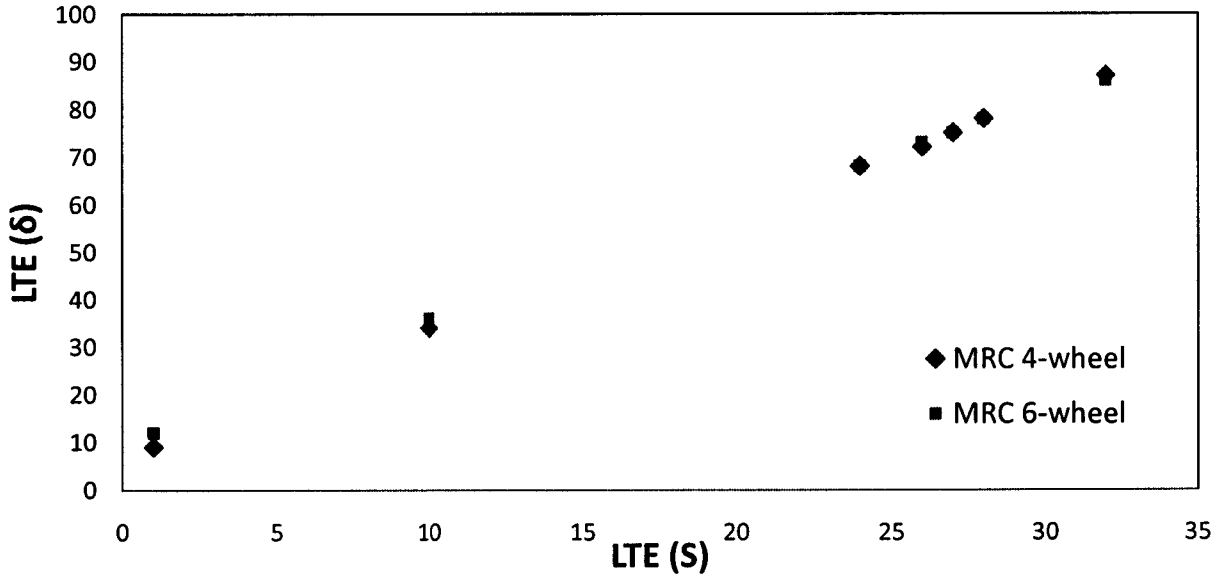

FIGURE 21(a): Relation between LTE (S) and LTE (δ) for 4-wheel and 6-wheel perpendicular gear position in MRC (15ft)

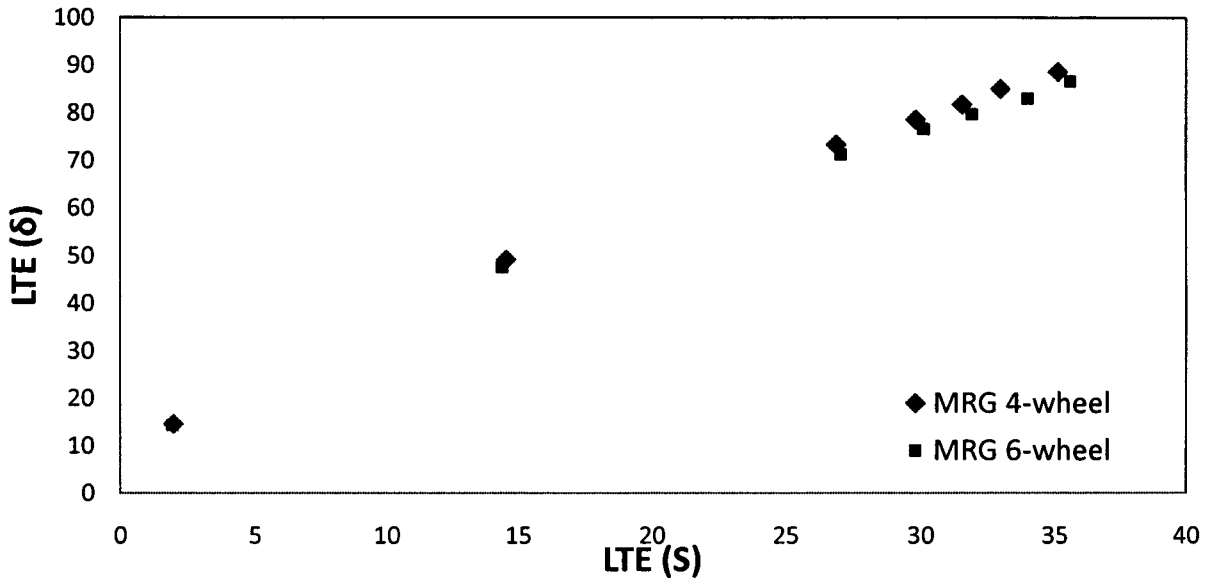

FIGURE 21(b): Relation between LTE (S) and LTE (δ) for 4-wheel and 6-wheel perpendicular gear position in MRG (15ft)

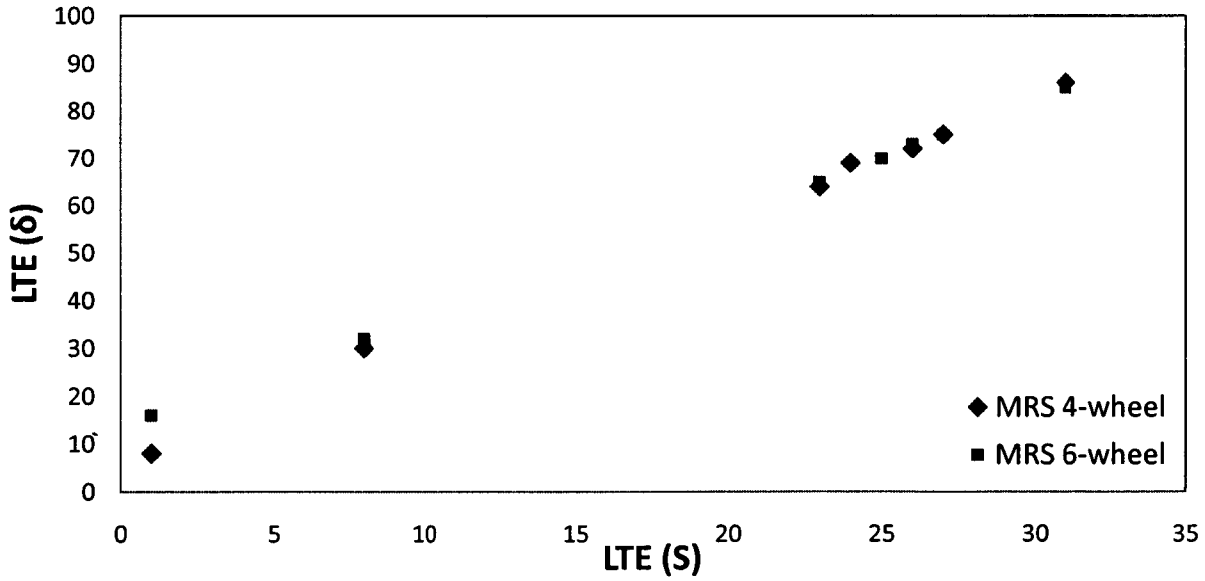

FIGURE 21(c): Relation between LTE (S) and LTE (δ) for 4-wheel and 6-wheel perpendicular gear position in MRS (15ft)

From the above figures, it is clear that the 25% LTE(S) is equivalent to 70- 80 % LTE (δ) depending upon the pavement subgrade configuration. However, this graph is valid only for static 4-wheel and 6-wheel loading when the gears are in perpendicular position. Figure 22(a), 22(b) and 22(c) displays the relation between LTE(S) and LTE (δ) for static 4-wheel and 6-wheel gear configurations in parallel position for each type of CC2 test item. Again, it was observed that 25% LTE(S) is equivalent to 70-80 % LTE (δ) depending upon the pavement subgrade configuration. However, the data points for relationship between LTE (δ) and LTE (S) for 4-wheel and 6-wheel gears in parallel position did not overlap with the perpendicular gear position which can be attributed to the difference in number of loaded areas along the joint under 4-wheel and 6-wheel loading in parallel gear position.

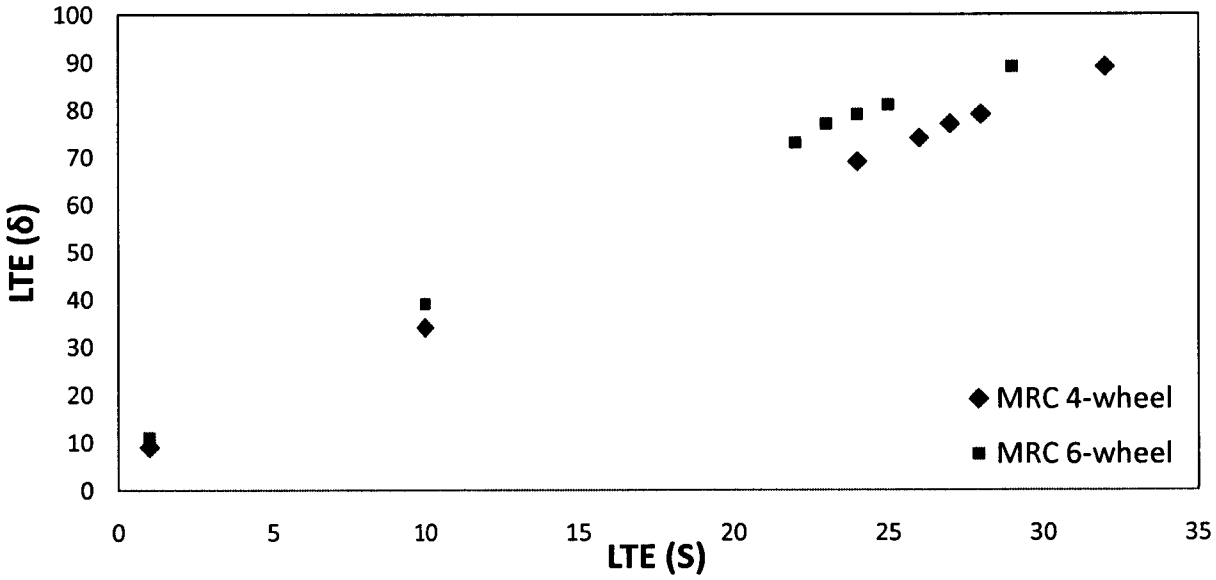

FIGURE 22(a): Relation between LTE (S) and LTE (δ) for 4-wheel and 6-wheel parallel gear position in MRC (15ft)

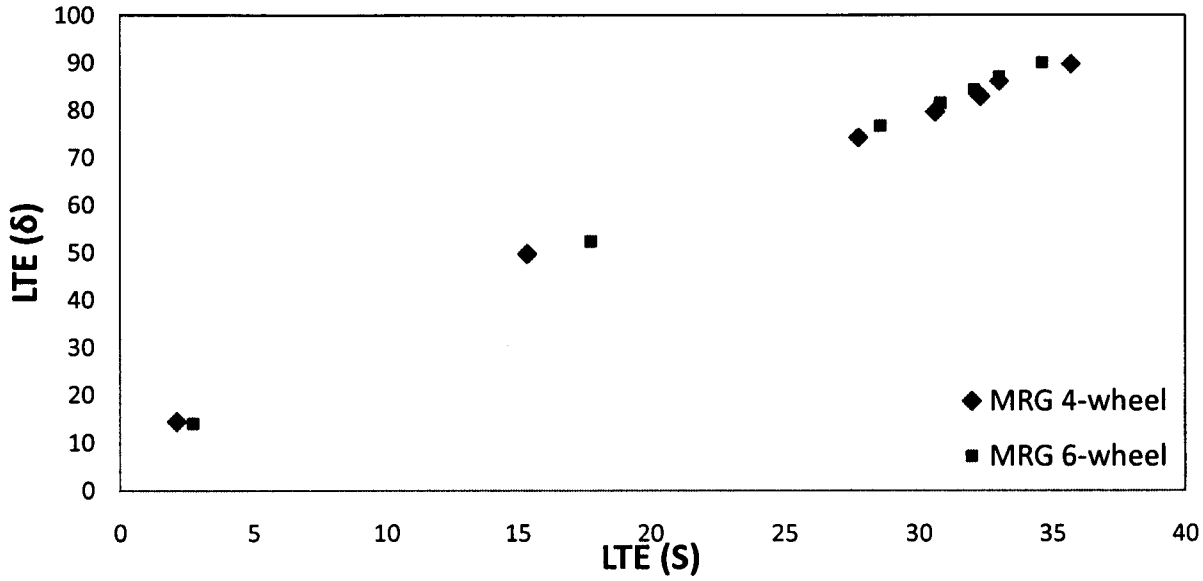

FIGURE 22(b): Relation between LTE (S) and LTE (δ) for 4-wheel and 6-wheel parallel gear position in MRG (15ft)

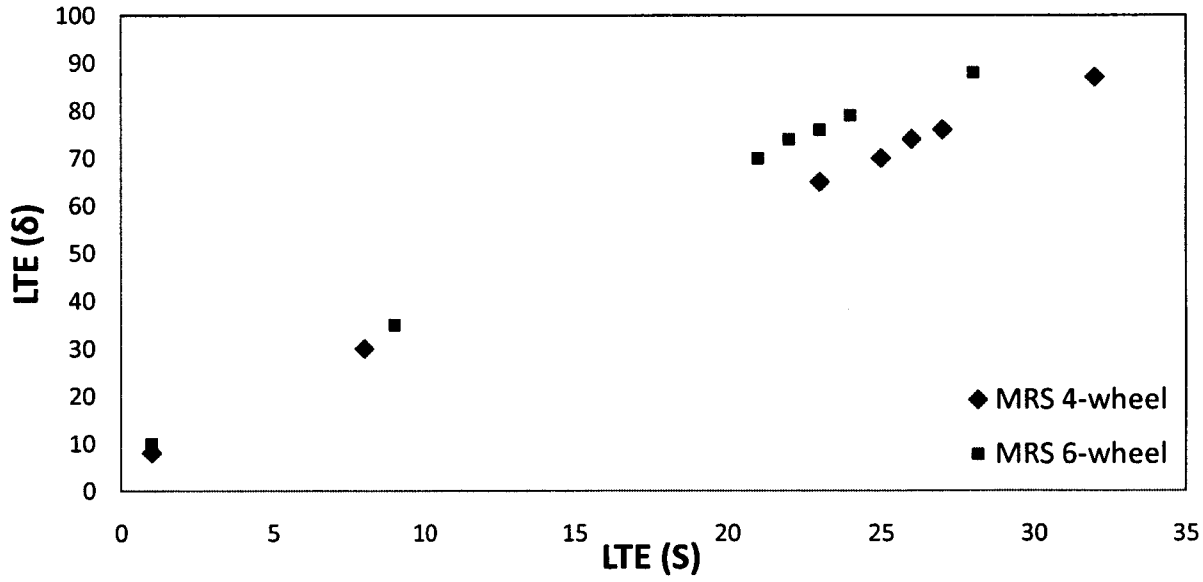

FIGURE 22(c): Relation between LTE (S) and LTE (δ) for 4-wheel and 6-wheel parallel gear position in MRS (15ft)

As mentioned earlier, the above analysis was conducted using a 9-slab model. The results significantly changed when a 2-slab model was used for analysis. Although the LTE (S) in 9-slab model increased by 11% on an average for the three test items (both

perpendicular and parallel positions) under a 4-wheel static loading, LTE (δ) remained almost the same under 2- slab or 9-slab model. Figure 23 shows the comparison of load transfer efficiencies for 4-wheel static loading while the gears are in parallel and perpendicular position using a 2 slab model. However, the same comparison for 6-wheel static loaded gears yielded significantly varying results. Figure 24 shows the comparison of load transfer efficiencies for 6-wheel static loading while the gears are in parallel and perpendicular position using a 2 slab model. While the difference in LTE (S) under perpendicular gear position using a 2-slab or 9-slab model was insignificant, it was found that LTE (S) under parallel gear position using a 2-slab model was lower by 55% as compared to that using a 9-slab model. This finding indicates that the proximity of the longitudinal joints relative to the locations of wheel have a certain influence on load transfer across transverse joints. In the case of 2-slab model, the two longitudinal edges are acting as free edge with zero load transfer. Hence, the stresses in the loaded slab are greater than that as compared to a case where loaded slab is surrounded by adjoining slabs on all sides (9-slab model).

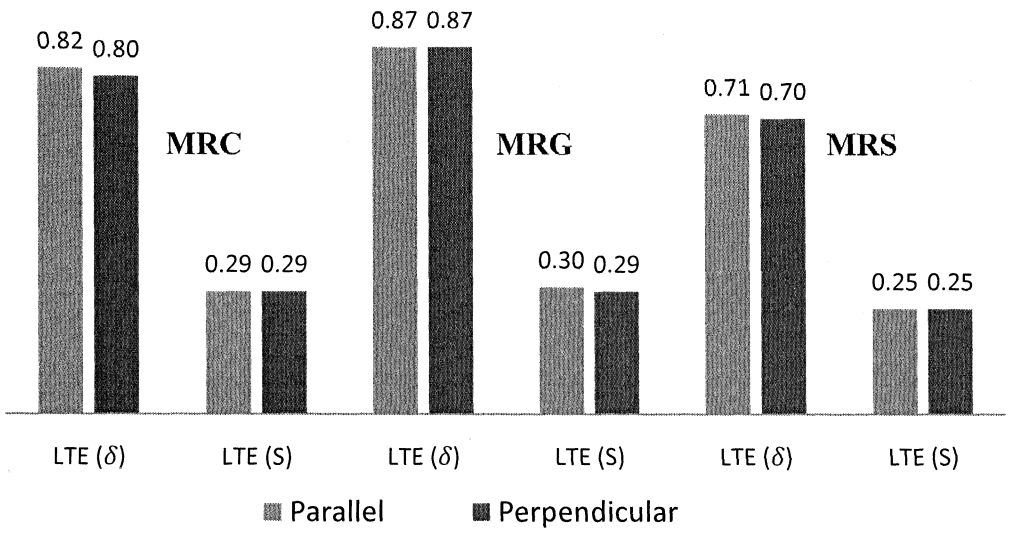

FIGURE 23: Comparison of LTE (S) and LTE (δ) under 4-wheel loading for parallel and perpendicular gear position using a 2 slab model.

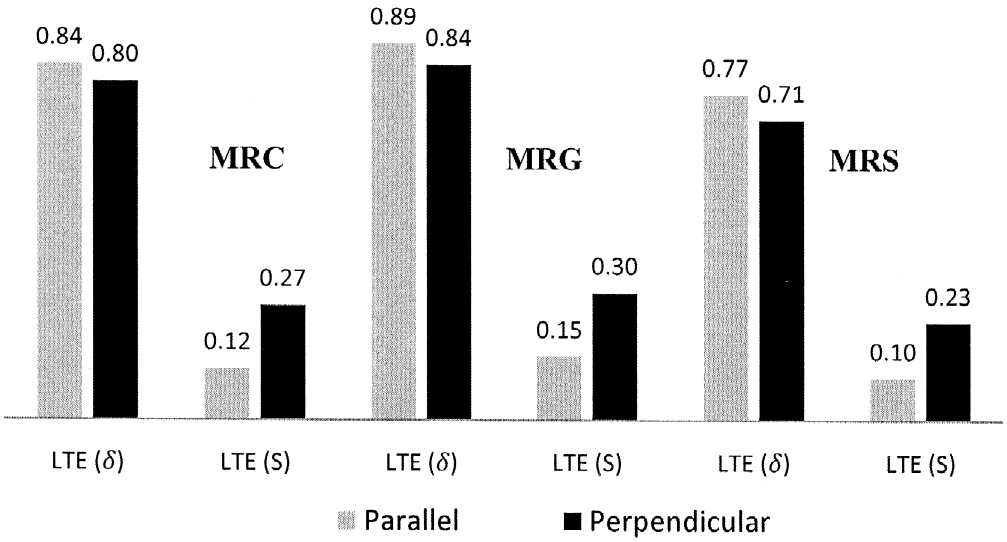

FIGURE 24: Comparison of LTE (S) and LTE (δ) under 6-wheel loading for parallel and perpendicular gear position using a 2 slab model.

The above analysis was carried out using a 15 feet x 15 feet slab. The analysis was repeated using a wider slab of size 20 feet x 20 feet. Figure 25 shows the comparison of load transfer efficiencies for 4-wheel static loading while the gears are in parallel and perpendicular position using a 2 slab model. The LTE values were similar in the two gear positions considered under a static 4-wheel gear load. Figure 26 shows the comparison of load transfer efficiencies for 6-wheel static loading while the gears are in parallel and perpendicular position using a 2 slab model. LTE (S) under parallel gear position was lower by 11% as compared to perpendicular case. Thus, slab size was found some effect on load transfer efficiency of joints when a 2-slab finite element model was used in the analysis. To study the effect of slab size using a multi-slab finite element model, more analysis was conducted using 9-slab model and different slab sizes as described in the next section.

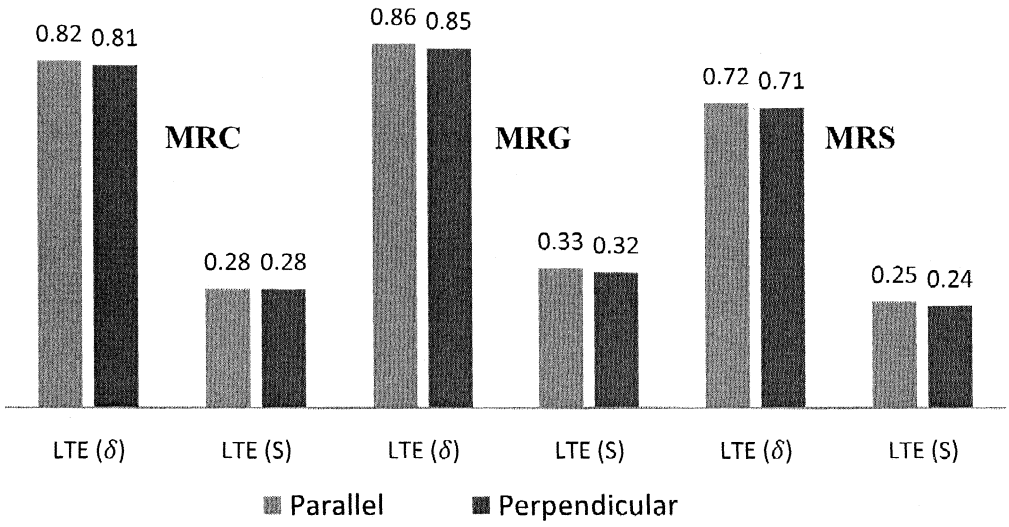

FIGURE 25: Comparison of LTE (S) and LTE (δ) under 4-wheel loading for parallel and perpendicular gear position using a 2 slab model and 20 feet x 20 feet slabs.

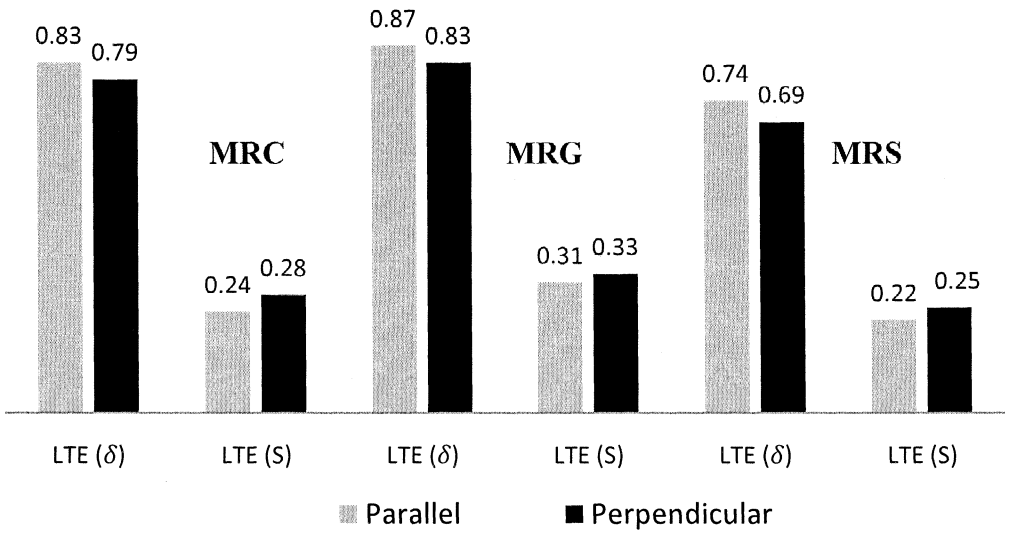

FIGURE 26: Comparison of LTE (S) and LTE (δ) under 6-wheel loading for parallel and perpendicular gear position using a 2 slab model and 20 feet x 20 feet slabs.

6.6 Effect of slab size on LTE across joint

In order to study the influence of slab size on load transfer efficiency of joints, the analysis performed using 15 ft x 15 ft slabs described in the above sections was repeated using 20 ft x 20 ft slab and 12 ft x 12 ft slab (using 9 slab model). The results were then

compared to determine if there were any differences in the load transfer efficiency of joints due to different slab sizes while the other parameters such as joint stiffness, subgrade modulus etc. remained the same. Table 16 summarizes the values of LTE (S) and LTE (δ) under a static 4-wheel and 6-wheel loading for different slab sizes and aircraft gear positions for the three test items.

TABLE 16: LTE (S) and LTE (δ) under static 4-wheel and 6-wheel loading for different slab sizes and aircraft gear positions

		LTE(S)					
		Perpendicular			**Parallel**		
		12 feet	15 feet	20 feet	12 feet	15 feet	20 feet
MRC	4-wheel	0.28	0.29	0.28	0.28	0.29	0.28
	6-wheel	0.29	0.29	0.28	0.22	0.26	0.26
MRG	4-wheel	0.32	0.32	0.32	0.32	0.33	0.32
	6-wheel	0.31	0.33	0.32	0.27	0.32	0.32
MRS	4-wheel	0.24	0.25	0.25	0.25	0.25	0.25
	6-wheel	0.24	0.25	0.25	0.20	0.23	0.23
		LTE (δ)					
		Perpendicular			**Parallel**		
		12 feet	15 feet	20 feet	12 feet	15 feet	20 feet
MRC	4-wheel	0.82	0.80	0.80	0.82	0.82	0.82
	6-wheel	0.78	0.79	0.79	0.83	0.82	0.82
MRG	4-wheel	0.85	0.84	0.84	0.86	0.85	0.86
	6-wheel	0.82	0.82	0.83	0.87	0.86	0.86
MRS	4-wheel	0.72	0.70	0.71	0.72	0.71	0.72
	6-wheel	0.69	0.68	0.69	0.75	0.73	0.73

From the above table, it can be concluded that the LTE values are almost the same for different slab sizes considered in the analysis. Thus it can be concluded that slab size had no significant effect on the load transfer efficiency of joints.

6.7 Summary

The effect of load types (static versus moving), various gear configurations and gear positions on LTE of joint was studied in this chapter. It was found that, similarity exists between the values of LTE (S) estimated from LTE (δ) measured by FWD and that calculated using finite element program for multiple wheel loads based on static analysis. However, significant differences exist in the value of LTE (S) estimated from LTE (δ) and that directly measured under dynamic loading from full scale testing. On an average, the LTE (S) values from static loading were lower by 38% as compared to moving loads (dynamic). The LTE was also affected by different gear configurations in different positions due to varying number of loaded areas along the joint. Overall, similar LTE values were observed for a 4-wheel or 6-wheel gear, denoting that different gear configuration or positions has negligible effect on degree of load transfer across a joint. The commonly used correlations were also verified accounting for the effect of various aircraft gear configurations and positions across the joint edge using 2D-FE analysis program JSLAB. The effect of differential stress distribution along the joint under various modern day aircraft gear configurations in different positions was also studied using a 3D-FE analysis program FEAFAA which is described in the next chapter.

CHAPTER 7

3D-FE analysis using FEAFAA

7.1 Introduction

In the previous chapter, it was found that degree of load transfer across a joint is different under a static and moving aircraft gear loading. The effect of differential stress distribution along the joint due to differential slab bending phenomenon under various aircraft gear configuration and positions with respect to the joint was also studied using a 2D-FE analysis program JSLAB in the previous chapter. The same effect is studied in this chapter using a 3D-FE analysis program FEAFAA developed by the FAA. Various modern day aircrafts in different position along the joint of a typical pavement structure was considered in the analysis. In addition, as load transfer efficiency under a static aircraft gear was critical as compared to moving gear loads, the LTE (S) under different modern day aircraft gears with different gross weights was also determined to see if 25% LTE (S) assumption was valid for a typical pavement layer configuration. The background of FEAFAA is explained in the next section.

7.2 Background of FEAFAA

The results of 3D-FE analysis using FEAFAA to study the effect of static aircraft gear configuration and gear position on LTE of joints are presented in this chapter. FEAFAA is a useful tool for computing accurate responses (stresses, strains and deflections) of rigid pavement structures to individual aircraft landing gear loads. FEAFAA's basic element type is an eight-node hexahedral (brick) solid element. The model uses only one element type for all structural layers. The bottommost layer of elements in the subgrade

consist of 8-noded "infinite" elements. However, infinite elements have special mapping functions that mathematically map the 8-node geometry onto a semi-infinite space. In this way, the FEAFAA model represents a rigid pavement structure on an infinitely deep foundation (NAPTF). A unidirectional spring element is used for modeling linear elastic joints between adjacent slabs. In FEAFAA, the joints act as continuous, linear elastic springs, transmitting vertical loads between adjacent slabs in shear through the joint. Joints in FEAFAA do not transmit moment, nor do they transmit horizontal forces. The shear force is assumed linearly proportional to the relative vertical displacement between slabs. The joint is characterized by equivalent shear stiffness, expressed in units of force per relative vertical displacement per unit length of the joint (Brill, 1998). The program was validated comparing the pavement responses using theoretical-solution-based program BISAR as well as layered elastic analysis program LEAF (FAA 2009). In general, there is a good agreement between the stresses calculated at the integration points by FEAFAA, BISAR and LEAF. In this study, FEAFAA was used to determine stresses and deflections in a rigid pavement section under edge loading condition to ultimately compute the joint LTE. The next section explains the input data preparation and analysis carried out using FEAFAA.

7.3 Input data

A typical pavement structure with a stabilized base was chosen for checking the sensitivity of various aircraft gear loads in different positions on degree of load transfer across the joint. The thicknesses of the pavement layers and material properties are shown in figure 27. In order to check the reliability of input parameters and boundary conditions, the results (stresses in two directions and deflections) under a single wheel load were compared with those calculated by 2D-FE program JSLAB. An interior loading case was considered to minimize the effect of joint and the maximum interior stresses at the slab bottom were determined. Table 17 shows the comparison between the results of FEAFAA and JSLAB under the single wheel interior loading case.

12" PCC, μ=0.15	E = 6,500,000 psi
6" Econocrete, μ=0.2	E = 700,000 psi
6" Crushed Aggregate, μ=0.4	E = 29,000 psi
Subgrade, μ=0.45	E= 10,500 psi

FIGURE 27: Pavement layers with material properties and thicknesses

TABLE 17: Stresses and deflections under single, 4 and 6 wheel loading

Gear Type	Parameter	FEAFAA	JSLAB
Single Wheel	Stress-X (psi)	322.73	328.17
	Stress-Y (psi)	305.01	314.08
	Deflection (inches)	0.0187	0.0102
4-Wheel	Stress-X (psi)	609.49	501.11
	Stress-Y (psi)	587.47	465.55
	Deflection (inches)	0.0801	0.0331
6- Wheel	Stress-X (psi)	816.71	578.50
	Stress-Y (psi)	681.98	423.82
	Deflection (inches)	0.1164	0.0405

The above table shows that while the results (stresses and deflections) matched closely under a single wheel loading case, the difference increased under a 4-wheel and 6- wheel gear loading. The differences observed can be attributed to the different modeling techniques in 2D (JSLAB) and 3D program (FEAFAA). The most important difference is how the pavement layers are handled. While a single value of spring constant simulating liquid foundation is defined in JSLAB, actual layer thicknesses with elastic moduli are defined in FEAFAA. In the case of a single wheel loading, a minimum number of springs are being compressed, however, in the case of 4 and 6 wheel loading a

relatively large number of springs are being compressed and the results vary as more of the base layer is engaged under the loads. FEAFAA can thus be reliably used for analysis in this study as actual layers thicknesses and material property can be defined. The differences in stresses using a 2D and 3D-FE analysis program were also observed in a study conducted to predict top down cracking of rigid airfield pavements (Evangelista and Roesler, 2010). The next section describes the analysis using four different aircrafts to study the effect of gear configuration and gear position on LTE using FEAFAA.

7.4 FEAFAA analysis

Different aircrafts were chosen to cover different wheel configuration namely Airbus A 380 (TDT), Boeing 777-200 baseline (TDT), Boeing 747-400 ER passenger (DT), DC-9-51 (DW). In addition, a single wheel footprint was also considered to study the effect of single wheel gear or FWD plate load. A previous study on parametric sensitivity using layered elastic design program showed that aircraft gross weight was one of the parameter the design life of rigid airfield pavements was highly sensitive to (Garg et al., 2006). The aircraft selected in this analysis cover a broad range of gear configurations and aircraft gross weights the details of which are tabulated in table 18. The layout of wheels with axle and wheel spacing is shown in figure 28 below.

A 15 feet x 15 feet slab was modeled in FEAFAA and the joints were assigned a stiffness value of 60 ksi. The aircrafts were place at the edge of the slab with the wheel tangential to the joint. When the main axis of the gear was oriented perpendicular to the joint the gear position was referred to as perpendicular while in the case when the main axis was parallel to the joint the gear position was referred to as parallel.

TABLE 18: Type of aircraft gears with gross weight of aircrafts considered in the analysis

Aircraft	A380	B777	B747	DC-9	FWD
Type of gear	6-wheel	6-wheel	4-wheel	2 wheel	Single-wheel
Gross Weight (lbs.)	1,239,00	537,000	913,000	122,000	36,000

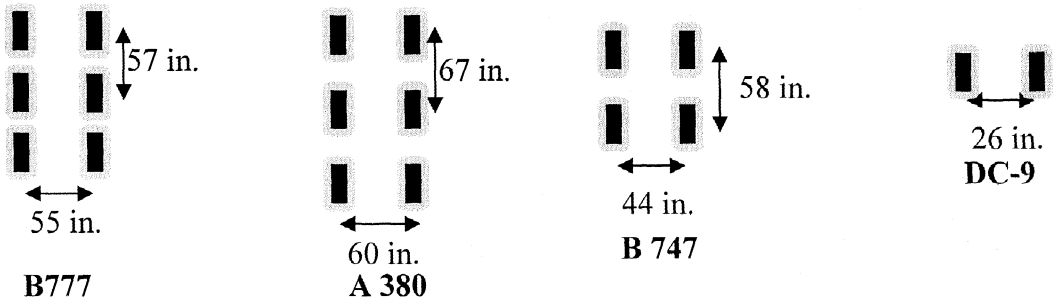

FIGURE 28: Aircraft gear configurations with wheel and axle spacing

The main purpose of this analysis was to study the effect of differential slab bending phenomena resulting in differential stress distribution under various gear configurations and positions along the slab edge. Figure 29 shows an example of Mises stresses in the slab in a 6-wheel and 4-wheel loading case in parallel position.

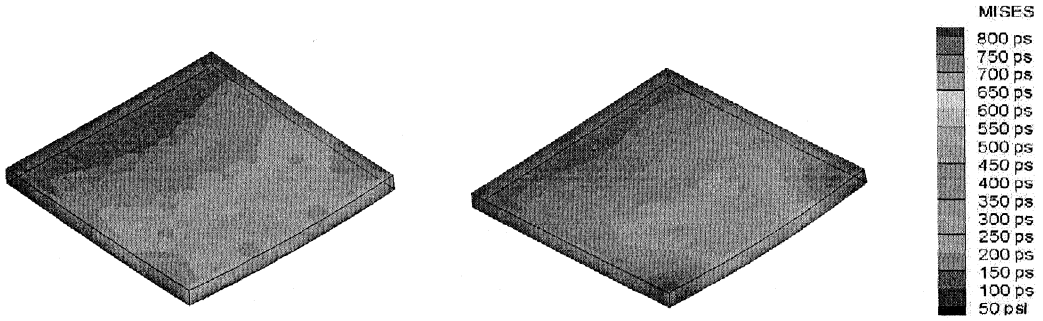

FIGURE 29: Differential stress distribution under a 6-wheel and 4-wheel loading case in parallel position.

Maximum stresses and deflection values were noted at a distance of 6 inches away from the joint on the loaded and unloaded side in order to compute the LTE (S) and LTE (δ) for the different aircrafts considered in the analysis. Table 19 shows the values of stresses and deflections and LTE values under a perpendicular gear position for various aircrafts while table 20 shows the same in parallel gear position.

TABLE 19: Stresses and deflections for various aircrafts under perpendicular position

Aircraft Type	Stress (psi)		LTE(S)	Deflection (in.)		LTE(δ)
	Loaded	Unloaded		Loaded	Unloaded	
Boeing 777	631.01	322.35	0.34	0.090	0.079	0.88
Boeing 747	781.97	394.74	0.34	0.105	0.092	0.88
DC-9-51	386.05	196.01	0.34	0.038	0.034	0.90
A380	1142.03	580.30	0.34	0.180	0.157	0.87
FWD (single plate)	432.74	147.58	0.25	0.025	0.022	0.88

TABLE 20: Stresses and deflections for various aircrafts under parallel position

Aircraft	# of Loads *	Stress (psi)		LTE(S)	Deflection (in.)		LTE(δ)
		Loaded	Unloaded		Loaded	Unloaded	
Boeing 777	3	556.45	323.37	0.37	0.110	0.101	0.92
Boeing 747	2	742.29	375.23	0.34	0.109	0.099	0.91
DC-9-51	1	497.37	191.68	0.28	0.036	0.031	0.87
A380	3	954.88	514.54	0.35	0.225	0.208	0.92
FWD	1	425.48	155.54	0.27	0.025	0.022	0.88

*Number of loaded areas at the edge of the joint

The above tables showed that the LTE (S) was same for all the aircraft considered in the analysis except under a single plate loading. The stresses at the bottom and deflection at center of the slab were larger for the aircraft with higher gross weight. While no significant differences in LTE (δ) of a single wheel and other aircrafts considered were observed in perpendicular gear cases (also observed in JSLAB analysis, see figure 16), LTE (S) under a single wheel was lower by 27%. In case of single wheel loading, the stresses are concentrated at the center of slab and are a function of only one loaded area at the slab. However, for other type of aircraft gears the stress distribution along the slab edge is a function of two loaded areas with two wheels tangential to the joint. Thus it appears that more number of dowels are responsible for transmitting forces on the

unloaded slab as the number of loaded areas along the joint increased in case of 6, 4 or 2 wheel gear configurations as compared to a single wheel case.

In case of parallel gear position, the values of LTE (δ) for a single wheel and 2-wheel gear configuration were slightly lower than those under other types of gear configurations. The LTE (δ) was found to be similar only under a 2-wheel and single wheel configuration. LTE (S) under 2-wheel and a single wheel gear was also relatively lower than that under a 4-wheel and 6-wheel or single wheel gear load. Apparently, as mentioned above, more number of dowels are likely to transfer the forces to the unloaded slab as the load is dispersed over a larger area (more number of loaded areas) along the joints in parallel gear position. The effect of transmission of shear forces along the joint diminishing linearly from the center of joint has been discussed in the past (Ioannides & Korovesis 1992). The length along which the joint is effective in transmitting forces has been found to be a function of radius of relative stiffness. In this study, the effect of number of loaded areas along the joint edge on degree of load transfer has been highlighted. In the case of parallel position, the stresses along the joint are a function of three loaded areas for a 6-wheel gear and two loaded areas for a 4-wheel gear. However, under a single wheel or 2-wheel gear configuration the stresses along a joint edge are function of only one loaded area. Hence the load transfer efficiency drops in case of DC-9-51 and a single wheel aircraft gear. The effect of number of loaded areas is also noticeable by comparing the LTE values of individual aircrafts in perpendicular and parallel gear position. As the number of loaded areas along the joint edge increased in parallel position (B-777, A-380) the LTE values were also found to be slightly higher, however, the values dropped as the number of loaded areas in parallel position decreased (DC-9-51). No change in LTE values was observed in perpendicular or parallel position when the number of loaded areas along a joint edge was equal (B-747). Overall, the above trends suggest that LTE (S) of 25% was met in all the cases for the typical pavement structure considered in the analysis. Moreover, since the differences in LTE values were small, the various aircraft gear positions and gear configurations can be said to have minimal effect on load transfer efficiency of rigid airfield pavement joints and thus the correlation between LTE (S) and LTE (δ).

On a side note, it is also important to note that LTE (S) trend for parallel gear position from JSLAB and FEAFAA are contradictory. It was observed that LTE (S) drops in JSLAB but increased slightly in FEAFAA (Boeing 777 and A 380) under a parallel gear position as compared to a perpendicular gear case. The reasons for this difference can be attributed to difference between the selection of nodes for determining unloaded bending stress values in perpendicular gear case. While in JSLAB, the maximum unloaded slab stress was found to be at a node at the center of slab edge, the same in FEAFAA was found to be at a node corresponding to the maximum stress node on loaded slab (near the wheel loaded area). Table 21 shows the values of stresses and LTE (S) values under a perpendicular gear position for various aircrafts. The unloaded slab stresses in this case was taken at the node present at the center of the slab edge. The LTE (S) values remained same or were more than those in parallel gears case which was consistent with trend observed in JSLAB. However, FEAFAA proves to more appropriate tool to select the nodes and determine the stress values.

TABLE 21: Comparison of Stresses and LTE (S) with different node selection methods under perpendicular position

Aircraft Type	Center of Slab Edge Node			Corresponding Node		
	Stress (psi)		LTE(S)	Stress (psi)		LTE(S)
	Loaded	Unloaded		Loaded	Unloaded	
Boeing 777	631.01	353.00	0.36	631.01	322.35	0.34
Boeing 747	781.97	448.71	0.36	781.97	394.74	0.34
DC-9-51	386.05	208.78	0.35	386.05	196.01	0.34
A380	1142.03	665.61	0.37	1142.03	580.30	0.34
FWD (single plate)	432.74	147.58	0.25	432.74	147.58	0.25

7.5 Summary

The effect of aircraft gear configuration and gear position on load transfer efficiency of joint was studied in this chapter using 3D-FE program FEAFAA. LTE (S) under a single wheel was found to be lower by 27% as compared to the same under a 6-wheel, 4-wheel and 2-wheel gear configuration in perpendicular position. LTE of a joint was governed by the number of loaded areas along the joint. As the number of loaded areas increases in case of a parallel gear position, LTE of the joints slightly increases. Since the differences in LTE values were small, the various aircraft gear positions and gear configurations can be said to have minimal effect on load transfer efficiency of rigid airfield pavement joints and thus the correlation between LTE (S) and LTE (δ). Overall, LTE (S) criterion of 25% was met for all the aircraft gears considered in the analysis. The next chapter summarizes the finding of this study.

CHAPTER 8

Summary of findings, conclusions and recommendations

The study examined the effect of different load types (static versus moving), various aircraft gear configuration and gear position on the load transfer efficiency of joints. The impact of the above effects on commonly used correlations between stress-based and deflection-based load transfer efficiency was studied. The research team successfully used the accelerated pavement tests data and the finite element analysis to demonstrate the changes in stress and deflection based LTE considering the above mentioned effects. The findings on the study and recommendations for future testing at FAA's NAPTF are listed in this chapter.

8.1 Summary of findings

1) From the analysis of concrete strain gage data, it was observed that average value of LTE (S) of CC2 test item joints were similar and of the order 0.46 during the initial phase of trafficking.
2) On an average, the LTE (S) values from static loading were lower by 38% as compared to moving loads (dynamic).
3) Values of deflection based load transfer efficiency were found to be similar when measured under a HWD or 4-wheel/ 6-wheel gear configuration and was lower for stabilized base as compared to similar configuration of joints over non-stabilized base. The value of LTE (δ) was 0.71 for MRS (stabilized base), 0.81 for MRC (conventional base), and 0.86 for MRG (over subgrade).
4) The LTE (δ) of longitudinal joints was much higher than that of the transverse joint in spite of the joint configuration being the same in both cases.

5) The sum of deflection parameter almost remained a constant which was clear from significantly low coefficient of variation and as anticipated for a flat slab case. The strain gage records indicated that the sum of strains on either sides of the joint were constant for the initial phases of trafficking analyzed in this research.
6) In case of gears oriented perpendicular to the joint, gear configuration had no effect on load transfer efficiencies defined by stresses and deflections . However, in case of parallel gear position, while the LTE (δ) saw an insignificant increase under 6-wheel gear, the LTE (S) dropped by 6% on an average and LTE (σ) dropped by 9 % on an average for the three test items.
7) In case of 4-wheel loading, gear position had no impact on LTE in parallel or perpendicular as per the analysis carried out using 2D-FE analysis program JSLAB. However, in case of 6-wheel loading, while LTE (δ) in perpendicular position dropped by 5.7% on an average for the three test items, an increase of 7.7% on an average was observed for LTE (S) in perpendicular as compared to parallel gear position.
8) LTE (S) under parallel gear position using a 2-slab model was lower by 55% as compared to that using a 9-slab model when 15 feet x 15 feet slab was used. The same difference reduced to 11% when a 20 feet x 20 feet slab was used.
9) LTE (S) under a single wheel using 3D-FE program FEAFAA was found to be lower by 27% as compared to the same under a 6-wheel, 4-wheel and 2-wheel gear configuration in perpendicular position.
10) The difference between 2D-FE analysis (JSLAB) and 3D-FE analysis program (FEAFAA) may be due to a single value of spring constant that simulates a liquid foundation was modeled in JSLAB, and actual layer thicknesses with elastic moduli was defined in FEAFAA.
11) In the case of a single wheel loading, in JSLAB, a minimum number of springs are being compressed and the results (stresses and deflections) are similar between JSLAB and FEFAA.
12) In the case of 4 and 6 wheel loading a relatively large number of springs are being compressed. Therefore, the difference in stresses and deflections between

JSLAB and FEAFAA is greater as more of the base layer is engaged under the loads.

13) Overall, LTE (S) criterion of 25% compared well under all the static aircraft gears considered on typical pavement structures considered in the analysis.

8.2 Conclusions

The conclusions based on the summary of findings are as follows:

1) The LTE (S) under moving aircraft gear was significantly higher than under static loads. It would be imperative to consider a higher value of LTE (S) for thickness design of runways where the loads are moving.
2) The values of LTE (S) estimated from LTE (δ) measured by FWD and that calculated using finite element program for multiple wheel loads based on static analysis were similar. However, significant differences exist in the value of LTE (S) estimated from LTE (δ) and that directly measured under dynamic loading from full scale testing.
3) The differences in LTE values under various static aircraft gear configurations and positions along the joint were insignificant and their effect on joint LTE and ultimately the correlation between stress-based and deflection-based LTE was negligible.
4) The LTE of joint was influenced by slab size when a 2-slab model was used, however, the slab size was found to have no effect on LTE of joint when a 9-slab model was used in the analysis.
5) LTE of a joint was governed by the number of loaded areas along the joint. As the number of loaded areas increased in case of a parallel gear position, LTE of the joints slightly increased.
6) The value of 25% LTE (S) assumed in the current airfield design procedure compared well with the LTE (S) values under static aircraft gear loads computed using finite element programs considering variables in current airfields such as modern day aircrafts in various positions and different pavement structures.

7) The full scale test data collected during Construction Cycle 2 (CC2) initiated at FAA's National Airport Pavement Test Facility proved to be an excellent source of data for the research.

8.3 Recommendations

From the above study, it is clear that the commonly used correlations between LTE(S) and LTE (δ) can be conveniently used in field evaluation of joint load transfer. However, the correlations are valid only for a static aircraft gear loading. A value of 25% load transfer efficiency assumed in the thickness design of airfield pavements is found to be appropriate under different kinds of modern day aircraft gears and typical pavement structures considered. From the analysis of recent available full scale test data, the study indicates that 25% stress-based load transfer efficiency value is conservative under a moving aircraft gear load. Following are some recommendations for future full scale testing of airfield pavements pertaining to load transfer efficiency.

1) More full scale testing under a static aircraft gear load is require to understand the degree of load transfer based on stresses under a static gear loading.
2) Vertical displacement transducers (VDT) shall be installed near the joints, in addition to the concrete strain gages (CSG) at an appropriate distance away from the concrete strain gages to record the deflections of the pavement slab under static or moving gear loads. Thus, actual deflection values under real airfield conditions can be recorded for computation of deflection-based load transfer efficiency.
3) The LTE (S) under moving loads was computed as the test vehicle travelled with its main axis perpendicular to the joint during the testing of CC2 test items. The effect of the case in which the test vehicle travels with its main axis parallel to the joint need to be studied to understand the joint load transfer efficiency under parallel moving gear position. This can be attained by installation of VDTs and CSGs at the longitudinal joints on either side of the joints.

4) It is important to understand whether low LTE leads to early cracking. Thus monitoring of cracking pattern recording the order of cracking as trafficking progresses becomes essential. In addition to visual distress surveys, mechanistic evaluation of cracking needs to be considered. This can be attained by installing the concrete strain gages at the top and bottom of the PCC slab thus providing information on whether the crack is just a surface or a full-depth crack.
5) The sensitivity of joint LTE on pavement thickness derived from FAA's thickness design program FAARFIELD needs to be studied under different aircraft traffic mixes and pavement layer configurations (using stabilized/ un-stabilized bases).
6) More research is needed to evaluate the damping effect due to moving aircraft wheel which probably results in higher value of LTE (S) under moving aircraft loading and ultimately lead to conservative thickness design.

REFERENCES

Ahlvin, R.G. (1991). "Origin of Developments for Structural Design of Pavements" *Technical Report GL-91-26*, US Army Corps of Engineers.

Brill, D.R. (1998). "Development of Advanced Computational Models for Airport Pavement Design" *Publication DOT/FAA/AR-97/47*. FAA, US Department of Transportation.

Brill, D.R. and Guo, E.H. (2001). "Load Transfer in Rigid Airport Pavement Joints" *Proceedings of the 26th International Air Transportation Conference*, San Francisco, June 18-21.

Evangelista, F. and Roesler, J. (2010). "Top-Down Cracking Predictions for Airfield Rigid Pavements" *2010 FAA Worldwide Technology Transfer Conference*, Atlantic City, New Jersey.

Federal Aviation Administration (1995). "Airport Pavement Design and Evaluation" *Advisory Circular 150/5320-6D.*

Federal Aviation Administration (2004). "Use of Nondestructive Testing in the Evaluation of Airport Pavements" *Advisory Circular 150/5370-11A.*

FAA (2009). "FEAFAA - 3D Finite Element Based Pavement Analysis Procedure" http://www.airporttech.tc.faa.gov/pavement/3dfem.asp

Garg, N. and Guo, E. (2006). "Parametric Sensitivity Analysis for the FAA's Airport Pavement Thickness Design Software LEDFAA-1.3" FAA Airport Pavement Working Group Meeting, AAR- 410, *FAA William J. Hughes Technical Center, Atlantic City, NJ.*

Galaxy Scientific Corporation (2004). "JSLAB 2004 User's Manual" Federal Highway Administration.

Guo, E.H., J.A. Sherwood and M.B Snyder. (1995). "Component Dowel Bar Model for Load Transfer Systems in PCC Pavements" *Journal of Transportation Engineering*, Vol.121, No.3, pp 289-298.

Guo, E.H. (2001). "Back-Estimation of Slab Curling and Joint Stiffness" *Proceeding of the 7th International Conference on Concrete Pavements,* Orlando, Florida, pp 39-54.

Guo, E.H. (2003). "Proof and Comments on Extensively Used Assumption in PCC Pavement Analysis and Evaluation." *ASCE Journal of Transportation Research*, 129 (2), 219-220.

Guo, E., and Marsey, W. (2001). "Verification of curling in PCC slabs at FAA National Airport Pavement Test Facility" The 2001 Airfield Pavement Specialty Conference.

Guo, E.H. (2009). "Joint Modeling for JPCP: Successes and Pending Problems" *Bearing Capacity of Roads, Railways and Airfields Conference (CD-ROM)*, University of Illinois and Urbana-Champaign, IL, USA.

Guo, H., Petch, F., and Ricalde, L. (2009). "Analysis of concrete pavement strain data and behaviour during joint formation" *International Journal of Pavement Engineering*, Vol 00, No. 00, pp 1-15.

Hall, K.T., and Mohseni A. (1991). "Back-calculation of Asphalt Concrete-OverlaidPortland Cement Concrete Pavement Layer Modulii" *Transportation Research Record: Journal of Transportation Research Board, No. 1293,*

Transportation Research Board of the National Academics, Washington D.C., 112-123.

Hammons, M.I. (1998). "Advanced Pavement Design: Finite Element Modeling for Rigid Pavement Joints, Report II: Model Development" *Publication DOT/FAA/AR-97/7.* FAA, U.S. Department of Transportation.

Hammons, M.I., Pittman, D.W., and Mathews, D.D. (1995). "Effectiveness of Load Transfer Devices" *Publication DOT/FAA/AR-95/80.* FAA, U.S. Department of Transportation.

Hayhoe, G. F. (2004). "Traffic Testing Results from the FAA's National Airport Pavement Test Facility" *2nd International Conference on Accelerated Pavement Testing*, University of Minnesota, Minneapolis, Minnesota.

Huang, Y.H. and Wang, S.T. (1973). "Finite Element Analysis of Concrete Slabs and its Implications for Rigid Pavement Design". *Highway Research Board, No. 446*, pp 55-69.

Huang, Y.H. and Chou, Y.T. (1978). "Discussion on Finite Element Analysis of Jointed or Cracked Pavements" *Transportation Research Record*, No. 671, pp 17-18.

Ioannides, A.M., and Korovesis, G.T. (1990). "Aggregate Interlock: A Pure Shear Load Transfer Mechanism" *Transportation Research Record No. 1286*, Transportation Research Board, Washington DC, pp 14-24.

Ioannides, A.M., and Korovesis, G.T. (1992). "Analysis and Design of Doweled Slab-On-Grade Pavement Systems" *Journal of Transportation Engineering*, 118, pp 745-768.

Kawa, I., Brill, D.R., and Hayhoe, G.F. (2007). "FAARFIELD – New Airport Thickness Design Software" FAA Worldwide Technology Transfer Conference. (CD-ROM), Atlantic City, NJ, USA.

Kawa, I., Guo, E.H., Hayhoe, G.F., and Brill, D.R. (2002). "Implementation of Rigid Pavement Thickness Design for New Pavements" FAA Technology Transfer Conference. (CD-ROM), Atlantic City, NJ, USA.

Khazanovich, L.,and Gotlif, A. (2005). "Evaluation of PCC Joint Stiffness Using LTPP Data" International Society for Concrete Pavements, 1120-1137.

Kreger, W.C. (1967) "Computerized Aircraft Ground Flotation Analysis – Edge Loaded Rigid Pavements" Research Report ERR-FW-572, Research Engineering Departments, General Dynamics.

Maitra, S.R., Reddy, K.S., and Ramachandra, L.S. (2009). "Load Transfer Characteristics of Dowel Bar system in Jointed Concrete Pavement" *Journal of Transportation Engineering*. Vol. 135, No. 11, pp 813-821.

"National Airport Pavement Test Facility" <http://www.airporttech.tc.faa.gov/naptf> (September 2008).

Nishizawa, T., Fukuda, T. and Matsuno, S. (1989). "A Refined Model of Doweled Joints for Concrete Pavement using FEM Analysis" Publication of Purdue University, pp 735-745.

Ricalde, L. (2007). "Analysis of HWD Data from CC2 Traffic Tests at the National Airport Pavement Test Facility" *FAA Worldwide Technology Transfer Conference*. (CD-ROM), Atlantic City, NJ, USA.

Ricalde, L. & McQueen, R. (2003). "Portland Cement Concrete Test Strip Pavement at The FAA National Airport Pavement Test Facility (NAPTF)" *Airfield Pavements. Challenges and New Technologies*, Las Vegas, Nevada, pp 217-230.

Sargand, S. (1998). "Validation of a Three-Dimensional Finite Element Pavement Model".

Shoukry, S. (2005). "Evaluation of Load Transfer Efficiency Measurement" *Publication WVU-2002-04*. Mid-Atlantic Universities Transportation Center.

Tabatabaie, A.M. and Barenberg, E.J. (1978). "Finite Element Analysis of Jointed or Cracked Concrete Pavements" *Transportation Research Board*, No. 671, pp 11-19.

Tayabji, S., and Colley, B., (1986). "Improved Rigid pavement Joints" *Publication FHWA/RD-86/040*. Federal Highway Administration.

Teller, L.W, and E.C. Sutherland (1935). "The Structural Design of Concrete Pavement Design Procedure" *Reprint from Public Roads*, Vol. 16, 17 and 23. 1935.

Yu, X., Zhou, Y., Peng, J., Tan, Z., Guo, E., (2010). "Joint Load Transfer Efficiency of Rigid Pavement Considering Dynamic Effects Under a Single Moving Load" *FAA Worldwide Technology Transfer Conference (CD-ROM)*, Atlantic City, NJ, USA.

War Department Corps of Engineers (1946). "Lockbourne No. 1 Test Track" *Ohio River Division Laboratories*, Mariemont, Ohio.

Appendix A

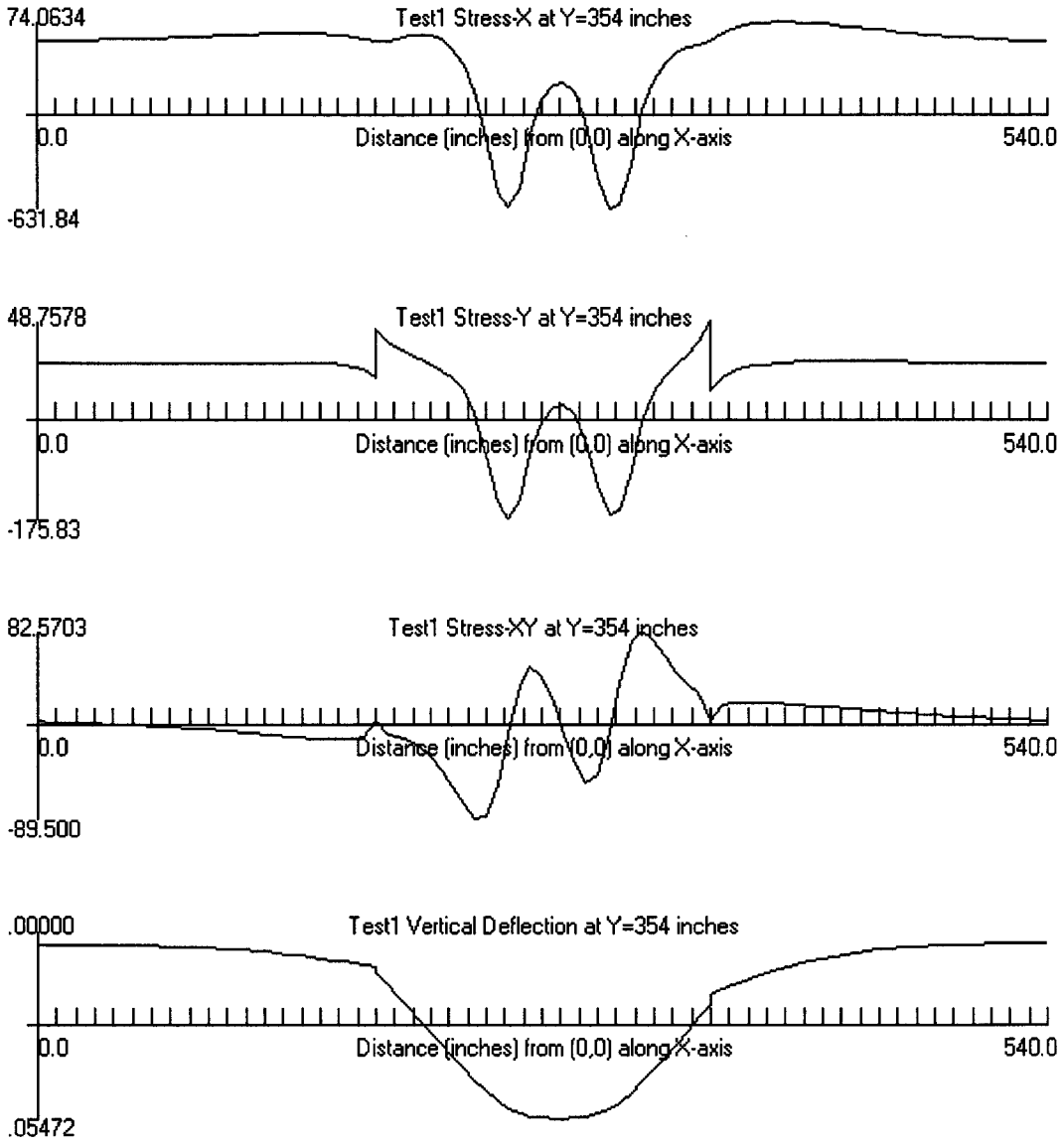

Figure B1: JSLAB output for MRC loaded 15ft slab under 4-wheel parallel loading

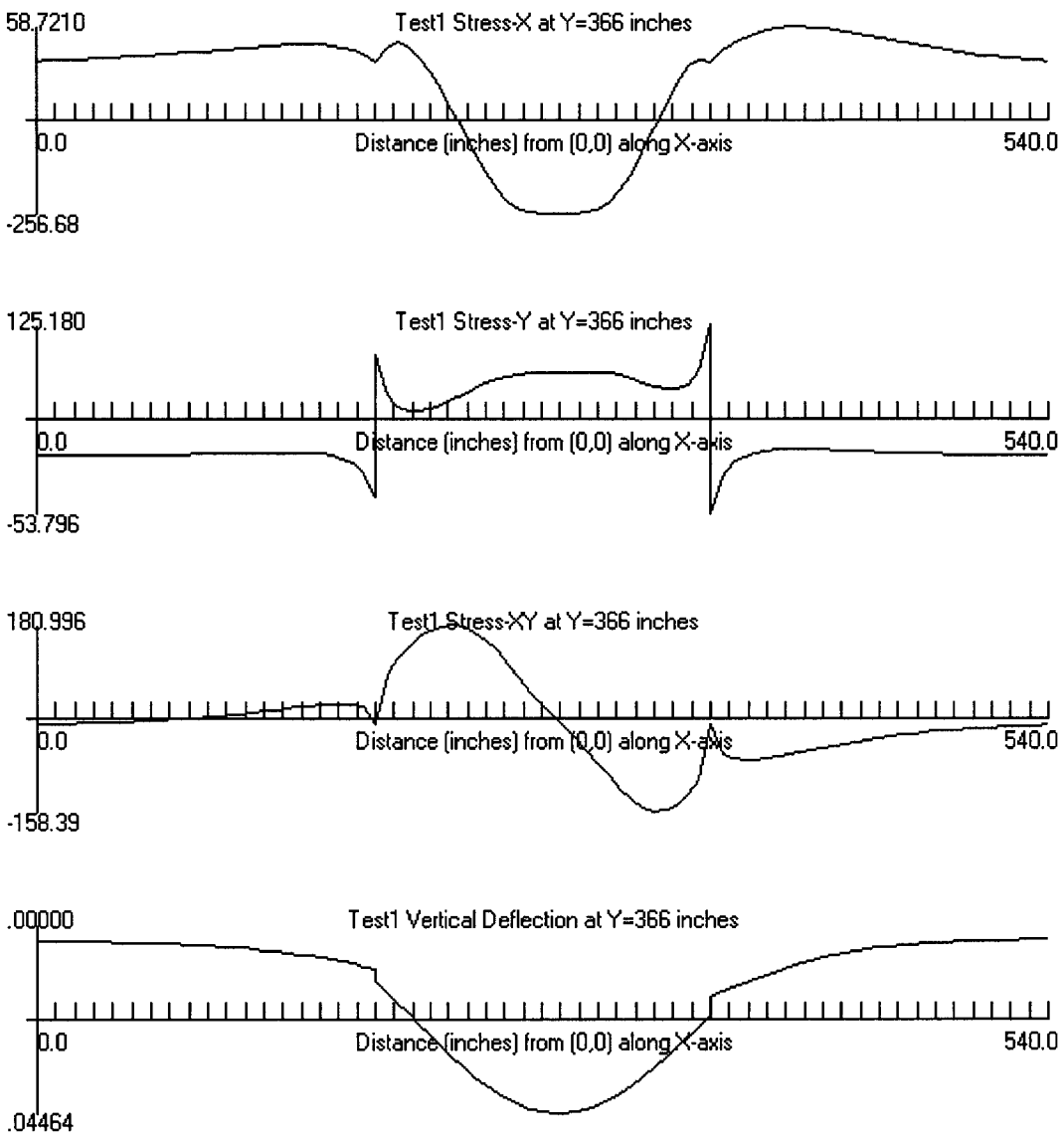

Figure B2: JSLAB output for MRC unloaded 15ft slab under 4-wheel parallel loading

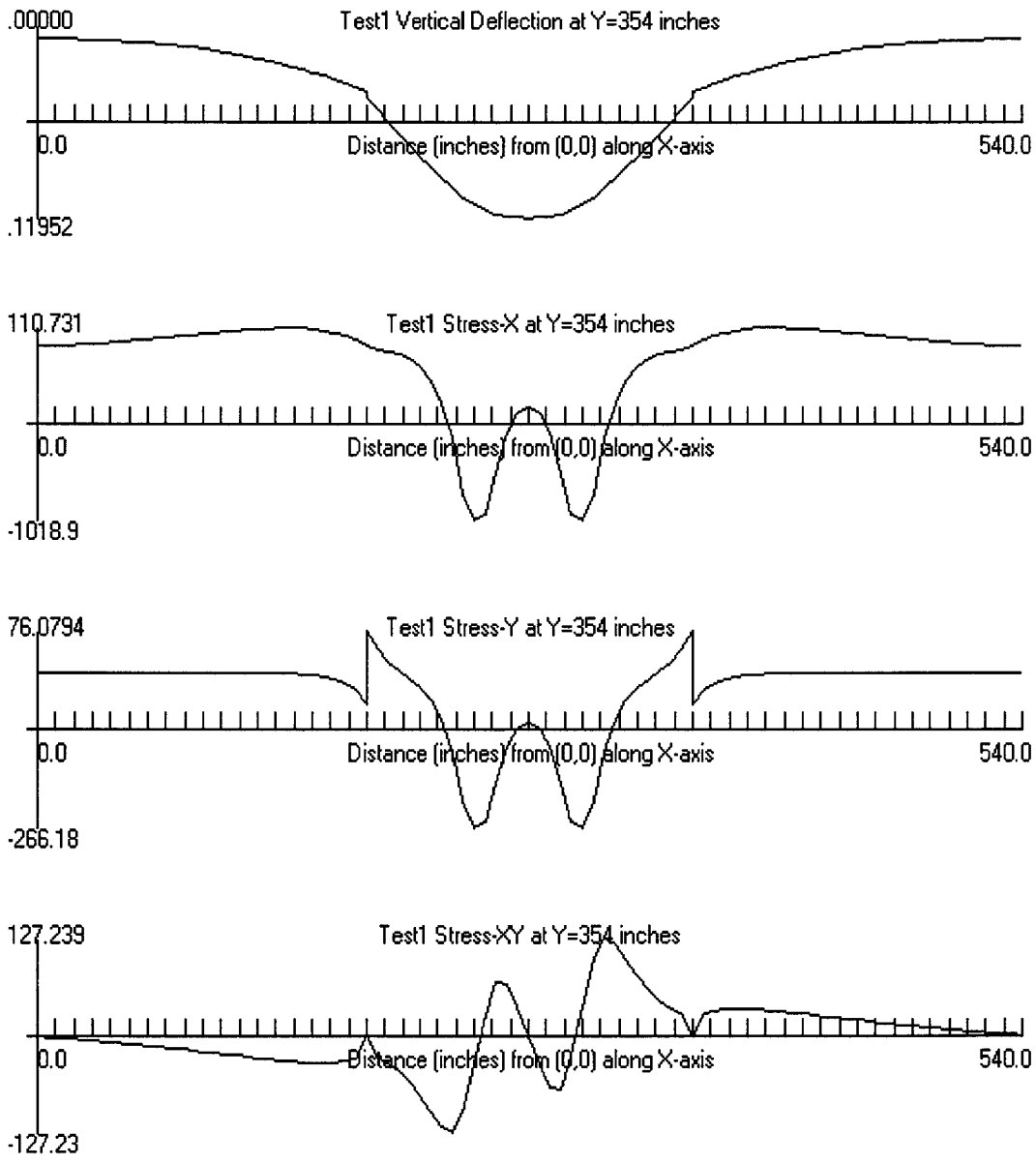

Figure B3: JSLAB output for MRG loaded 15ft slab under 4-wheel parallel loading

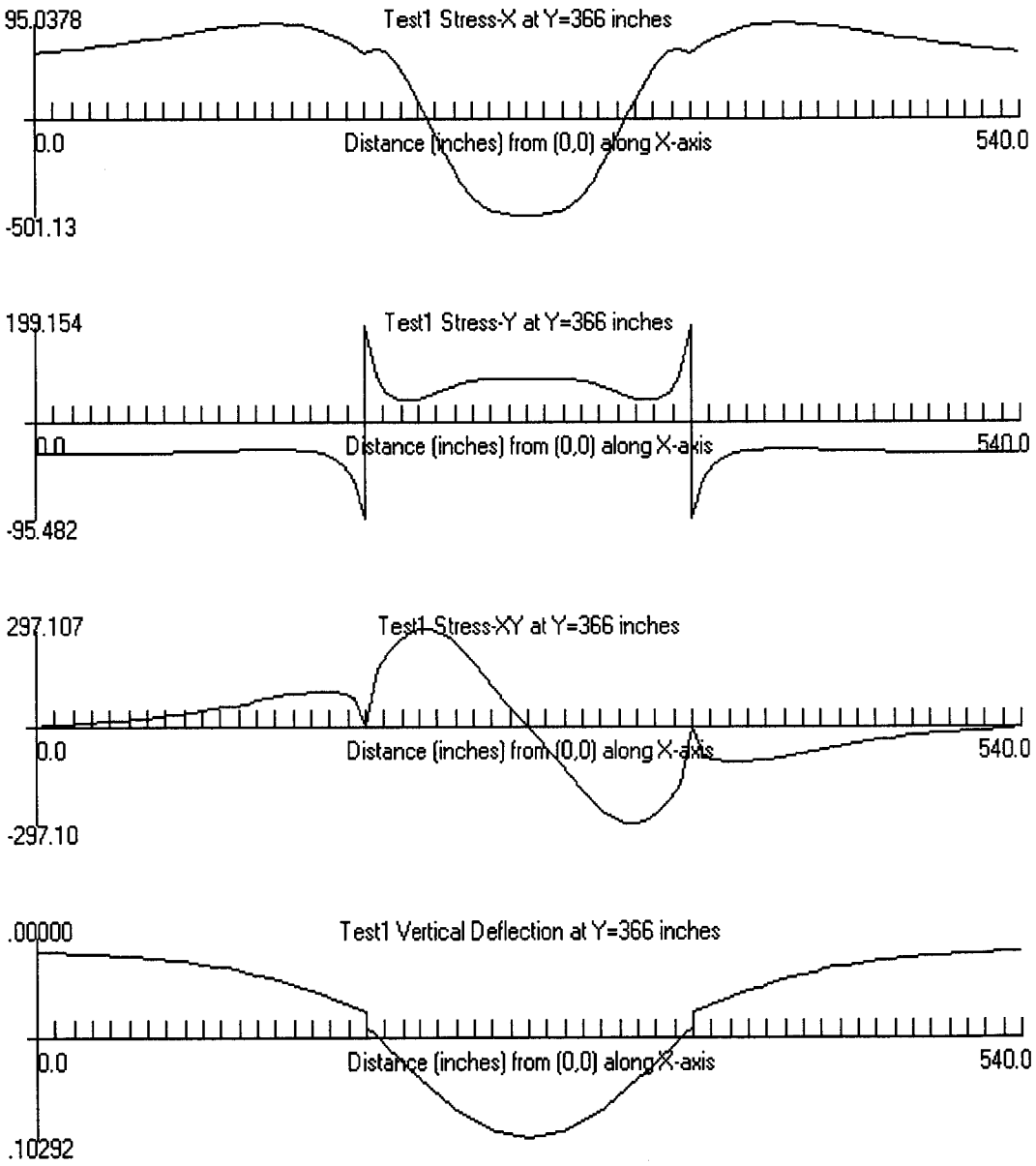

Figure B4: JSLAB output for MRG unloaded 15ft slab under 4-wheel parallel loading

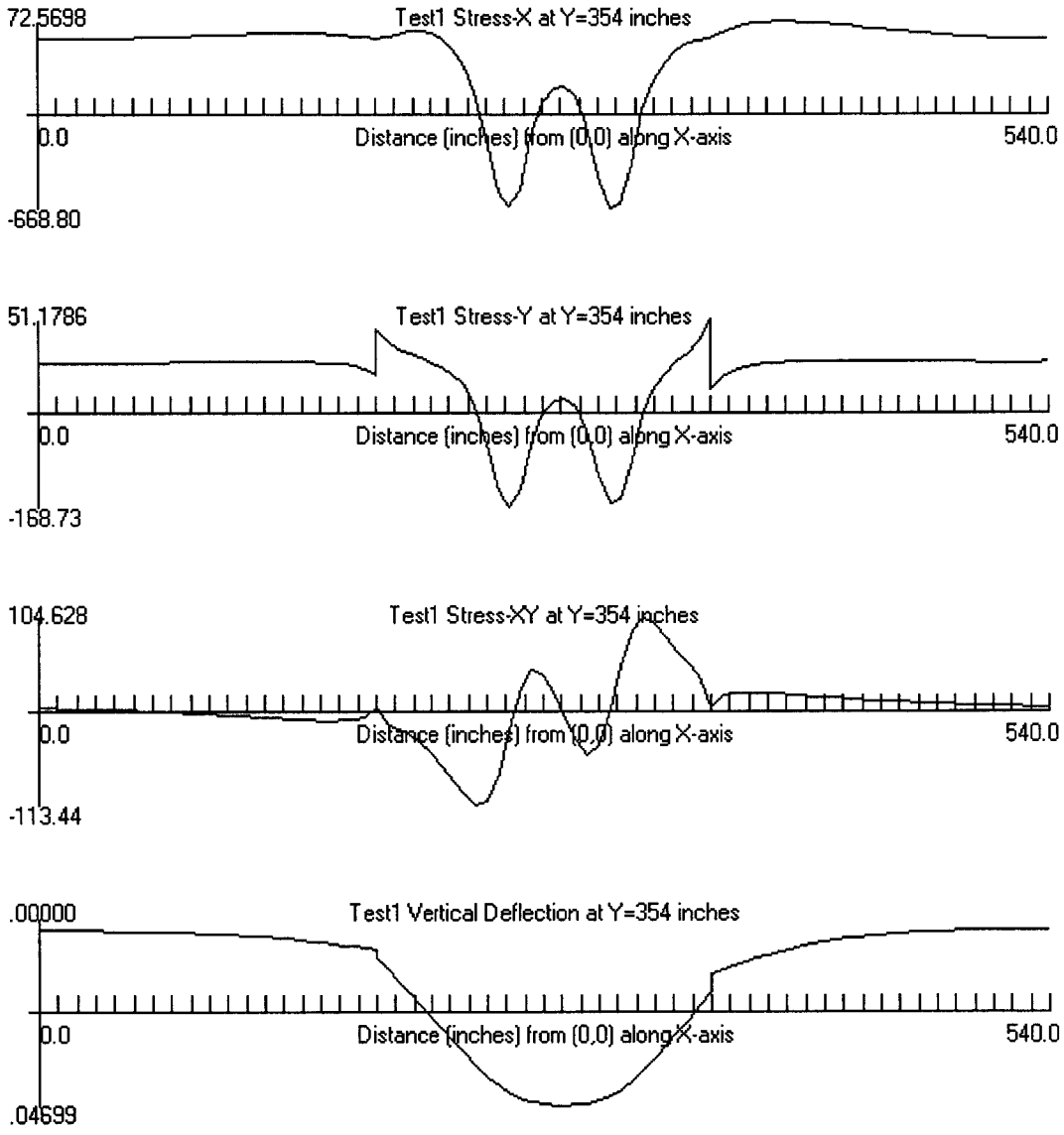

Figure B5: JSLAB output for MRS loaded 15ft slab under 4-wheel parallel loading

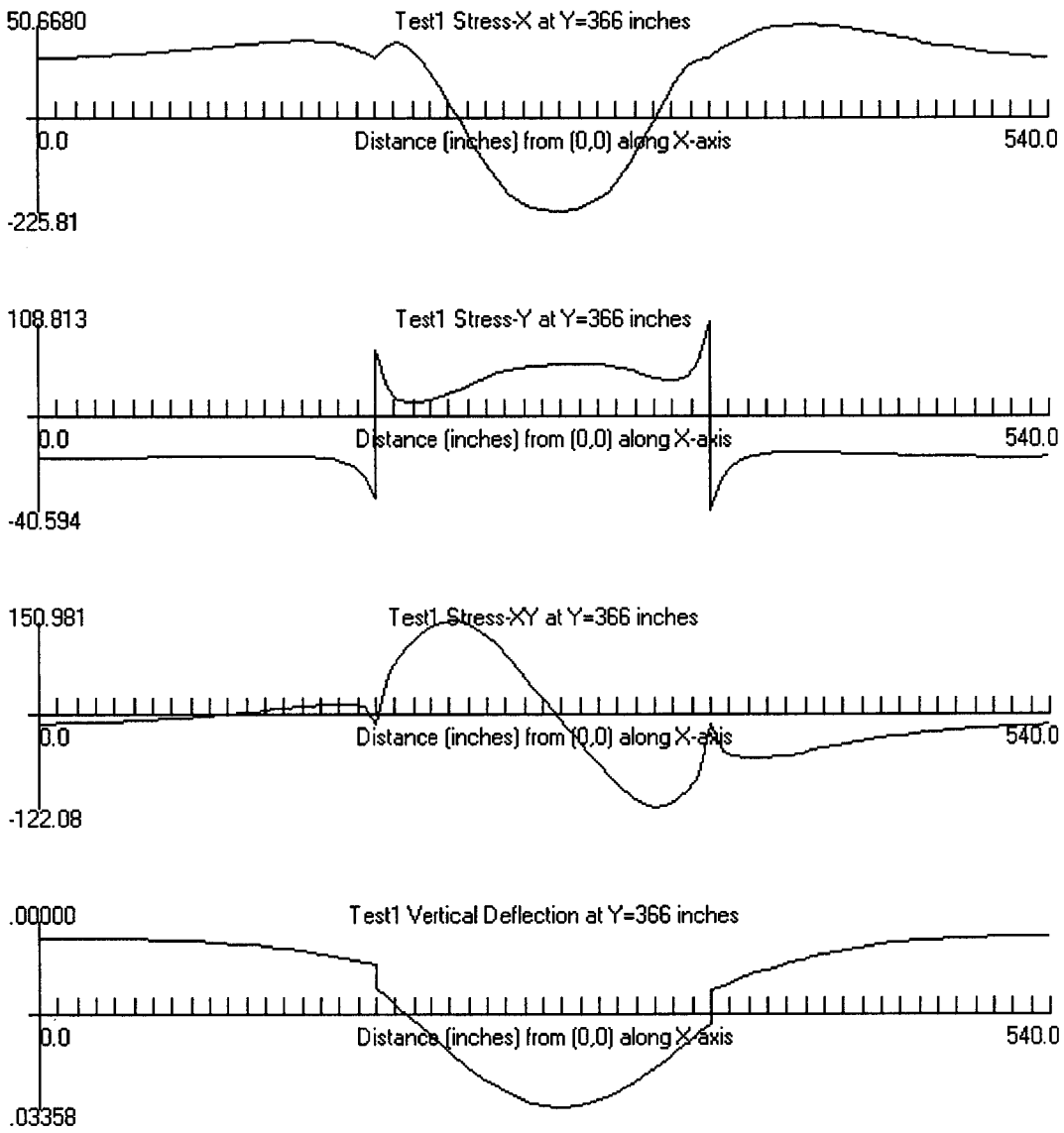

Figure B6: JSLAB output for MRS unloaded 15ft slab under 4-wheel parallel loading

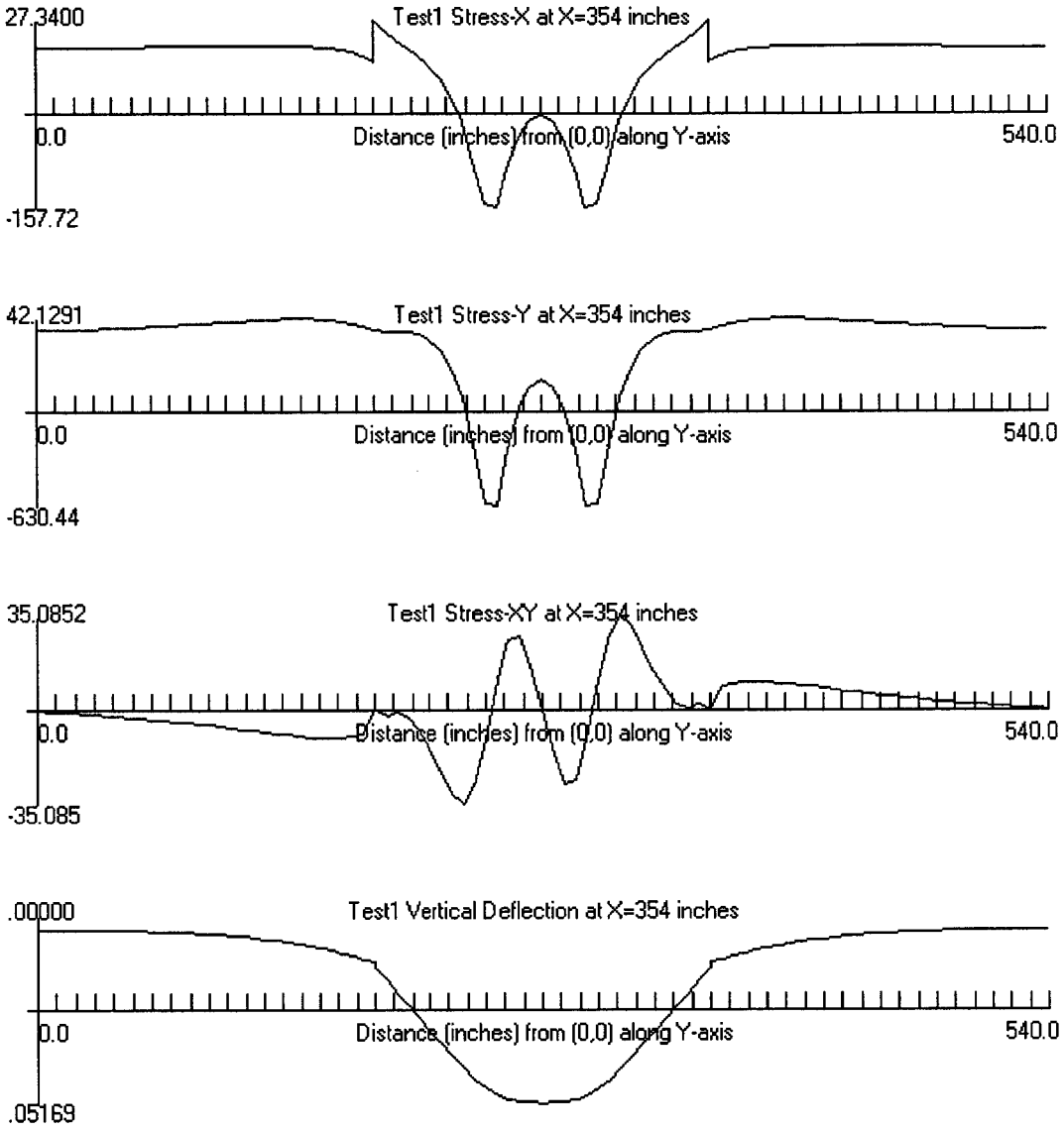

Figure B7: JSLAB output for MRC loaded 15ft slab under 4-wheel perpendicular loading

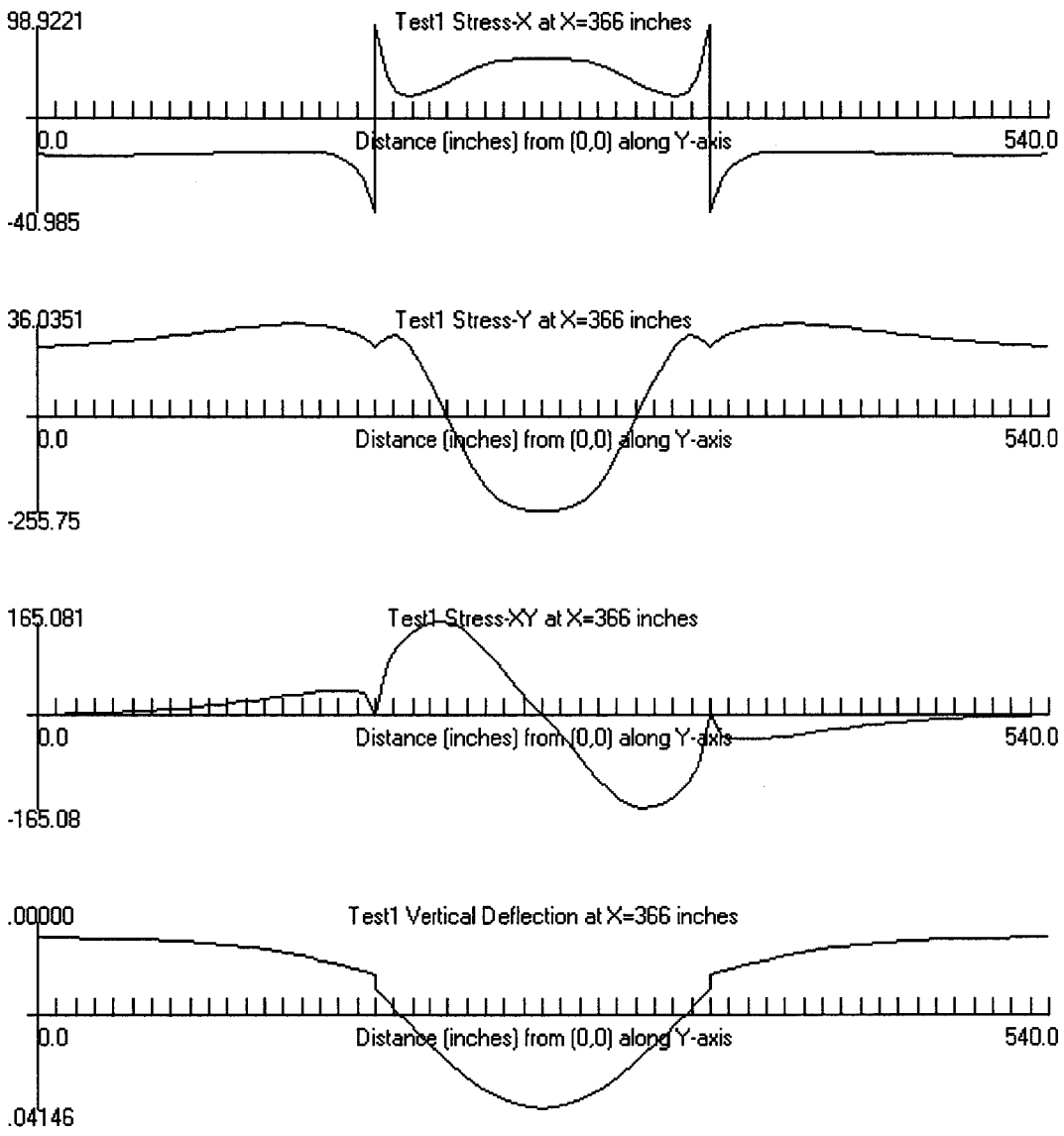

Figure B8: JSLAB output for MRC unloaded 15ft slab under 4-wheel perpendicular loading

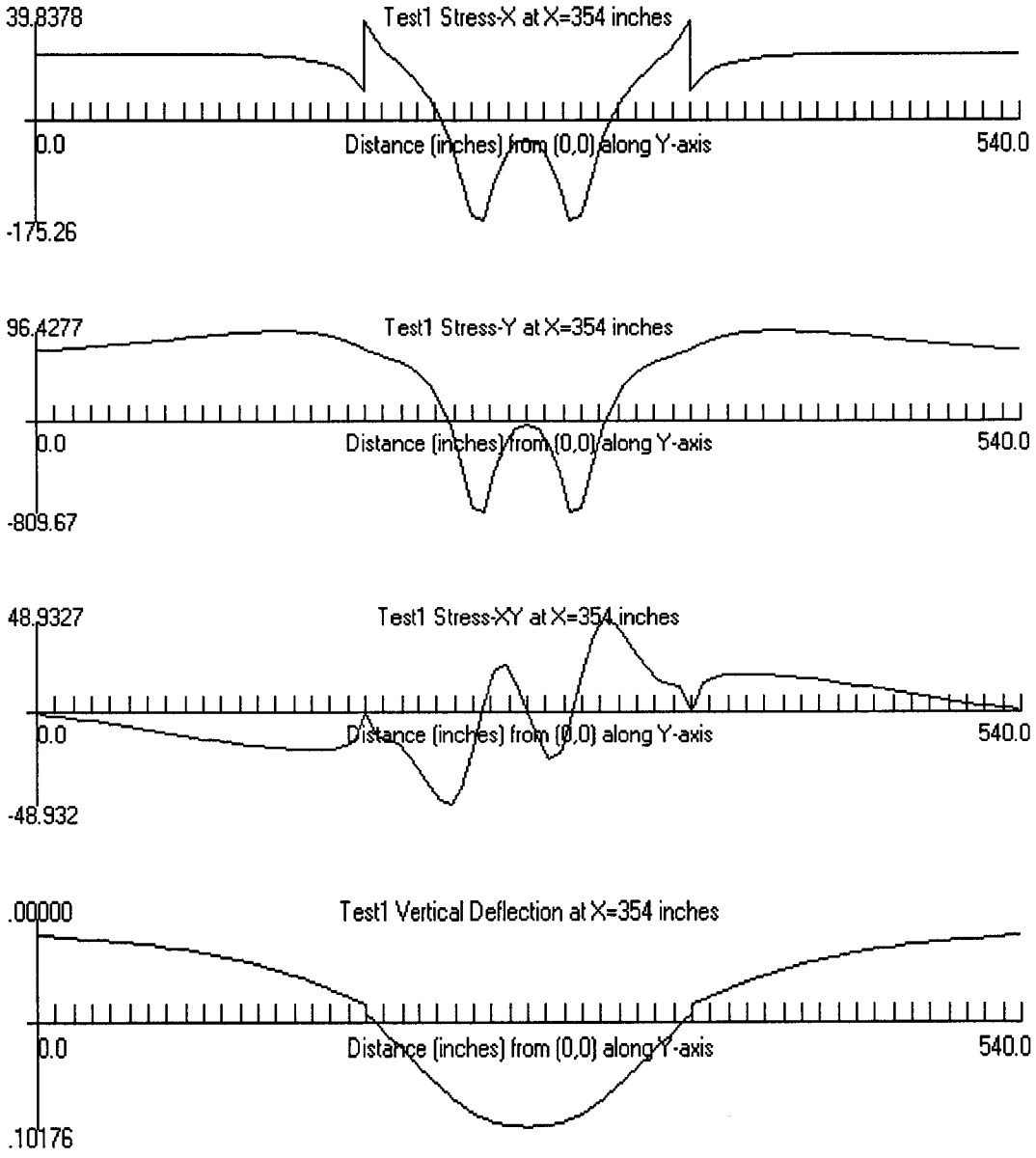

Figure B9: JSLAB output for MRG loaded 15ft slab under 4-wheel perpendicular loading

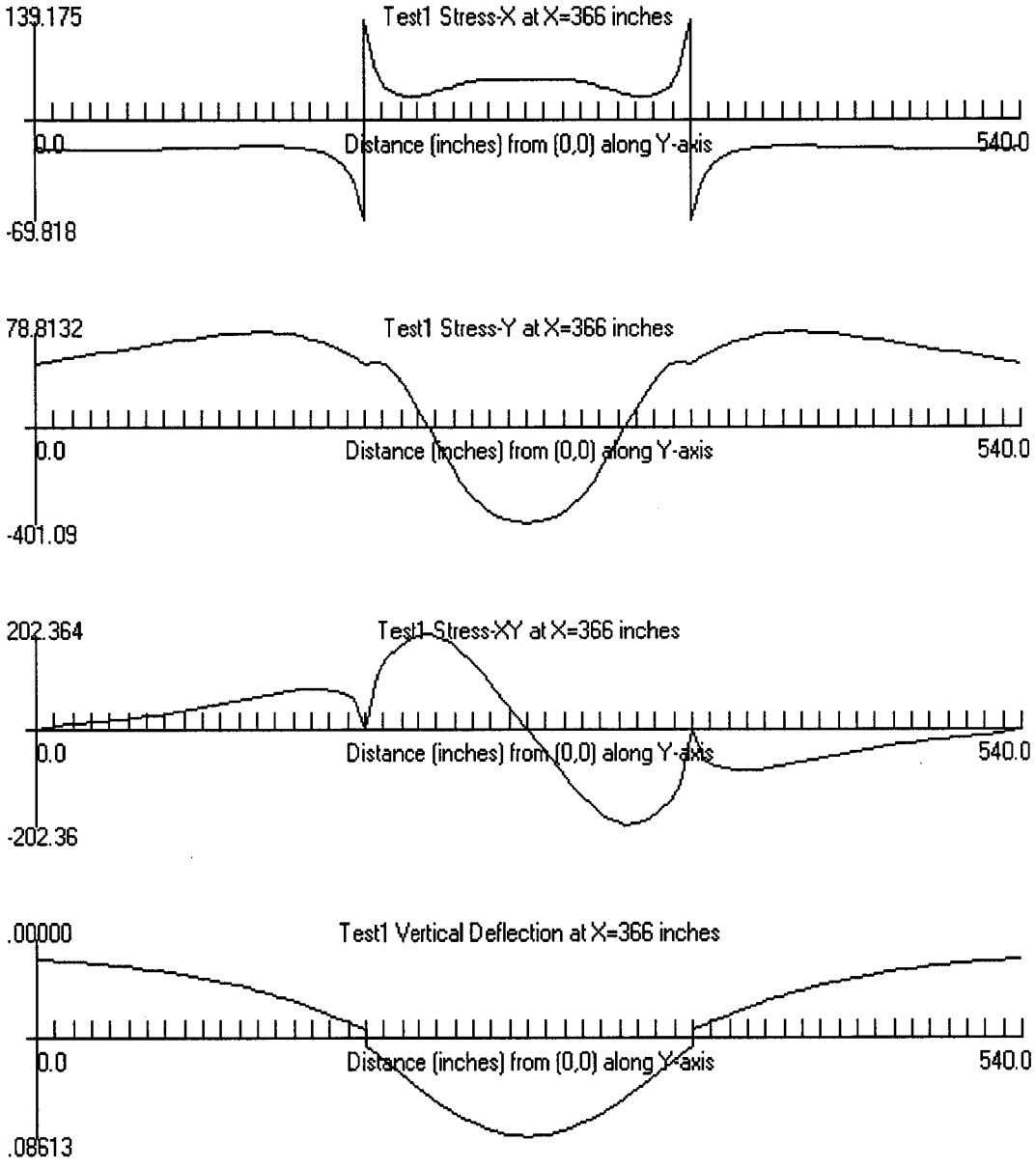

Figure B10: JSLAB output for MRG unloaded 15ft slab under 4-wheel perpendicular loading

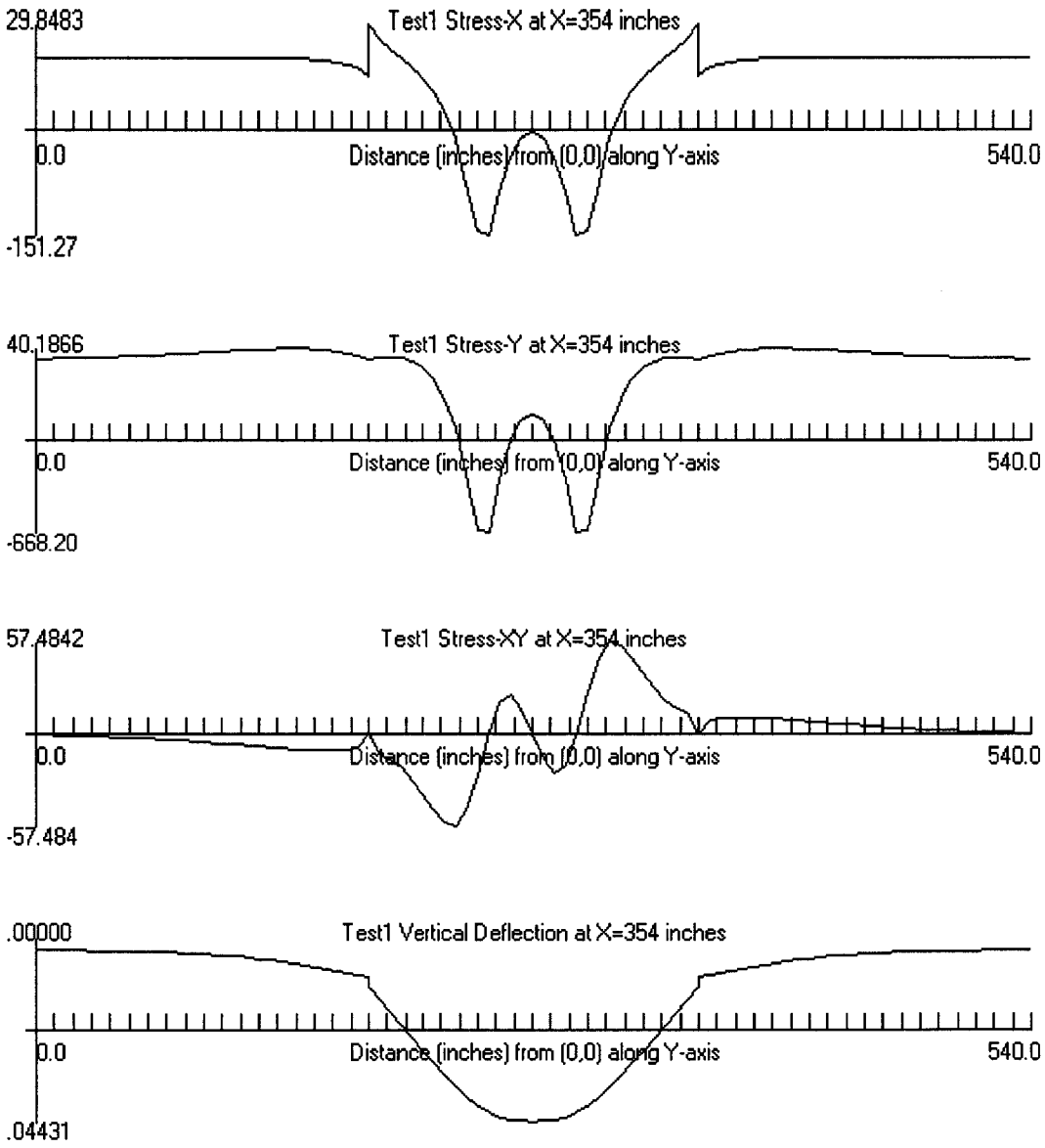

Figure B11: JSLAB output for MRS loaded 15ft slab under 4-wheel perpendicular loading

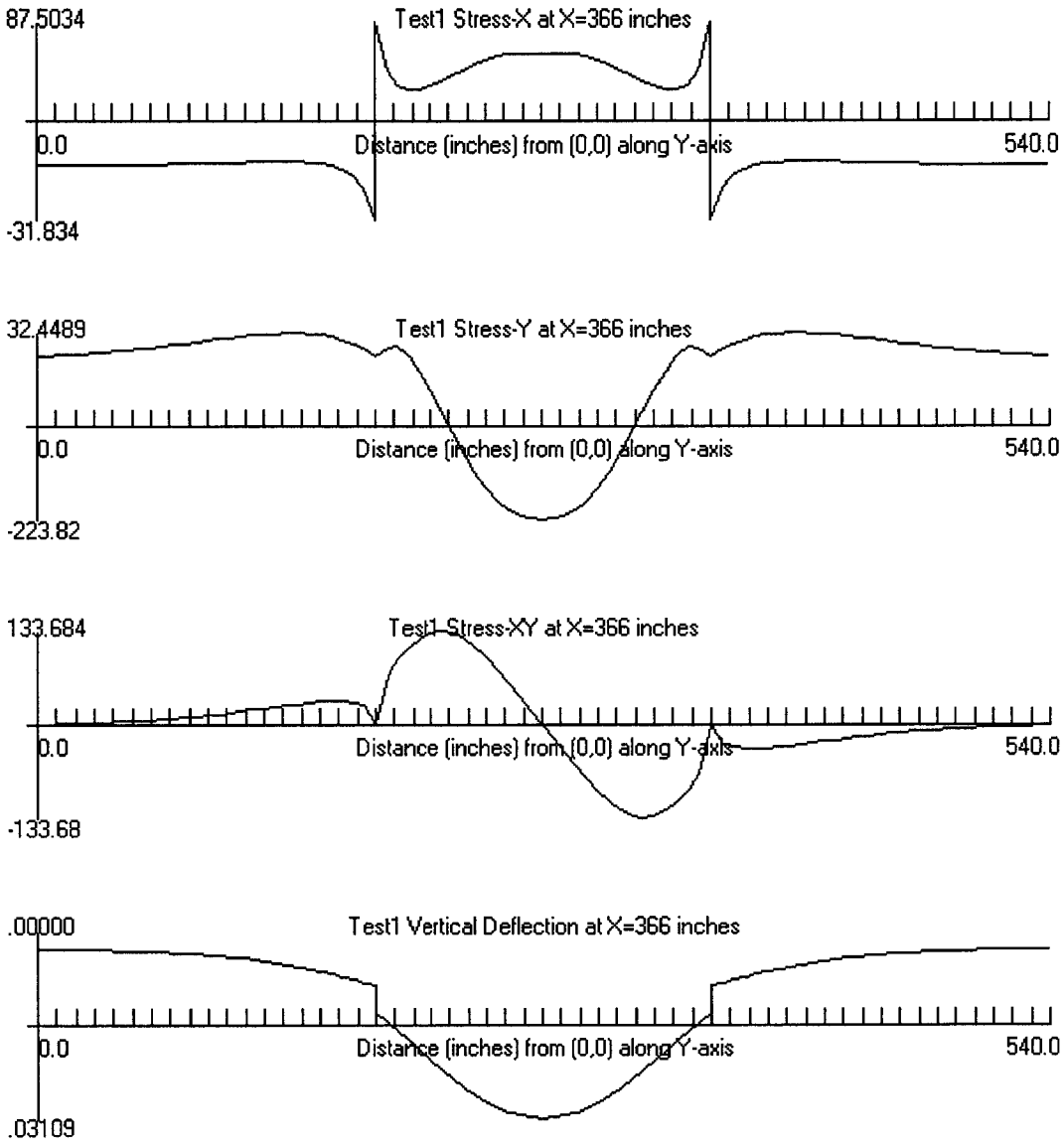

Figure B12: JSLAB output for MRS unloaded 15ft slab under 4-wheel perpendicular loading

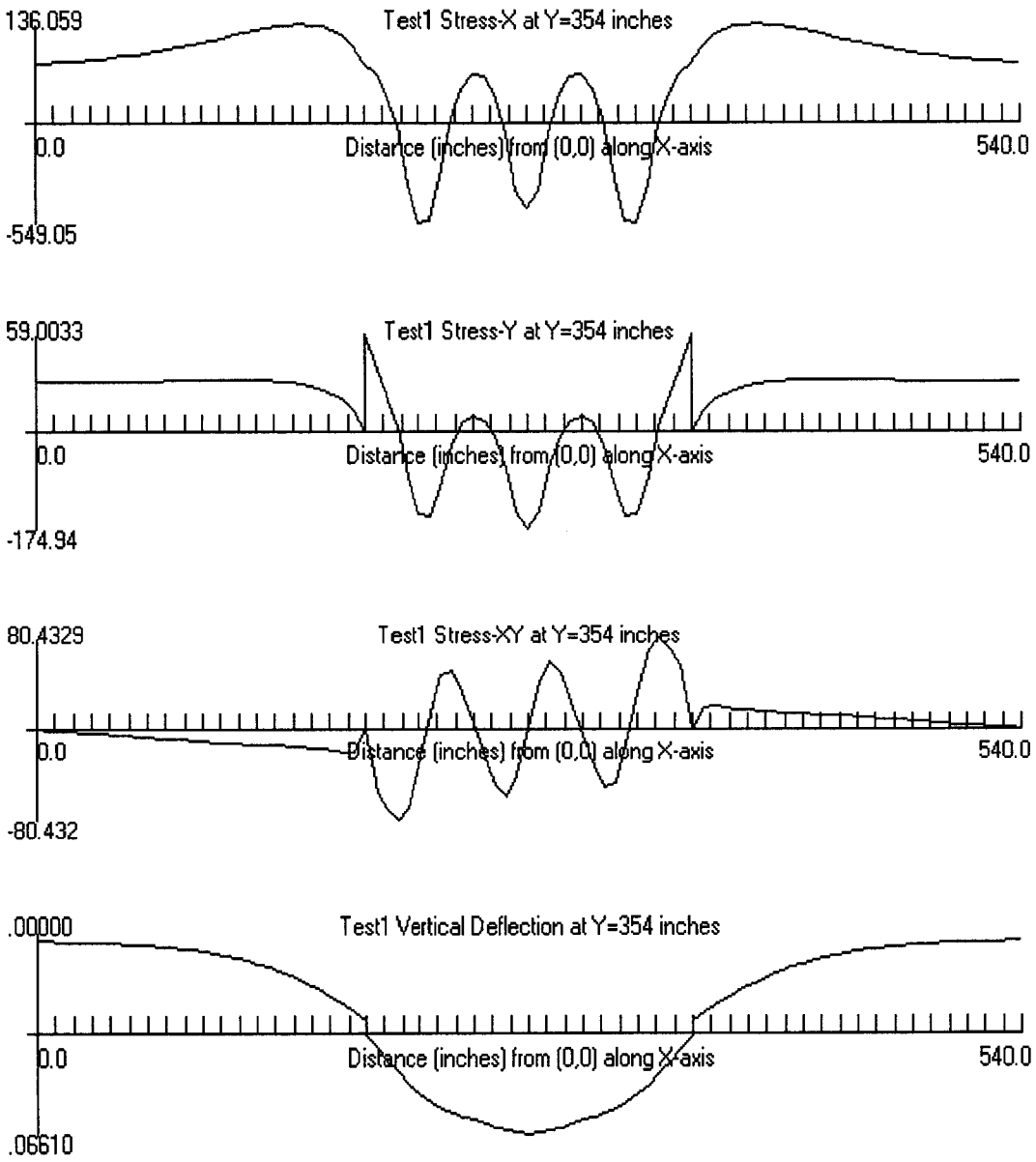

Figure B13: JSLAB output for MRC loaded 15ft slab under 6-wheel parallel loading

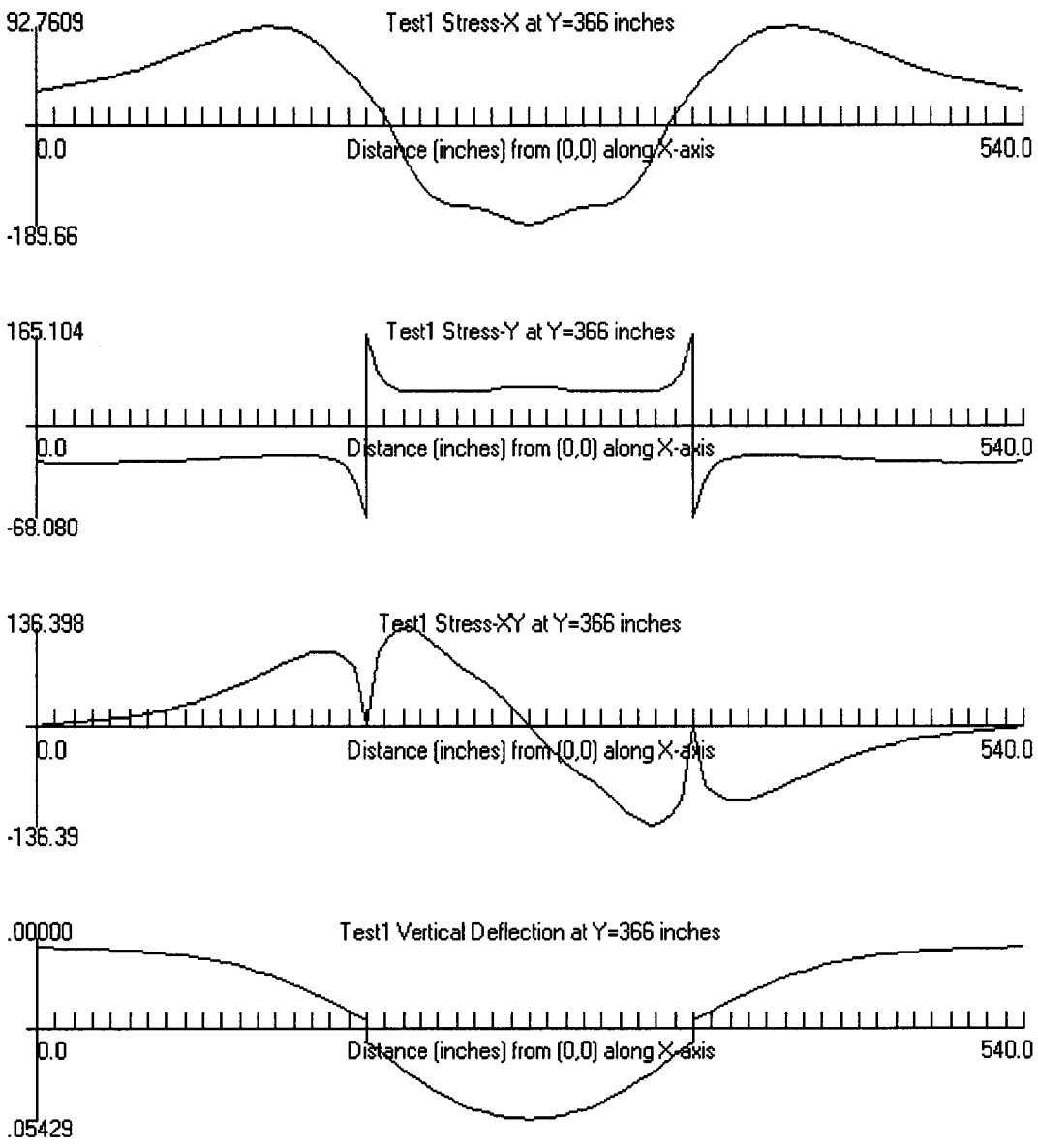

Figure B14: JSLAB output for MRC unloaded 15ft slab under 6-wheel parallel loading

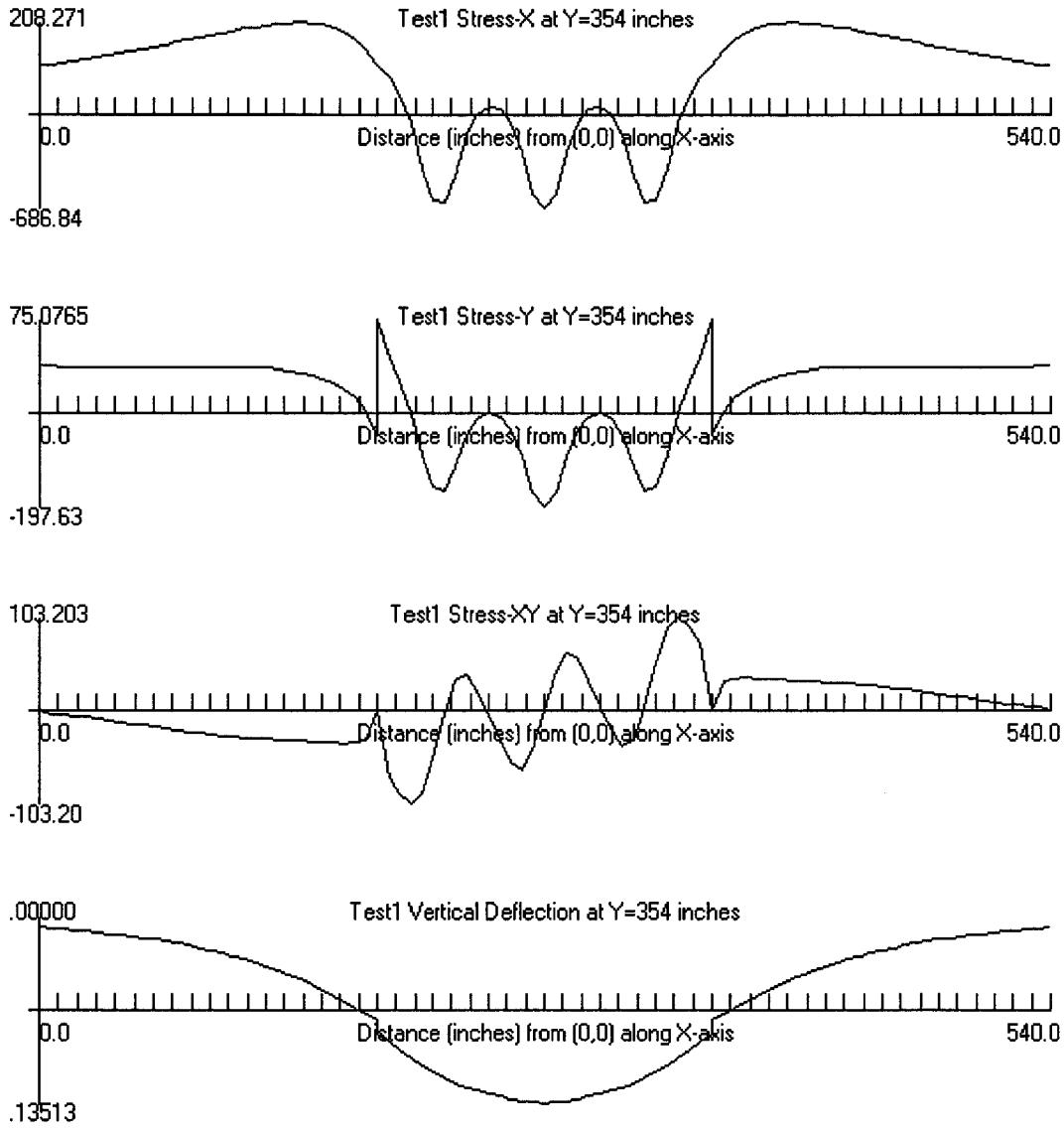

Figure B 15: JSLAB output for MRG loaded 15ft slab under 6-wheel parallel loading

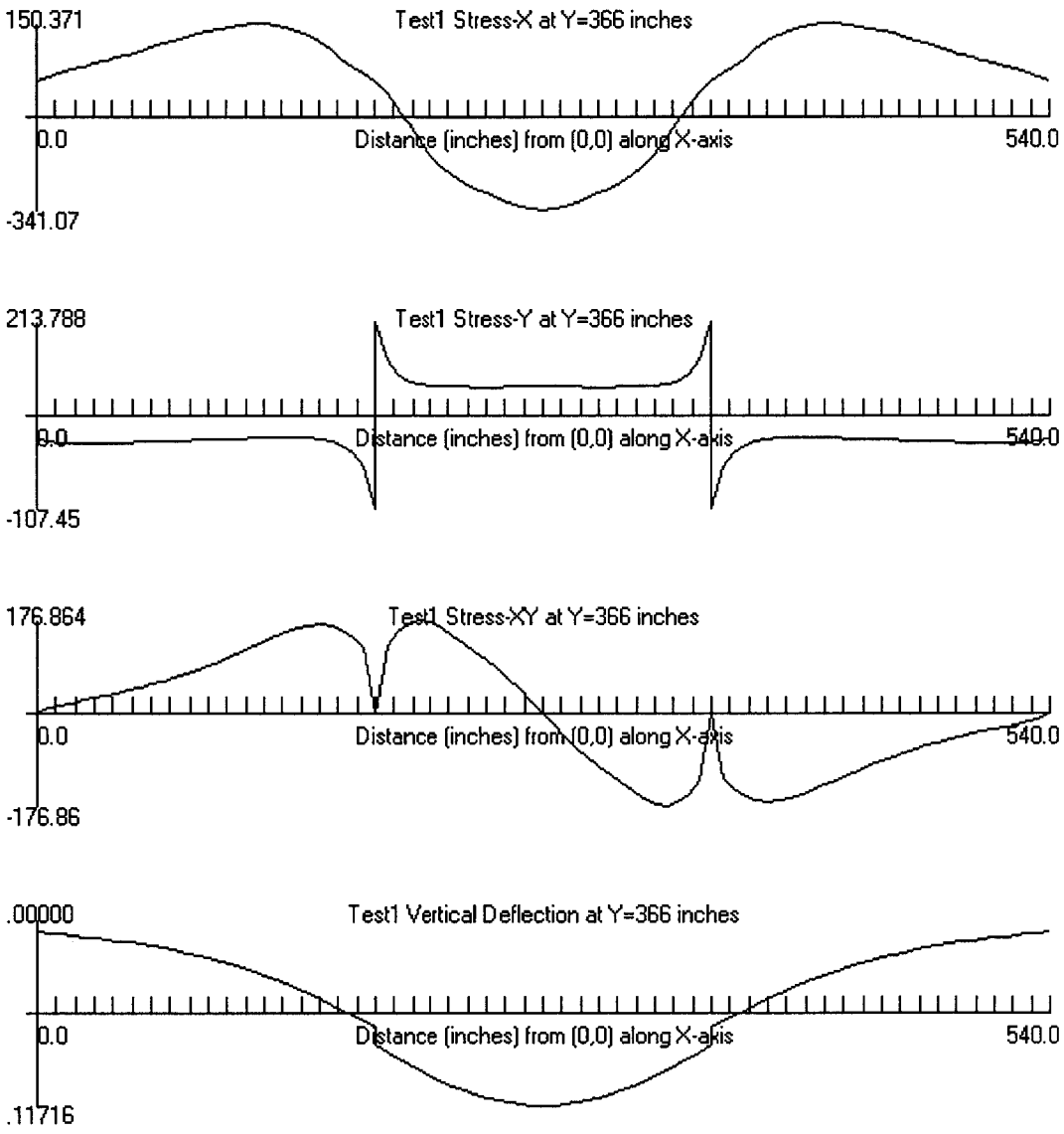

Figure B16: JSLAB output for MRG unloaded 15ft slab under 6-wheel parallel loading

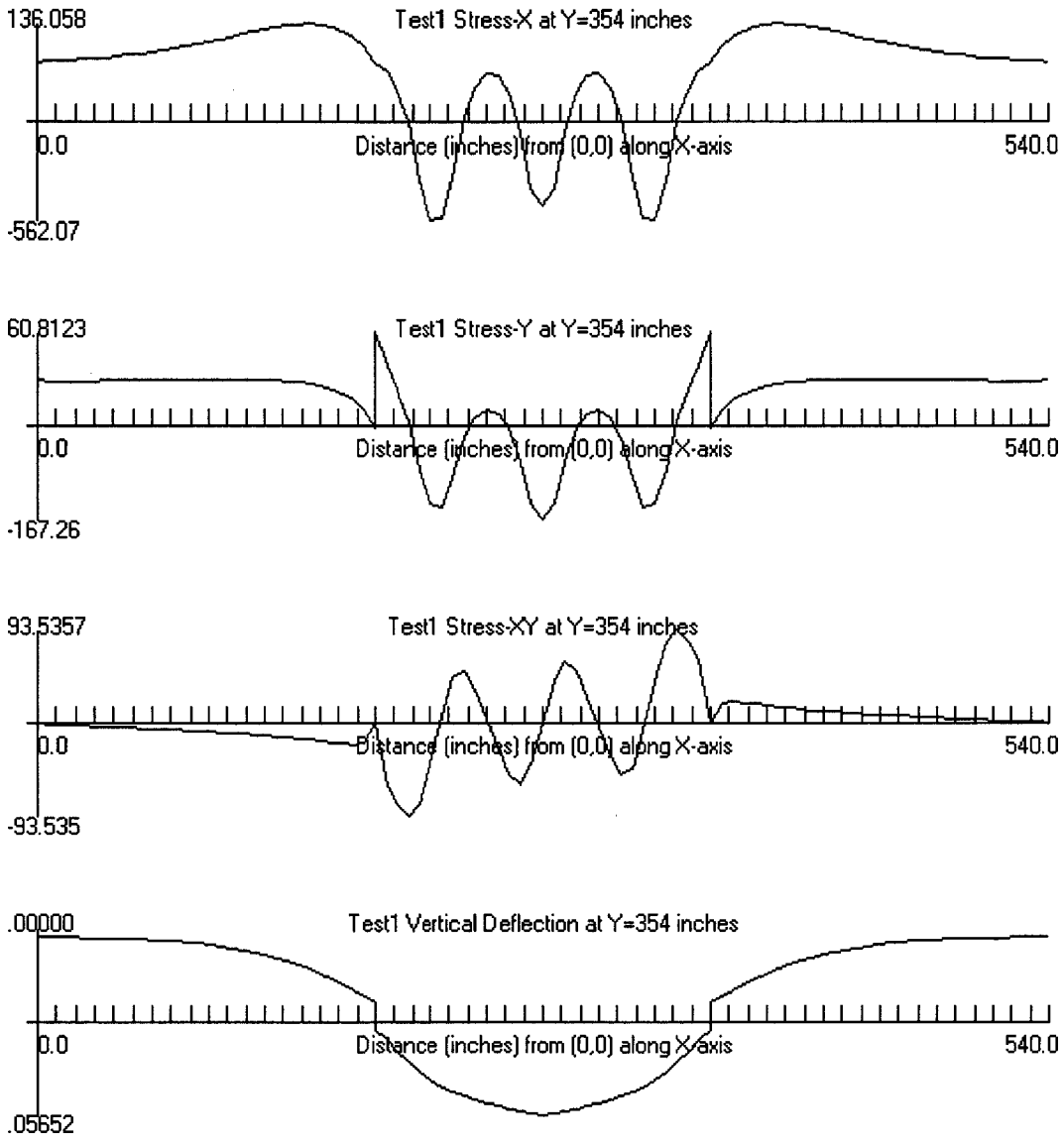

Figure B17: JSLAB output for MRS loaded 15ft slab under 6-wheel parallel loading

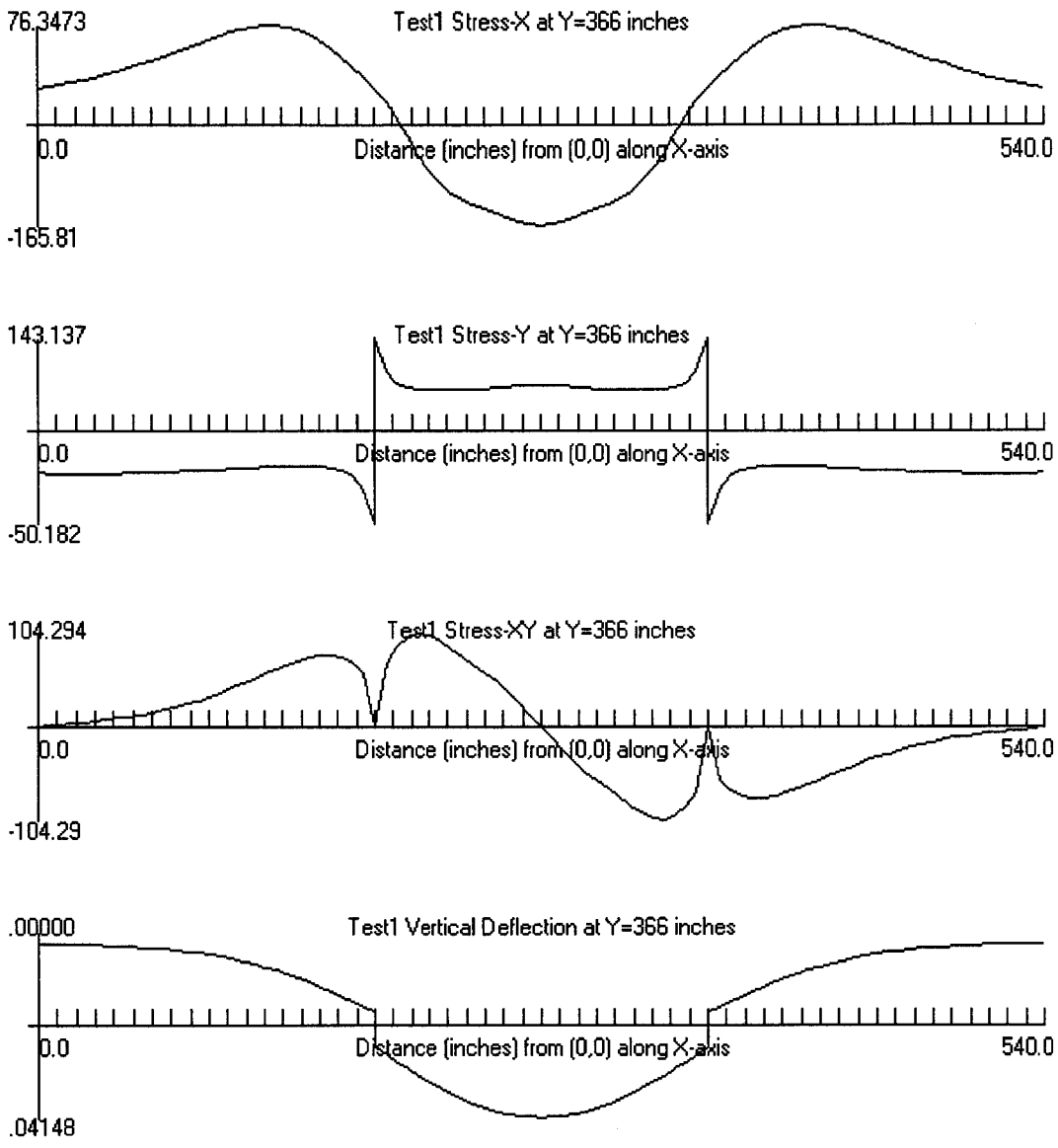

Figure B18: JSLAB output for MRS unloaded 15ft slab under 6-wheel parallel loading

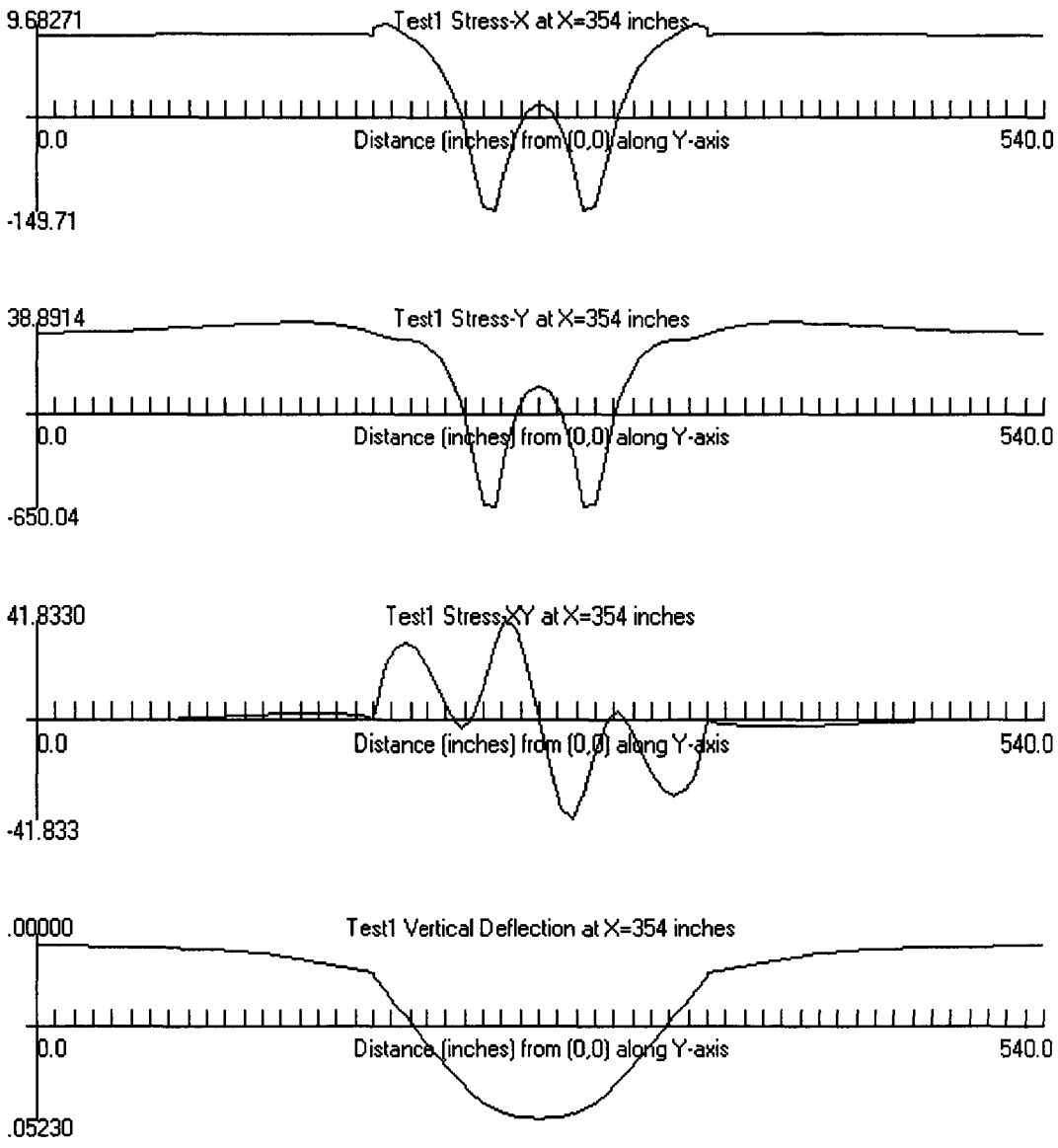

Figure B19: JSLAB output for MRC loaded 15ft slab under 6-wheel perpendicular loading

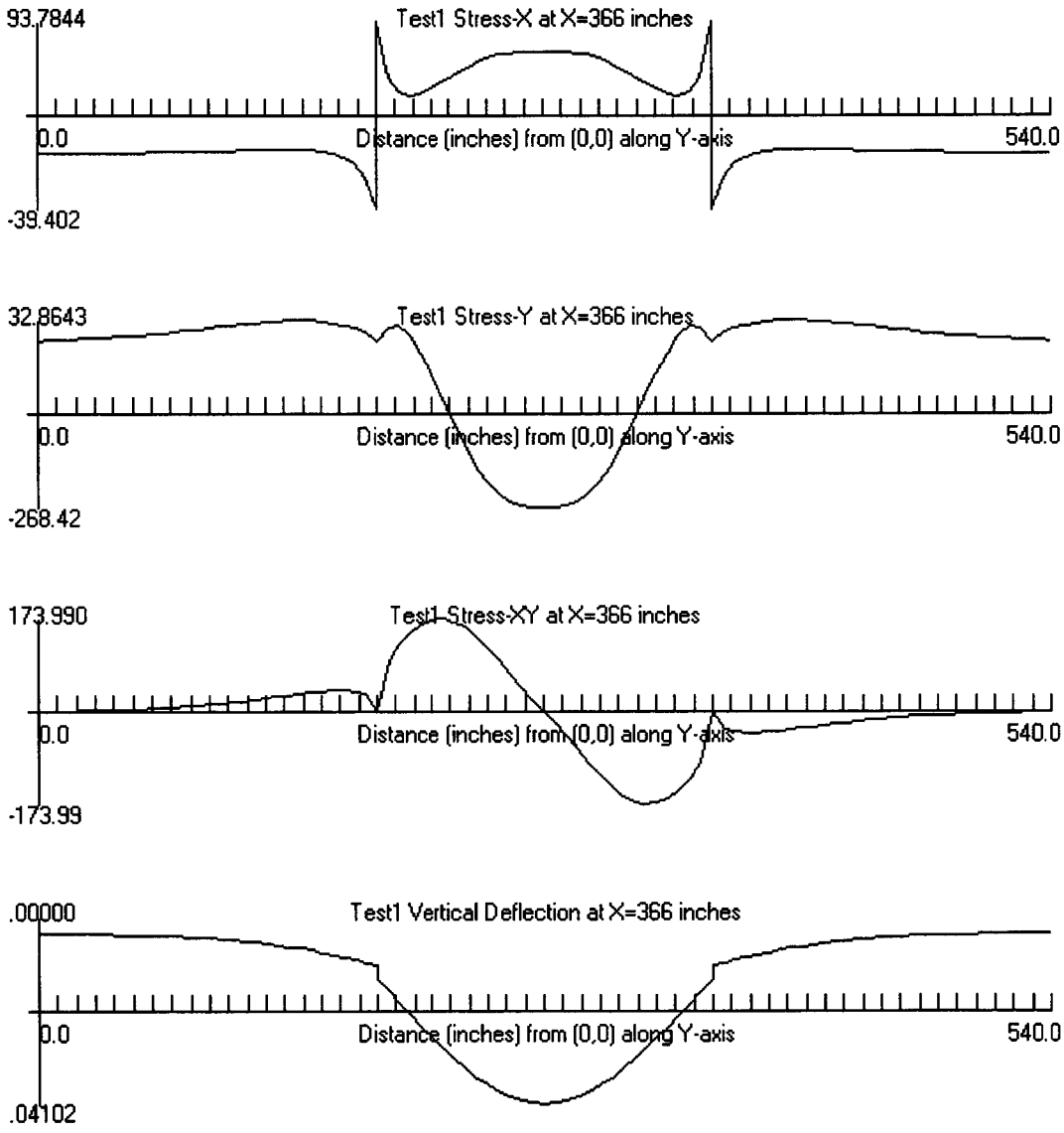

Figure B20: JSLAB output for MRC unloaded 15ft slab under 6-wheel perpendicular loading

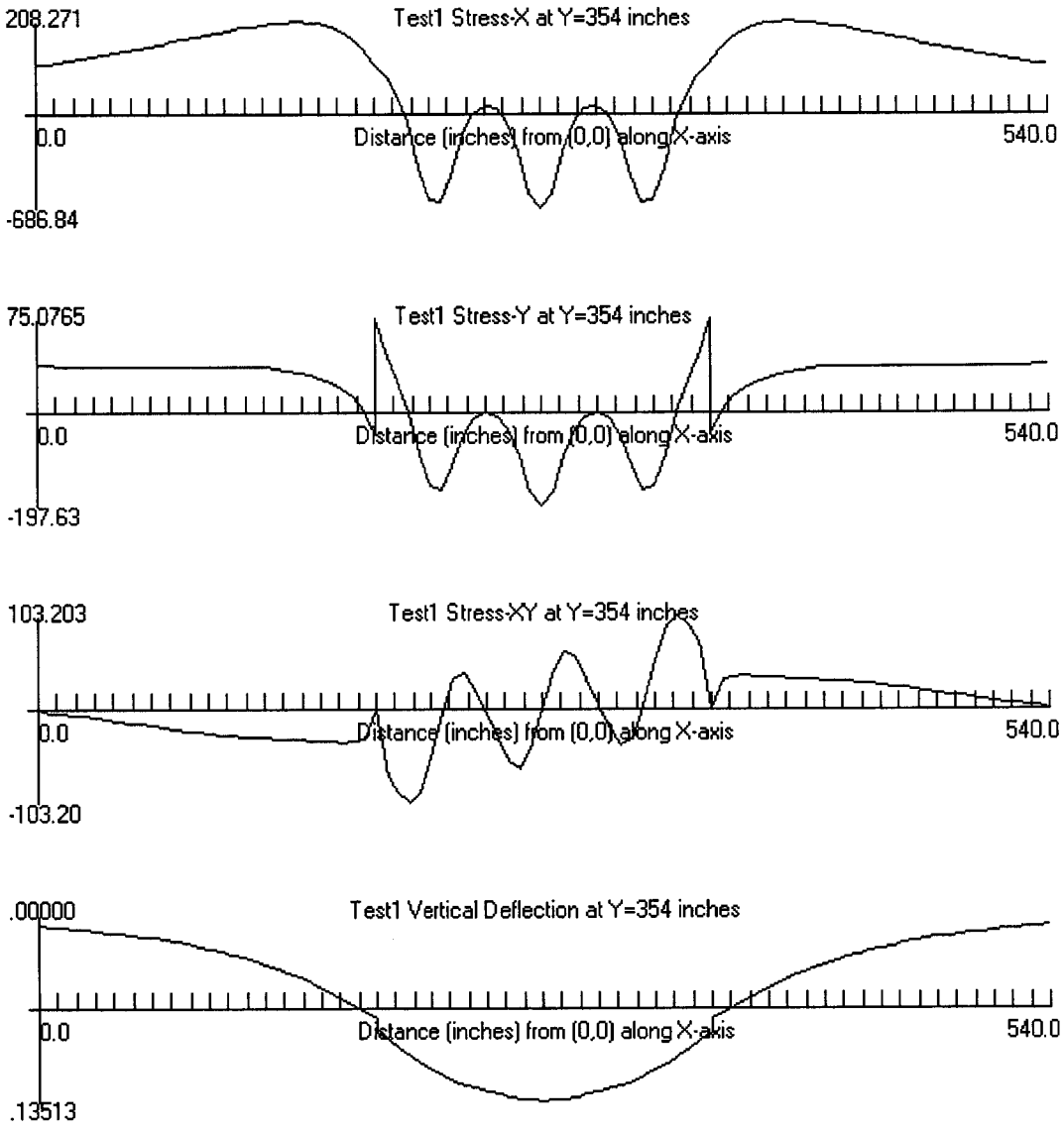

Figure B21: JSLAB output for MRG loaded 15ft slab under 6-wheel perpendicular loading

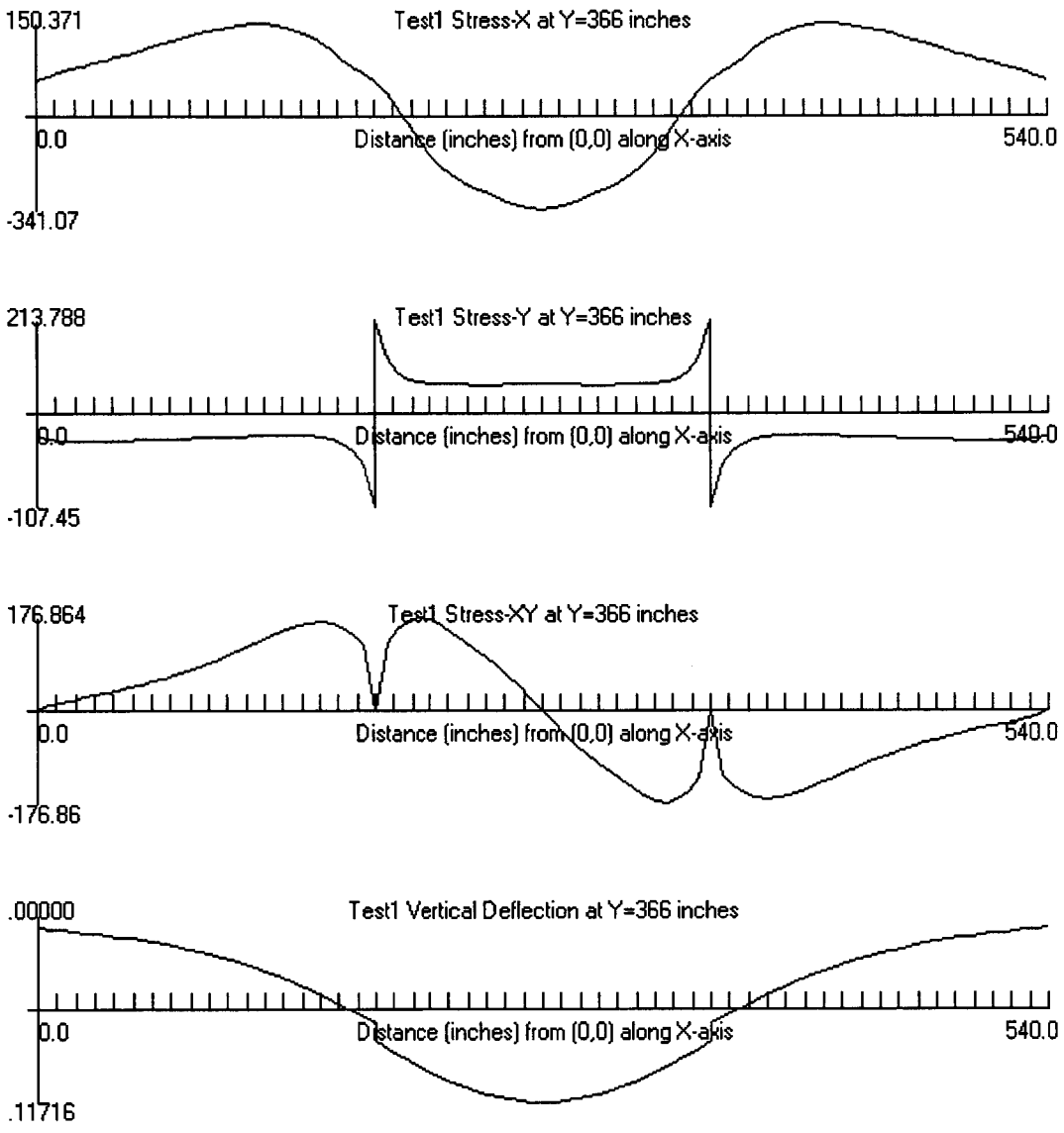

Figure B22: JSLAB output for MRG unloaded 15ft slab under 6-wheel perpendicular loading

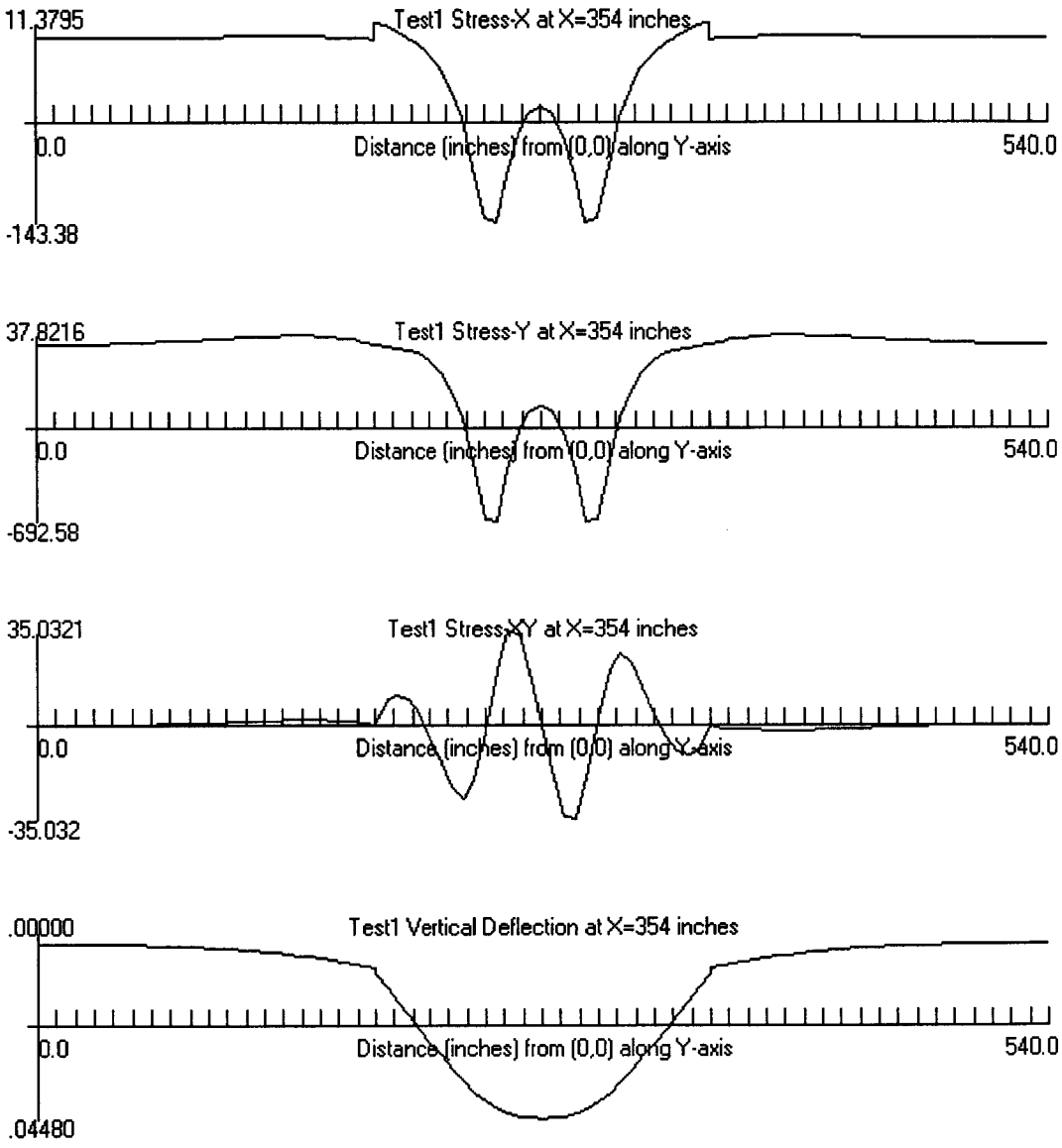

Figure B23: JSLAB output for MRS loaded 15ft slab under 6-wheel perpendicular loading

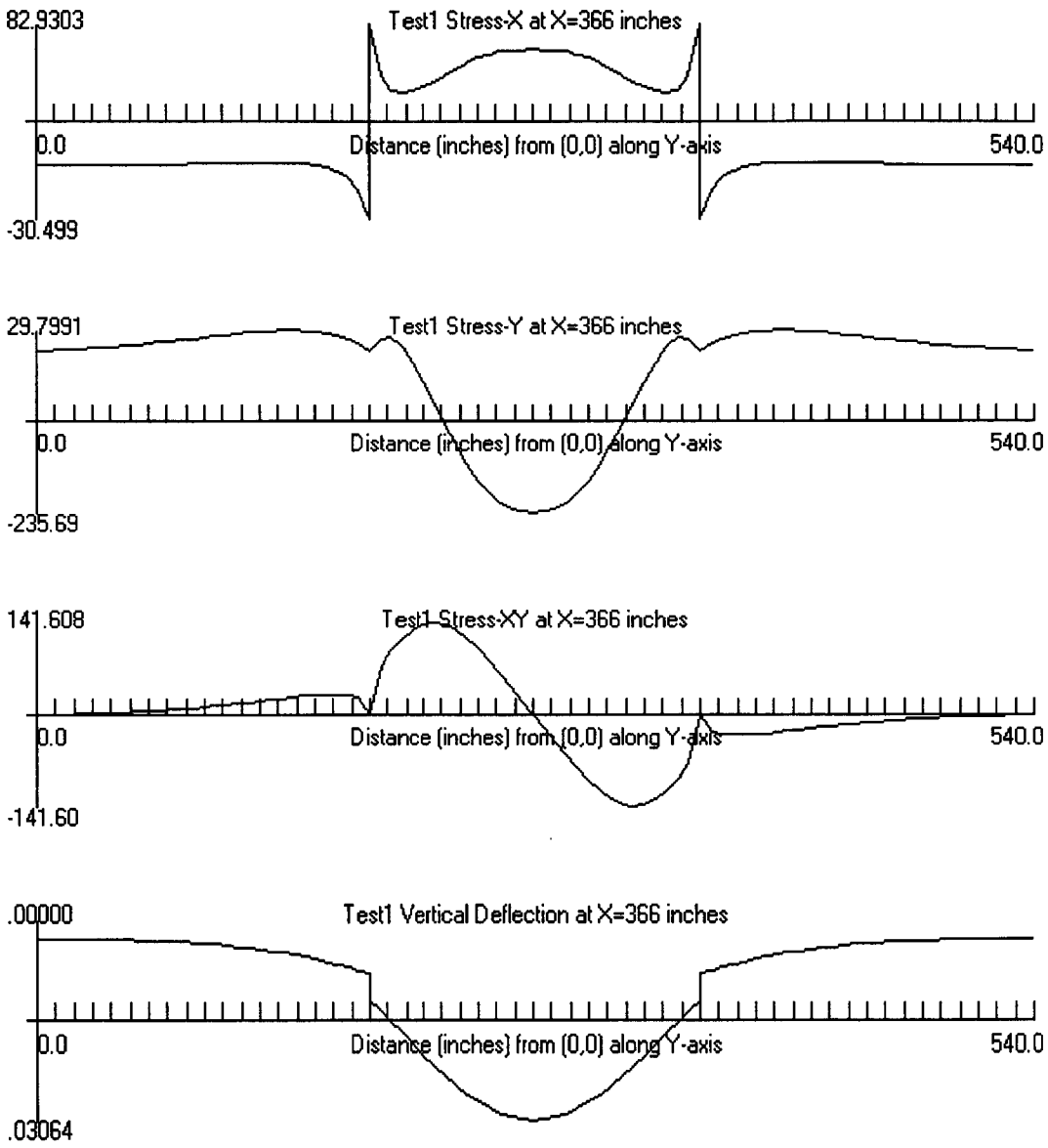

Figure B24: JSLAB output for MRS unloaded 15ft slab under 6-wheel perpendicular loading